Extended Analysis of the CARES Aerosol Chemistry Data to Characterize Sources and Processes of Organic Aerosol in the Sacramento Valley of California

REPORT TO THE

California Air Resources Board Research Division

Project # 10-305

Prepared by

Dr. Qi Zhang

Department of Environmental Toxicology
University of California, Davis
One Shields Avenue, Davis, CA, 95616

November 2013

DISCLAIMER

The statements and conclusions in this report are those of the contractor and not necessarily those of the California Air Resources Board. The mention of commercial products, their source, or their use in connection with material reported herein is not to be construed as actual or implied endorsement of such products.

ACKNOWLEDGEMENTS

Table of Contents

LIST OF FIGURES AND TALBES

LIST OF ACRONYMS

AMS: Aerosol mass spectrometer

BBOA: Biomass burning organic aerosol.

CARES: Carbonaceous Aerosol Radiative Effects Study (A DOE funded campaign conducted in the Sacramento and Sierra foothill region of northern California during June 2-28, 2010)

CCN: Cloud condensation nuclei

HOA: Hydrocarbon-like organic aerosol estimated from factor analysis of AMS spectra. HOA is typically used as a surrogate of POA due to the similarity of its spectra with those from primary sources, and the strong correlation of its time series with those of primary tracers (CO, NOx, EC, etc.).

HR-ToF-AMS: Aerodyne Aerosol Mass Spectrometer equipped with a high-resolution time-of-flight mass spectrometer

LO-OOA: Less oxidized oxygenated organic aerosol

LV-OOA: Low-volatility OOA, more aged and oxygenated, less volatile fraction of OOA, estimated from factor analysis of AMS spectra in several studies.

MO-OOA: More oxidized oxygenated organic aerosol

MSA: methanesulfonic acid

NPE: New particle events

OA: Organic aerosol, i.e., the organic fraction of airborne particulate matter.

OOA: Oxygenated organic aerosol estimated from factor analysis of AMS spectra. OOA is typically used as a surrogate of SOA due to the similarity of its spectra with those from chamber SOA and ambient highly aged OA, and the correlation of its time series with those of secondary tracers (e.g., ozone, nitrate, and sulfate)

PMF: Positive matrix factorization

POA: Primary organic aerosol emitted into the atmosphere directly into the particle phase

Q-AMS: Quadrupole-based Aerodyne aerosol mass spectrometer. It provides unit-resolution mass spectra.

SMPS: Scanning Mobility Particle Sizer

SOA: Secondary organic aerosol created by chemical reactions leading to a decrease in species volatility and increased partitioning to the particle phase

SOAR-1: Study of organic aerosols in Riverside, phase 1

SV-OOA: Semi-volatile, less aged and oxygenated, more volatile fraction of OOA, estimated from factor analysis of AMS spectra in several studies.

TD: Thermodenuder

ABSTRACT

This report explores the characteristics, sources, and processes of submicrometer particles in northern California via integrated analyses of atmospheric observation data obtained during the Carbonaceous Aerosols and Radiative Effects Study (CARES) that took place in the Sacramento and western Sierra Foothills area in June 2010. We focus on reporting aerosol chemistry, physical properties, and diurnal and temporal variations at Cool (denoted as the T1 site of the project) at the foothills of the Sierra Nevada Mountains, where intense biogenic emissions are periodically mixed with urban outflow transported by daytime southwesterly winds from the Sacramento metropolitan area. During CARES, the average mass loading of submicrometer particles (PM_1) was 3.0 µg m^{-3}, dominated by organics (80%) and sulfate (9.9%). The organic aerosol (OA) had a nominal formula of $C_1H_{1.38}N_{0.004}O_{0.44}$, thus an average organic mass-to-carbon (OM/OC) ratio of 1.70. Two distinct oxygenated OA factors were identified via Positive matrix factorization (PMF) of the high-resolution mass spectra of organics. The more oxidized MO-OOA (O/C = 0.54) was interpreted as a surrogate for secondary OA (SOA) influenced by biogenic emissions whereas the less oxidized LO-OOA (O/C = 0.42) was found to represent SOA formed in photochemically processed urban emissions. LO-OOA correlated strongly with ozone and MO-OOA correlated well with two 1st generation isoprene oxidation products (methacrolein and methyl vinyl ketone), indicating that both SOAs were relatively fresh. A hydrocarbon like OA (HOA) factor was also identified, representing primary emissions mainly due to local traffic. On average, SOA (= MO-OOA + LO-OOA) accounted for 91% of the total OA mass and 72% of the PM_1 mass observed at Cool. Twenty three periods of urban plumes from T0 (Sacramento) to T1 (Cool) were identified using the Weather Research and Forecasting model coupled with Chemistry (WRF-Chem). The average PM_1 mass loading was considerably higher in urban plumes than in air masses dominated by biogenic SOA. The change in OA mass relative to CO ($\Delta OA/\Delta CO$) varied in the range of 5-196 µg/m^3/ppm, reflecting large variability in SOA production. The highest $\Delta OA/\Delta CO$ was reached when air masses were dominated by anthropogenic emissions in the presence of a high concentration of biogenic volatile organic compounds (BVOCs). This ratio, which was 97 µg/m^3/ppm on average, was much higher than when urban plumes arrived in a low BVOC environment (~36 µg/m^3/ppm) or during other periods dominated by biogenic SOA (35 µg/m^3/ppm). These results demonstrate that SOA formation is enhanced when anthropogenic emissions interact with biogenic precursors.

During CARES, regional new particle formation and growth events (NPE) were observed on most days over the Sacramento and western Sierra Foothills area. Simultaneous particle measurements at both the T0 (Sacramento, urban site) and T1 sites of CARES indicate that the NPE usually occurred in the morning with the appearance of an ultrafine mode centered at ~15 nm (in mobility diameter, D_m) followed by the growth of this mode to ~50 nm in the afternoon. These events were generally associated with southwesterly winds bringing urban plumes from Sacramento to the T1 site. The growth rate was on average higher at T0 (7.1±2.7 nm/hr) than at T1 (6.2±2.5 nm/hr), due to stronger anthropogenic influences at T0. Using a high-resolution time-of-flight aerosol mass spectrometer (HR-ToF-AMS), we investigated the evolution of the size-resolved chemical composition of new particles at T1. Our results indicate that the growth of new particles was driven primarily by the condensation of oxygenated organic species and, to a lesser extent, ammonium sulfate. New particles appear to be fully neutralized during growth,

consistent with high NH$_3$ concentration in the region. Aminium species, although presenting at very low concentrations in particles, enhanced significantly during the NPE days. Our results also indicate that the bulk composition of the ultrafine mode organics during NPE was very similar to that of anthropogenically-influenced secondary OA (SOA) observed in transported urban plumes. In addition, the concentrations of species representative of urban emissions (e.g., black carbon, CO, and toluene) as well as the photo-oxidation products of biogenic VOC were significantly higher during the NPE days compared to the non-event days. These results indicate that the frequently occurring NPE over the Sacramento and Sierra-Nevada regions were promoted by the interaction between biogenic emissions and urban plumes.

1. INTRODUCTION

1.1. Background Information and Motivations

Aerosol particles are a key determinant of air quality and an important player in the Earth's climate system [*Ghan and Schwartz*, 2007; *IPCC*, 2007]. Yet, they represent some of the largest uncertainties that confound the understanding of climate change issues and complicate the assessment of air quality policies [*IPCC*, 2007; *NOAAresearch*, 2008]. Properties that determine aerosol's impacts on air quality, climate, human health, and ecosystems are intrinsically linked to the chemical composition of airborne particulate matter (PM), of which the organic fraction (i.e., organic aerosol, OA) is an important constituent.

OA typically accounts for 20-80% of the total fine PM mass in California and globally [*M. Kanakidou et al.*, 2005a; *Seinfeld and Pankow*, 2003; *Zhang et al.*, 2007b]. It is known to affect air quality and climate on both regional and global scales [*Fuzzi et al.*, 2006; *Hallquist et al.*, 2009a; *Jacobson et al.*, 2000; *Kanakidou et al.*, 2005a]. A thorough understanding of the chemical and physical properties, sources, and processes of atmospheric OA is crucial to quantifying the various effects of aerosol and improving the fidelity and predictive capability of air quality and climate models. Characterization and modeling of these variables, however, are challenging because OA comprises thousands of compounds with vastly different properties such as oxidation degree, volatility, and hygroscopicity [*Fuzzi et al.*, 2006; *A Goldstein and Galbally*, 2007; *Jacobson et al.*, 2000; *Kanakidou et al.*, 2005a; *Murphy*, 2005; *Saxena and Hildemann*, 1996; *Seinfeld and Pankow*, 2003]. Also complicated are the sources and evolution (aging) processes of atmospheric OA and their gas phase precursors [e.g., *de Gouw and Jimenez*, 2009; *Jimenez et al.*, 2009].

Particulate organic materials can be classified as either primary OA (POA) from direct emissions, e.g., fossil fuel and biomass burning, or secondary OA (SOA) from the oxidation of gas-phase precursors [*M. Kanakidou et al.*, 2005a]. POA and volatile organic compounds (VOCs) are emitted from numerous biogenic and anthropogenic sources [e.g., *Joost de Gouw and Jimenez*, 2009]. The formation of SOA may involve countless reaction pathways that convert VOCs into low volatility species [*Hallquist et al.*, 2009a; *Kroll and Seinfeld*, 2008]. In addition, the composition and properties of both POA and SOA may change dynamically throughout the aerosol lifetime, due to intertwined processes such as emission, oxidation, gas-to-particle partitioning, and cloud processing [*Blando and Turpin*, 2000; *Donahue et al.*, 2006; *Jimenez et al.*, 2009; *Kroll and Seinfeld*, 2008; *Ng et al.*, 2010a].

To this date, the emission sources, formation mechanisms, and evolution processes of atmospheric OA remain poorly characterized [*de Gouw and Jimenez*, 2009; *Holzinger et al.*,

2007a]. A consequence of this knowledge gap is the poor performance of current models in simulating OA concentrations and properties. In particular, there is critical need for better representation of SOA formation mechanisms in models. SOA is a ubiquitous and frequently dominant component of ambient aerosols [*Zhang et al.*, 2007b]. Its concentration is usually higher than that of POA, even in densely populated urban areas (e.g., the LA and NYC metropolitan areas) where combustion emissions of POA from transportation are intense [*Docherty et al.*, 2008; *Sun et al.*, 2010; *Zhang et al.*, 2007b]. SOA is even more dominant (> 80% of total OA mass typically) in rural and remote atmospheres [*Zhang et al.*, 2007b].

Most models, however, vastly underestimate the importance of SOA and inaccurately simulate its properties. According to several recent studies, model calculations constrained by chamber study data underpredict SOA concentrations in urban and regional polluted atmosphere by up to a factor of ~10 [*de Gouw et al.*, 2005; *Johnson et al.*, 2006; *Kleinman et al.*, 2008b; *Volkamer et al.*, 2006]. Top-down estimates based on budgets of organic species in the atmosphere suggest sizeable underestimation of global SOA loading as well [*Goldstein and Galbally*, 2007]. Furthermore, a recent study by Dzepina et al. [*Dzepina et al.*, 2009] found that even models incorporating newly identified mechanisms cannot accurately predict its volatility and degree of oxidation (thus hygroscopicity). Because the results from model predictions often guide emission control strategies and regulatory policies [2010; *Schwartz*, 2008], an improved understanding and model representation of airborne organic PM is critical to effectively combat air pollution and mitigate its detrimental effects on air quality, climate, and human health. This is especially important for California since over the years the state's emission control programs have not reduced OA loading as rapidly as the reductions in inorganic particulates and black carbon. This means that further fine particle control in the state may need to focus on OA.

Development and improvement of aerosol models require phenomenological descriptions of ambient PM and their gas phase precursors. Due to the enormous complexities inherent in the composition and lifecycle processes of atmospheric OA, simulation and representation of OA properties and impacts in models are extremely challenging. Field measurement data must be relied upon to unravel these complexities and to elucidate the properties, sources, formation, and evolution/aging processes of aerosol-phase organics. Highly time-resolved measurements of the composition and the chemically-resolved size distributions of ambient particles using Aerodyne Aerosol Mass Spectrometers (AMS) are essential to this need.

The AMS is the only current instrument that provides *real-time, quantitative, and size-resolved* information on submicron non-refractory (NR) aerosol chemistry with a time resolution of a few minutes or better [e.g., *Allan et al.*, 2003; *Canagaratna et al.*, 2007; *Jayne et al.*, 2000; *Jimenez et al.*, 2003]. The HR-ToF-AMS, i.e., AMS built with a high-resolution time-of-flight mass spectrometer, is further able to determine the elemental ratios and oxidation degrees of organic species in PM [*Aiken et al.*, 2007; *Aiken et al.*, 2008; *Aiken et al.*, 2009b; *DeCarlo et al.*, 2006a; *Sun et al.*, 2009]. Fig. 1-1 shows the type of information on aerosol that can be obtained directly with an HR-ToF-AMS: 1) concentration and composition of NR species (i.e., sulfate, nitrate, ammonium, chloride, and organics), 2) size distributions of aerosol species, and 3) elemental ratios (thus OM/OC ratios) of organics. In addition, although not measured directly, particle shape (physical morphology) and the mixing state (internal vs. external) of chemical species can be inferred by combining the size measurements by an AMS and a scanning mobility particle sizer (SMPS) [*DeCarlo et al.*, 2004; *Salcedo et al.*, 2007; *Zhang et al.*, 2004]. Aerosol chemical and physical properties are fundamental information required to evaluating and quantifying the impacts of atmospheric aerosols on air quality, climate, human health, and

1. Quantitative composition

2. Size-resolved composition

3. Elemental comp. ($C_nH_mN_pO_zS_w$)
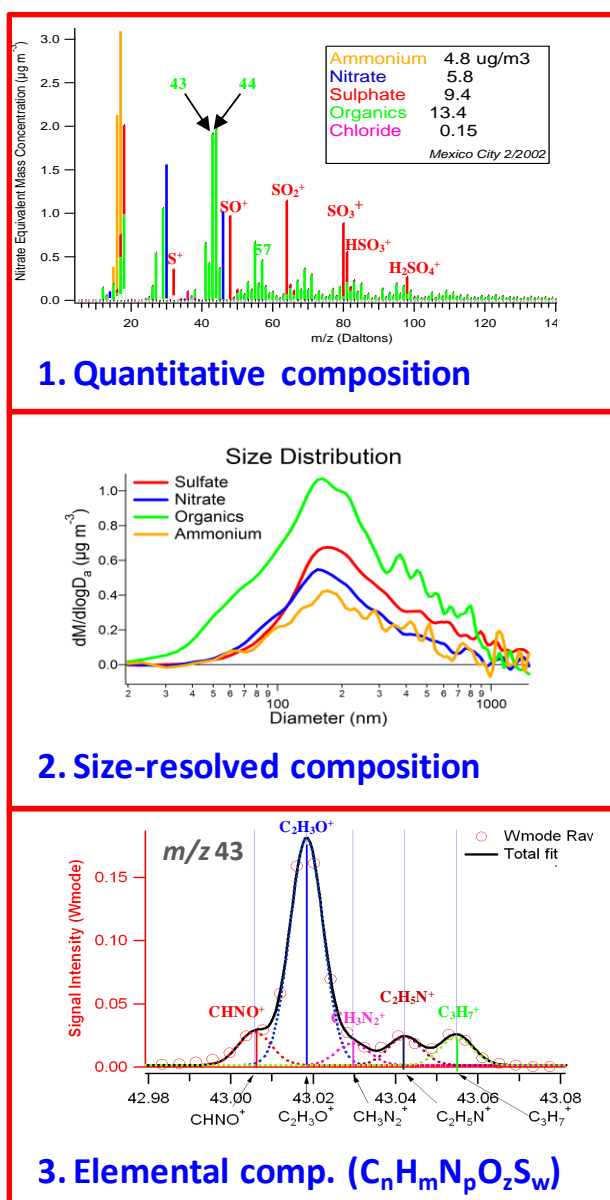
Figure 1-1. *Examples of the types of aerosol information provided directly by the Aerodyne HR-ToF-AMS.*

ecosystems. The high time resolution of the AMS data also reveals details about the dynamic variations of aerosol chemistry and microphysics – information that is vital to addressing the sources and physico-chemical processes of atmospheric PM [e.g., *Cubison et al.*, 2006; *Takegawa et al.*, 2006; *Volkamer et al.*, 2006; *Zhang et al.*, 2005a; *Zhang et al.*, 2007a; *Zhang et al.*, 2004]. All of these data are crucial for development and validation of air quality and climate models [*Ghan and Schwartz*, 2007].

The U.S. Department of Energy (DOE) sponsored Carbonaceous Aerosols and Radiative Effects Study (CARES) took place in the Sacramento Valley, which corresponds to the northern part of the Central Valley of California, between June 2nd and June 28th 2010. The valley forms a northwest-southeast axis and its shape is defined by mountains on the west (various Coast Ranges), north (Siskiyou Mountains) and east (Sierra Nevada Mountains). A mid-size metropolitan area (Sacramento and its suburbs) lies on the south edge of the valley, while the rest of the valley is heavily forested and contains large agricultural regions. The Sacramento Valley has faced air pollution problems such as high ozone concentrations promoted by meteorological conditions (strong sunlight and high temperatures in summer) coupled with high VOCs and NO_x emissions (Murphy et al., 2007). In summer, the region is subjected to constant winds, which bring air masses from the Pacific Ocean to the Sacramento metropolitan area, and push northeast to the Sierra Nevada Mountains, bringing urban outflow from Sacramento to the foothills (Dillon et al., 2002). Recent studies performed at the University of California-Blodgett Forest Research Station (UC-BFRS; Goldstein et al., 2000), which is located on the western slope of the Sierra Nevada ~ 75 km downwind from Sacramento and surrounded by a ponderosa pine plantation, pointed out that large amounts of reactive VOCs are emitted by the surrounding forests (e.g., Bouvier-Brown et al., 2009) and that SOA formation in this region is mainly driven by oxidation of monoterpenes and isoprene (Cahill et al., 2006; Worton et al., 2011) mediated primarily by ozone (Holzinger et al., 2005). New particle formation and growth events have been frequently observed as well (Lunden et al., 2006; Creamean et al., 2011), indicating the importance of secondary aerosol formation processes in

the region. Several studies also focused on chemical processes occurring in urban plumes brought from Sacramento (Dillon et al., 2002; Spaulding et al., 2003), but anthropogenic influences were found to be small at the UC-BFRS, probably because the site is too far from significant urban emission sources.

The CARES campaign was designed to take advantage of the regular wind pattern to better understand the life-cycle processes and radiative properties of carbonaceous aerosols in a region influenced by both anthropogenic and biogenic emissions (Zaveri et al., 2012; Fast et al., 2012). Within the framework of CARES, a wide range of instruments were deployed between June 2 and 28, 2010 at two ground sites located in Sacramento (T0, urban site) and Cool, CA at the foothills of the Sierra Nevada Mountains (T1, rural site), respectively, to measure aerosol chemical composition, size distribution, and optical and hygroscopic properties, as well as trace gases and meteorological data (Zaveri et al., 2012). In coordination with the two ground-based operations, two aircrafts conducted regular flights through and around the Sacramento plumes during CARES. Zaveri et al. (2012) provide a complete overview of the CARES field campaign, including a description of the experimental design and key observations from the two ground-based sites and aircraft platforms.

1.2. Objectives

The primary goals of this project are to achieve a process-level understanding of organic aerosols in Northern California and to bridge between observations and models via synthesizing and translating the results and insights generated from this research into data products and formulations that may be directly used to inform and evaluate air quality models. To achieve this goal, we performed integrated analysis of the measurement data of aerosol particles, trace gases, and meteorological conditions acquired from the T1 site, focusing on the aerosol chemistry and size distribution data acquired with a high-resolution time-of-flight aerosol mass spectrometer and a scanning mobility particle sizer. Based on these results, as well as observations from T0, we interpret the sources and processes of submicrometer particles over the Sierra foothills region.

1.3. Report Structure

This report is comprised of five chapters, including introduction (Chapter 1) and conclusions (Chapter 5).

Chapter 2 provides an overview of the characteristics size resolved composition and temporal variation of submicrometer aerosol particles at Sierra foothills

Authors note: The work in chapter 2 has been published in the journal Atmospheric Chemistry and Physics and may be cited in any future studies as "Setyan, A., Q. Zhang, M. Merkel, W. B. Knighton, Y. Sun, C. Song, J. E. Shilling, T. B. Onasch, S. C. Herndon, D. R. Worsnop, J. D. Fast, R. A. Zaveri, L. K. Berg, A. Wiedensohler, B. A. Flowers, M. K. Dubey, and R. Subramanian (2012), Characterization of submicron particles influenced by mixed biogenic and anthropogenic emissions using high-resolution aerosol mass spectrometry: results from CARES, Atmospheric Chemistry & Physics, 12, 8131-8156, 10.5194/acp-12-8131-2012"

Chapter 3 presents a study on the frequent regional new particle formation and growth events in the Sacramento Valley Air Basin.

Authors note: The work in chapter 3 will be submitted for publication at a future date.

2. CHARACTERISTICS, SOURCES, AND PROCESSES OF SUBMICROMETER PARTICLES AT SIERRA FOOTHILLS

2.1. Introduction

Atmospheric aerosols significantly affect the Earth's climate [IPCC, 2007], human health [*Pope et al.*, 2009], the ecological balance [*Mahowald*, 2011], and visibility [*Watson*, 2002]. Aerosols consist of a wide range of chemical compounds. Analyses of many datasets from around the world showed that organic species generally represent the dominant fraction and account for 20-90% of the mass in submicron particles [*Zhang et al.*, 2007c]. Organic aerosols (OA) are classified into primary (POA) or secondary (SOA). POA refers to aerosols directly emitted by a source, such as fossil fuel combustion, biomass burning or food cooking, while SOA are generated by reactions of gaseous precursors. In addition, OA can also be classified depending on their sources, e.g., biogenic or anthropogenic.

Models have been developed to improve understanding of aerosol processes and properties, and to evaluate their effects on climate. Even if some uncertainties still remain, the processes controlling the formation and evolution of secondary inorganic aerosol compounds are now well understood [*Zaveri et al.*, 2008]. However, since SOA formation is controlled by very complex processes, including photo-oxidation of volatile organic compounds (VOCs), nucleation or gas-to-particle partitioning of low volatile compounds into preexisting particles, and aqueous-phase and heterogeneous processes [*Ervens et al.*, 2011; *Hallquist et al.*, 2009b; *M. Kanakidou et al.*, 2005b], current models have difficulty predicting accurately SOA concentrations and/or properties [*K. Dzepina et al.*, 2009; *Spracklen et al.*, 2011; e.g., *R. Volkamer et al.*, 2006]. Recent studies suggest that anthropogenic and biogenic emissions may interact and increase SOA formation [*Allen H. Goldstein et al.*, 2009; *Hoyle et al.*, 2011; *Maria Kanakidou et al.*, 2000; *Weber et al.*, 2007; *Worton et al.*, 2011]. Thus, field campaigns have been undertaken in locations subjected to both urban and natural influences to study the enhancement effects of SOA production in mixed biogenic and anthropogenic emissions. These studies are important for identifying missing SOA sources in current models and closing the gaps between simulated and measured SOA concentrations and properties [*Zaveri et al.*, 2012a].

The Sacramento Valley, which corresponds to the northern part of the Central Valley of California, is a place of choice to study processes of organic species from biogenic and anthropogenic sources. The valley forms a northwest-southeast axis and its shape is defined by mountains on the west (various Coast Ranges), north (Siskiyou Mountains) and east (Sierra Nevada Mountains). A mid-size metropolitan area (Sacramento and its suburbs) lies on the south edge of the valley, while the rest of the valley is heavily forested and contains large agricultural regions. The Sacramento Valley has faced air pollution problems such as high ozone concentrations promoted by meteorological conditions (strong sunlight and high temperatures in summer) coupled with high VOCs and NO_x emissions [*J G Murphy et al.*, 2007]. In summer, the region is subjected to constant winds, which bring air masses from the Pacific Ocean to the Sacramento metropolitan area, and push northeast to the Sierra Nevada Mountains, bringing urban outflow from Sacramento to the foothills [*Dillon et al.*, 2002]. Recent studies performed at the University of California-Blodgett Forest Research Station [UC-BFRS; *A. H. Goldstein et al.*, 2000], which is located on the western slope of the Sierra Nevada ~ 75 km downwind from Sacramento and surrounded by a ponderosa pine plantation, pointed out that large amounts of reactive VOCs are emitted by the surrounding forests [e.g., *Bouvier-Brown et al.*, 2009] and that

SOA formation in this region is mainly driven by oxidation of monoterpenes and isoprene [*Cahill et al.*, 2006; *Worton et al.*, 2011] mediated primarily by ozone [*Holzinger et al.*, 2005]. New particle formation and growth events have been frequently observed as well [*Creamean et al.*, 2011; *Lunden et al.*, 2006], indicating the importance of secondary aerosol formation processes in the region. Several studies also focused on chemical processes occurring in urban plumes brought from Sacramento [*Dillon et al.*, 2002; *Spaulding et al.*, 2003], but anthropogenic influences were found to be small at the UC-BFRS, probably because the site is too far from significant urban emission sources.

The Carbonaceous Aerosols and Radiative Effects Study (CARES), which was sponsored by the U.S. Department of Energy (DOE), took place in northern California in summer 2010. The aim of this field campaign was to better understand the evolution and ageing of carbonaceous aerosols in a region influenced by mixed anthropogenic and biogenic precursors, and to integrate this knowledge into models used for simulating their direct and indirect radiative effects on climate [*Fast et al.*, 2012; *Zaveri et al.*, 2012a]. Measurements were conducted at two ground-based sites: one within the Sacramento urban area (denoted T0 to represent the urban emission origin of the project) and one at Cool, CA (denoted T1 to represent a rural receptor site located ~ 40 km northeast of Sacramento, i.e., downwind from T0). In coordination with the two ground-based operations, two aircrafts conducted regular flights through and around the Sacramento plumes during CARES. *Zaveri et al.* [2012a] provide a complete overview of the CARES field campaign, including a description of the experimental design and key observations from the two ground-based sites and aircraft platforms.

Here, we present results obtained at the T1 site of CARES, where we deployed an Aerodyne high resolution time-of-flight aerosol mass spectrometer (HR-ToF-AMS) in parallel with a scanning mobility particle sizer (SMPS) to characterize the concentration, composition, size distribution, and temporal variation of PM_1. We performed positive matrix factorization (PMF) of the high resolution mass spectra to identify distinct OA factors and determine their concentrations and mass spectra. These results were combined with collocated measurements of other aerosol properties, trace gases, and meteorological conditions to elucidate the sources of and processes controlling PM_1 at T1. Finally, periods of urban plumes from Sacramento and other air masses dominated by biogenic emissions were determined by the WRF-Chem model [*Fast et al.*, 2012]. Aerosols during different periods are compared to study the influence of anthropogenic emissions on the formation of biogenic SOAs.

2.2. Methods

2.2.1. Sampling site, Instrumentation, Meteorological Conditions, and Time
The CARES field campaign took place in the Sacramento Valley between June 2nd and June 28th 2010. A map of the Sacramento Valley with the location of the two ground-based sites is given in Fig. 2-1(a). Measurements reported in this paper were performed at Cool (T1 site; 38°53′ N, 121°00′ W) in a maintenance parking lot on the campus of the Northside School. Cool is a small town (2500 inhabitants) located in the foothills of the Sierra Nevada Mountains at an elevation of ~ 460 m above sea level. The sampling site is surrounded by forests, and located ~ 200 m from the California State Route 49. During summer, Cool is influenced by highly consistent winds bringing urban outflow from Sacramento during the afternoon [*Dillon et al.*, 2002]. A complete description of the meteorological conditions during the CARES is given by *Fast et al.* [2012]. In summary, the meteorological conditions were spring like, with high

Figure 2-1. *(a)* *Map of the Sacramento Valley with the location of the two ground-based sites (T0 and T1), the University of California-Blodgett Forest Research Station (UC-BFRS, site of the BEARPEX 2007 and 2009 studies) and the refineries identified in the region.* *(b)* *Wind rose plots for every 3-hour period at the T1 site (height: 3 m), colored by wind speed. Radial scales correspond to the frequency, and are kept the same in each wind rose.* *(c)* *Schematic drawing of the instrumental setup.*
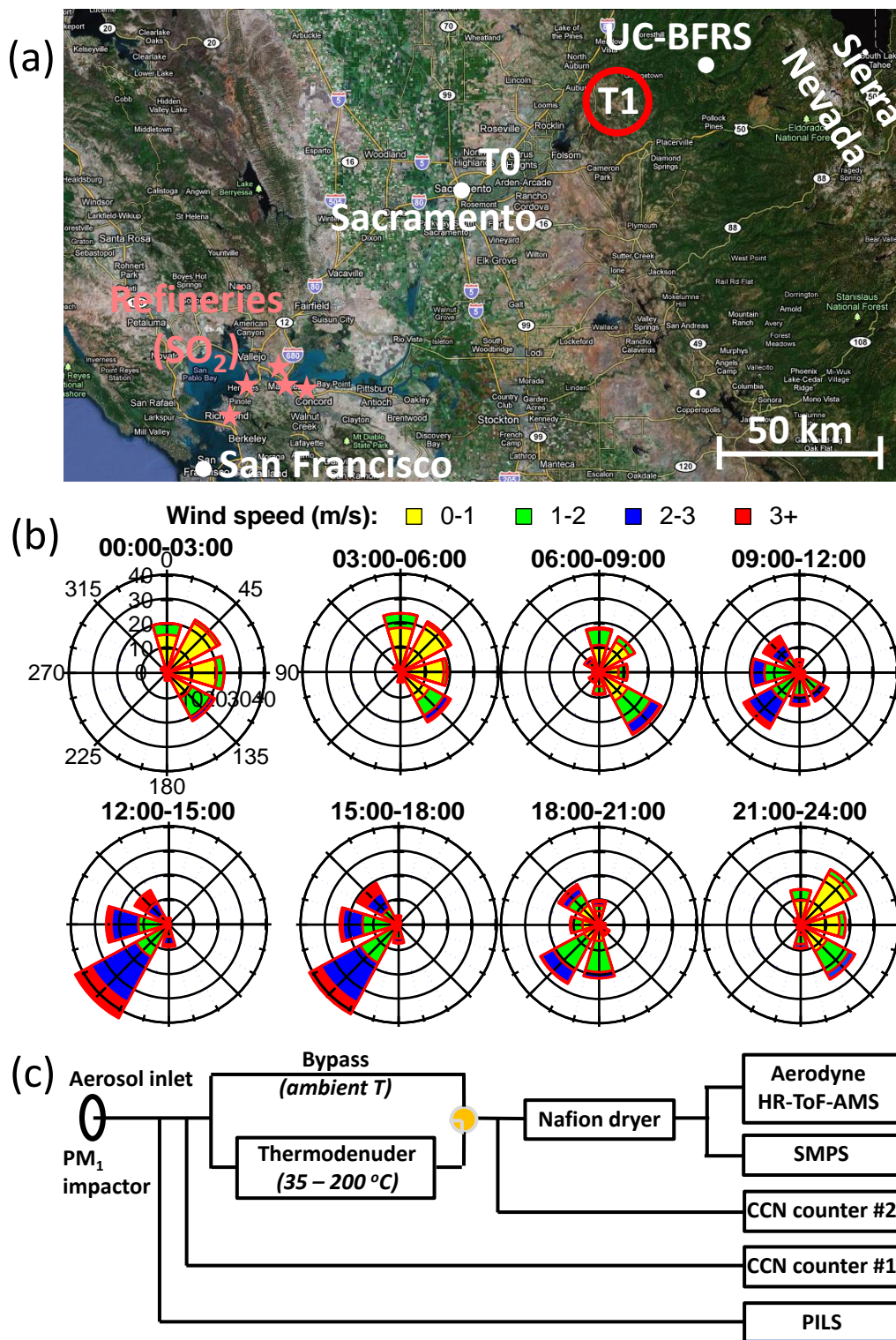
Figure 2-2. Time series of (***a***) temperature, relative humidity and broadband solar radiation (from precision spectral pyranometer [PSP]), (***b***) wind direction colored by wind speed (height: 3m), (***c***) concentrations of CO2, O3 and NOx, (***d***) monoterpenes, isoprene and sum of methacrolein (Macr) and methyl vinyl ketone (MVK), (***e***) formaldehyde, methanol and acetone, (***f***) acetonitrile, benzene and toluene. Shaded regions indicate 23 periods of urban plumes transported from T0 to T1 (orange) and 3 periods subjected to influences from northwesterly wind (green). The remaining periods correspond mainly to downslope flows from the Sierra Nevada to the foothills.
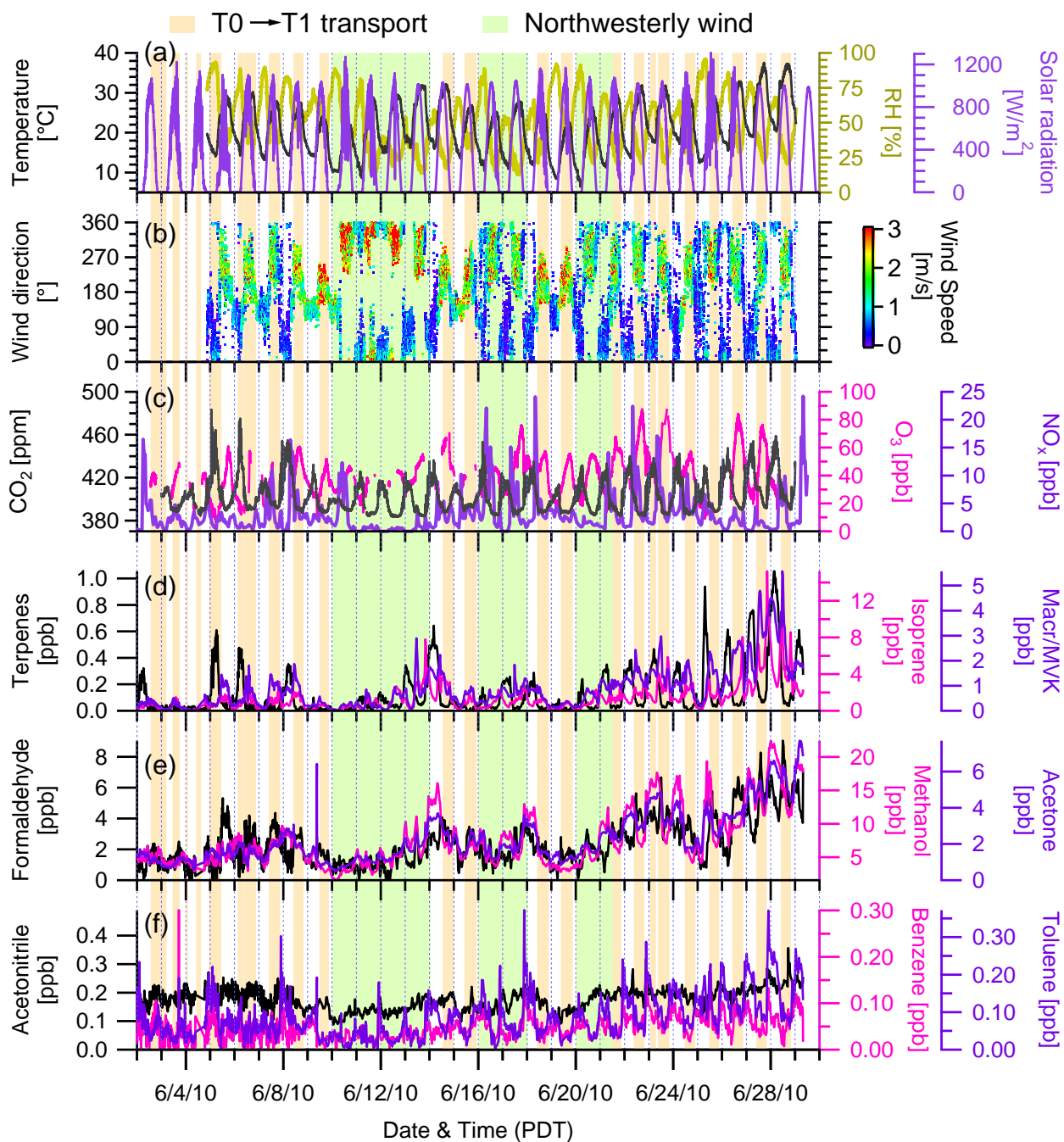
temperatures on average 27ºC during the day and 14ºC in the night (Fig. 2-2). The prevailing wind was from the southwest during the day and from the northeast in the night (Fig. 2-1b). The weather was sunny during the entire campaign, except for two cloudy periods on June 4 and 24, 2010. In addition, during the present study, transport of pollutants from Sacramento over the Sierra Nevada foothills occurred almost every afternoon except for three periods (June 10-13, June 16-17, June 20-21) [*Fast et al.*, 2012].

Various instruments installed in two adjacent trailers were deployed to measure the concentration, chemical composition, size distribution, mixing state, radiative and optical properties, and cloud condensation nuclei (CCN) activities of particles, as well as trace gas concentrations and meteorological conditions [*Zaveri et al.*, 2012a]. A schematic drawing of the instrumental setup for PM_1 is given in Fig. 1c. Particles were sampled through a common inlet equipped with a PM_1 impactor (Brechtel Manufacturing Inc., Hayward, CA; model 8003) at a total flow rate of ~15 l/min. The sampling line was constituted of a total of 14 feet of tubing, including 3 feet of stainless steel tube with an inner diameter of 3/4 inch, 8 feet of copper tube with an inner diameter of 1/4 inch, 2 feet long temperature-controlled thermodenuder (TD), and 1 feet long Nafion dryer. Instruments connected to this system include a particle into liquid sampler (PILS), a CCN counter, and a thermodenuder. The sampling line downstream of the TD was split again in three parts to connect to an AMS, an SMPS, and a second CCN counter. The Nafion dryer was included in the system to dry particles analyzed by the AMS and SMPS. Additional instruments measuring aerosol size and composition, including a single particle soot photometer (SP2) and a particle analysis by laser mass spectrometry (PALMS) system, aerosol optical properties, and trace gases (e.g., VOCs by proton transfer reaction mass spectrometer [PTR-MS], CO by infrared absorption, CO_2 and CH_4 by cavity ring-down spectroscopy [CRDS], and ozone by ultra-violet photometry) were also deployed at T1, but shared other common inlets.

All dates and times reported in this paper are in Pacific Daylight Time (PDT), which was the local time during this study. PDT corresponds to the Coordinated Universal Time (UTC) minus 7 hours and the Pacific Standard Time (PST) plus 1 hour.

2.2.2. High Resolution Time-of-Flight Aerosol Mass Spectrometer Operation and Data Analysis

An HR-ToF-AMS was used to measure the size-resolved chemical composition of non-refractory submicron aerosols (NR-PM_1) in the size range 35-1000 nm in D_{va}. The D_{va} measured by the AMS corresponds to the mobility diameter (D_m) times the particle density (1.4 g cm^{-3} on average during this study), assuming sphericity [*P F DeCarlo et al.*, 2004].

In brief, particles are sampled into a high vacuum system (~10^{-5} Pa) through a 100 μm critical orifice and an aerodynamic lens installed at the inlet of the instrument. The narrow particle beam formed after the passage through the lens crosses a particle time-of-flight (PToF) region, where the measurement of the velocity allows the determination of the particle diameter D_{va}. Particles are then transmitted into a detection chamber, where non-refractory components (organics, sulfate, nitrate, ammonium, and chloride) are vaporized upon impact on a metallic surface heated up to ~ 600˚C, and ionized by electron impact (70 eV). The chemical composition of the particles is finally determined by a high resolution time-of-flight mass spectrometer operated alternatively in two modes - "V" and "W". The V-mode is more sensitive than the W-mode, while the mass resolution of the W-mode is much higher (~ 5000 vs. ~ 2500 for V-mode).

The data acquisition was performed using the ToF-AMS Data Acquisition software v3.0.29, available online at http://cires.colorado.edu/jimenez-group/wiki/index.php/ToF-AMS_DAQ. Between June 2 and June 17, 2010, the HR-ToF-AMS was operated in V- and W-mode alternatively every 2.5 minutes. From June 17 till the end of the field campaign (June 28), a temperature-stepping thermodenuder was operated upstream of the AMS, SMPS and CCN #2 (Fig. 2-1c). During this period, a valve switched automatically every 5 minutes to alternate the air flow sampled by the instruments between a bypass (ambient temperature) and the heated section of the thermodenuder. During the bypass period, the AMS was still operated in V- and W-mode (2.5 minutes each), while during the thermodenuder period, two runs in V-mode were acquired (also 2.5 minutes each). PToF data was systematically acquired in V-mode, but not in W-mode, due to low signal/noise ratio.

The ionization efficiency (IE) of the HR-ToF-AMS was calibrated at the beginning, in the middle and at the end of the field campaign, following a standard protocol previously published [*J. T. Jayne et al.*, 2000]. The IE/air beam ratio varied less than 3% between the beginning and the end of the campaign, indicating that the instrument remained remarkably stable during the four weeks of the study. For the relative ionization efficiencies (RIEs) of the main chemical species, we used values previously published for organics (1.4), nitrate (1.1) and chloride (1.3) [*M. R. Alfarra et al.*, 2004]. The RIE of ammonium was determined at 4.0 following the NH_4NO_3 analysis during the IE calibrations, and that of sulfate was determined at 1.4 following the analysis of pure $(NH_4)_2SO_4$. The particle sizing was calibrated at the same time as the IE calibration using polystyrene latex spheres of known sizes (Duke Scientific, Palo Alto, CA). A total 13 different sizes in the range of 22-700 nm were used. Finally, two particulate-free periods were recorded before and after the campaign using a HEPA filter (Pall Corporation, Port Washington, NY; model 12144), for subsequent adjustment of the fragmentation table and determination of the detection limits of individual species.

The data analysis was performed using SQUIRREL v1.51 and PIKA v1.10, the standard ToF-AMS analysis toolkits written in Igor Pro 6.2.2.2 (WaveMetrics Inc., Lake Oswego, OR) and available online at http://cires.colorado.edu/jimenez-group/ToFAMSResources/ToFSoftware/index.html. The V-mode and PToF data were processed with SQUIRREL to determine the mass concentrations and size distributions of NR-PM$_1$ species. The ammonium concentrations, however, were determined from PIKA analysis of the V-mode data since those from the SQUIRREL analysis are too noisy (see Fig. 2-3 for a comparison of the ammonium time series). The W-mode data was processed with PIKA to obtain high resolution mass spectra and the elemental composition of organic species.

In order to apportion correctly the ToF-MS signal to the different chemical species, the fragmentation tables of SQUIRREL and PIKA were modified according to the method presented by *J. D. Allan et al.* [2004]. A critical modification was the incorporation of a time-dependent correction of the gas-phase CO_2 at *m/z* 44. This point was very important, since the gas-phase CO_2 showed a strong diurnal pattern (the CO_2 concentration was on average 420 ppm during the night and 390 ppm during the day) and that the gas-phase CO_2 signal accounted for up to 75% of the total signal of the CO_2^+ fragment during periods of low organics mass loading. The detection limit of individual species was determined as three times the standard deviation of the corresponding signal in particle-free air [*Zhang et al.*, 2005b]. The 2.5-minute detection limits (DLs) are 0.075 (organics), 0.011 (sulfate), 0.018 (nitrate), 0.01 (ammonium), and 0.017 $\mu g\ m^{-3}$ (chloride). These values are between 2 and 10 times higher than the DLs (scaled to 2.5-min)

reported by *DeCarlo et al.* [2006b], which were 0.014 (organics), 0.0033 (sulfate), 0.002 (nitrate), 0.024 (ammonium), and 0.008 (chloride) ng/m^3.

Figure 2-3*. Time series of NH_4^+ using Squirrel and Pika, both in V-mode.*
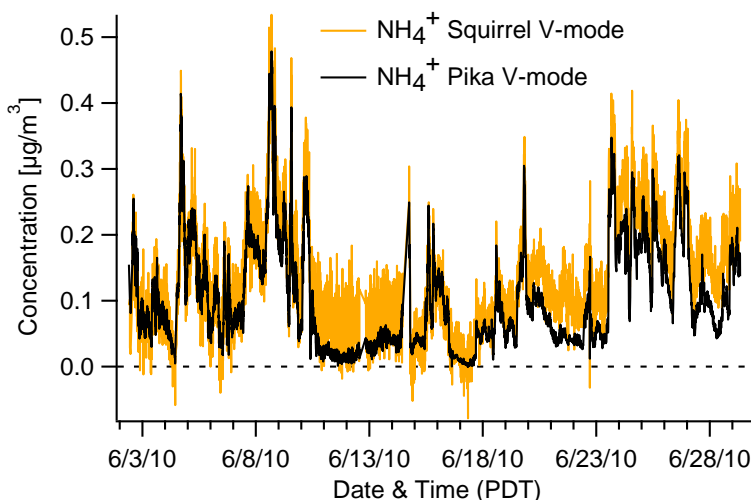
A collection efficiency (CE) was introduced to take into account of incomplete detection of aerosols, due to e.g., particle bounce at the vaporizer [*Matthew et al.*, 2008]. In many previous field campaigns, a constant CE of 0.5 for all the species has been found to be consistent with results obtained with collocated instruments [*A. C. Aiken et al.*, 2009a; e.g., *DeCarlo et al.*, 2008; *J Y Sun et al.*, 2010; *Sun et al.*, 2011]. However, CE may increase depending on the chemical composition (e.g., mass fraction of NH_4NO_3), acidity, water content and the phase of the particle [*Lawrence I. Kleinman et al.*, 2007; *Middlebrook et al.*, 2012]. We use a constant CE of 0.5 for all the species in this study, because 1) particles were dominated by organics during the entire campaign, 2) they appeared to be fully neutralized (Fig. 2-5), and 3) the air flow was dried (relative humidity – RH < 30%) prior to the AMS analysis. This choice has been validated by the inter-comparison between AMS+BC mass and SMPS volume (Fig. 2-4).

Figure 2-4. *Scatterplot of AMS total + BC mass vs. SMPS volume in the size range 25-714 nm (D_m), colored by time. The data fitting was performed using the orthogonal distance regression (ODR).*
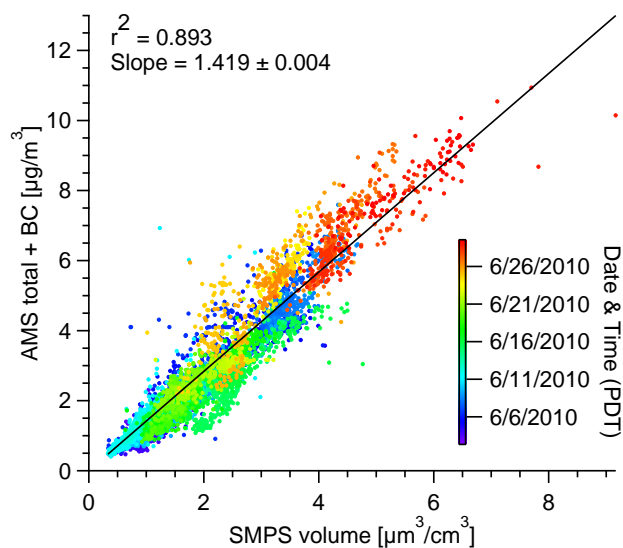
Figure 2-5. *Scatterplot of NH_4^+ measured vs. NH_4^+ predicted, colored by time. The data fitting was performed using the orthogonal distance regression (ODR).*

$$r^2 = 0.951$$
$$Slope = 0.971 \pm 0.001$$

NH4$^+$ measured [μg/m^3]

NH4$^+$ predicted [μg/m^3]

$$(= [2 \cdot 18/96 \cdot SO_4^{2-}] + [18/62 \cdot NO_3^-] + [18/35.5 \cdot Cl^-])$$

Date & Time (PDT)

6/26/2010
6/21/2010
6/16/2010
6/11/2010
6/6/2010
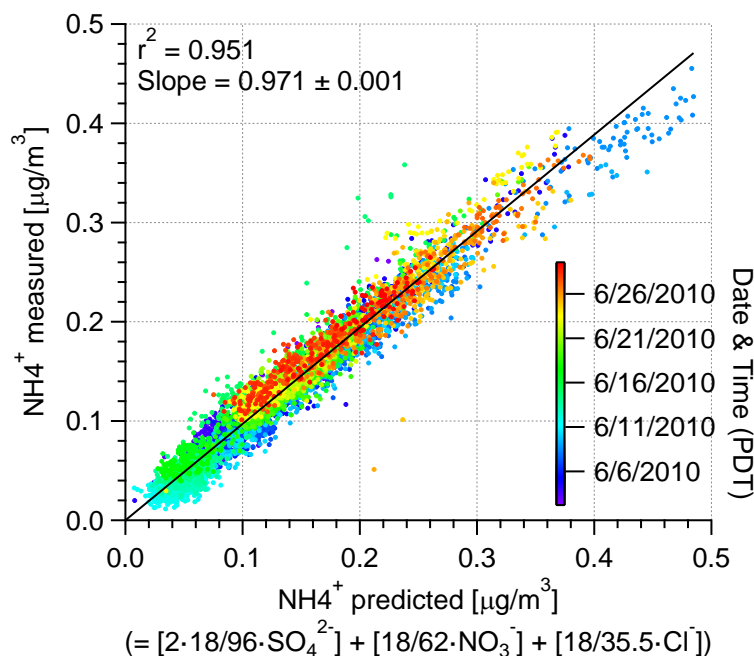
PMF analysis was performed on the high resolution mass spectra of organic species to determine the mass spectra of distinct organic factors and their time-dependent concentrations. This technique was described by *Paatero and Tapper* [1994a], while its application to AMS datasets was discussed previously [*Lanz et al.*, 2007b; *I M Ulbrich et al.*, 2009; *Ulbrich et al.*, 2012; *Q Zhang et al.*, 2011]. Data and error matrices were first generated in PIKA. We took into account ions up to *m/z* 100, given that bigger ions had low signal/noise ratio and more biases because of insufficient mass resolution. Isotopes were systematically constrained in PIKA, but were removed from the data and error matrices, since their presence would have given excess weight to the parent ions in the PMF analysis. The error matrix was then further adjusted to take into account of the counting error of ions by the detector [*I M Ulbrich et al.*, 2009]. Ions with a signal-to-noise ratio (S/N) < 0.2 were removed from the data and error matrices, whereas ions whose average S/N between 0.2 and 2 were down-weighed by a factor of 3. Four organic ions scaled to the CO_2^+ signal (O^+, HO^+, H_2O^+, and CO^+) were removed from the data and error matrices prior to the PMF analysis. They were reintroduced in the mass spectra after the PMF analysis. PMF analysis was performed using the PMF Evaluation Tool Software v2.03A described in *I M Ulbrich et al.* [2009], available online at http://cires.colorado.edu/jimenez-group/wiki/index.php/PMF-AMS_Analysis_Guide. The PMF solution has been tested from 1 to 10 factors and for FPEAK values between -1 and +1 (step: 0.1). The robustness of the solution has been examined by running the PMF algorithm from different random starting points (SEED values from 0 to 10, delta=1). Detailed procedures listed in Table 1 of *Q Zhang et al.* [2011] were followed to evaluate various PMF solutions. A summary of the evaluation of the PMF results is given in Fig. 2-6. The 3-factor solution with FPEAK=0 was chosen as the final solution and the results were validated based on interpretation of the characteristic mass spectral signatures, the temporal and diurnal variation patterns of the OA factors in reference to meteorological conditions, and the correlations with tracer compounds.

Figure 2-6. *Summary of the evaluation of the PMF results: (a) Q/Q_exp as a function of number of factors (P); (b) Q/Q_exp as a function of fPeak values for the 3-factor solution; (c) fractions of OA factors as a function of fPeak values; (d) correlation between the 3 OA components in terms of mass spectrum and time series (1: biogenic SOA, 2: urban transport, 3: HOA); (e) Q/Q_exp values for each ion; (f) box plot of the scaled residuals for each ion; (g) time series of the measured organic mass concentration and the reconstructed organic mass (= biogenic SOA + urban transport + HOA); (h) time series of the residual (= measured - reconstructed) of the fit; (i) time series of Q/Q_exp.*
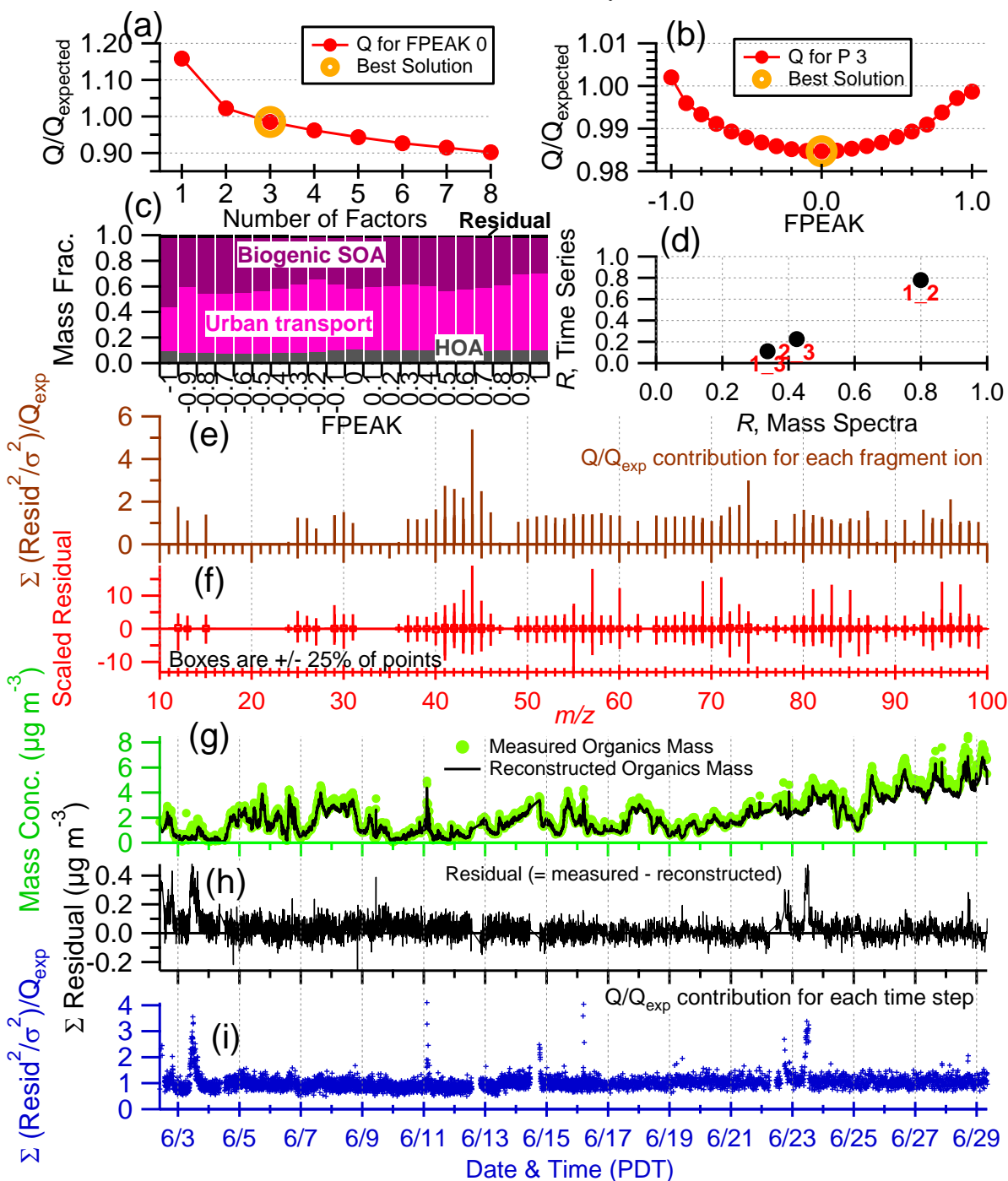
2.2.3. Collocated Measurements

An SMPS was used to measure the particle number size distribution in the range from 8 to 858 nm in D_m. The SMPS used during this study followed a recommended standard design of the European supersites [*Wiedensohler et al.*, 2012] for atmospheric measurements and was manufactured by the WMO-GAW World Calibration Center for Aerosol Physics (WCCAP) hosted at the Leibnitz Institute for Tropospheric Research (IFT) at Leipzig, Germany. The instrument consists of a neutralizer (Po^{210}), a Hauke-type differential mobility analyzer [DMA; design described by *Winklmayr et al.*, 1991] and a condensation particle counter (CPC; TSI Inc., Shoreview, MN; model 3772). The SMPS alternated between two modes – the "upscan" mode (from 8 to 858 nm) and the "downscan" mode (from 858 to 8 nm) – every 2.5 minutes. The data was recorded every 5 minutes, corresponding to the average of the "upscan" and "downscan" modes alternatively. The aerosol sampling flow was set at 1 l/min, and was obtained by using a vacuum pump (GAST Manufacturing Inc., Benton Harbor, MI; model DOA-P704-AA) connected to the outlet of the CPC. The sheath flow was set at 5 l/min. The data acquisition software applied two corrections to the particle size distribution during the data inversion, in order to take into account the DMA transfer function [*Birmili et al.*, 1997] and the bipolar charge distribution [*Wiedensohler*, 1988]. The corrections for the CPC efficiency and the internal diffusion losses were applied after the data inversion. The diffusion losses were calculated following the methods of the "equivalent length" [*Wiedensohler et al.*, 2012].

A PTR-MS [*J. de Gouw and Warneke*, 2007] was used for online monitoring of VOCs. Briefly, H_3O^+ ions are produced in a hollow-cathode discharge in water vapor, and are injected into the drift tube reaction region where they interact with the ambient sample. These reagent ions are pulled through the ambient sample at reduced pressure (~ 2 mbar) under the influence of an applied electric field where they will transfer a proton to any component having a proton affinity greater than that of water. A fraction of the reagent ions and product ions formed are sampled through a small aperture at the end of the drift tube and mass analyzed using a quadrupole mass spectrometer operated in the ion counting mode. For the present study, the ratio between the electric field strength and the buffer gas density (E/N ratio) was 133-136 Td between June 2 and 4, 2010, and 139 Td from June 4 until the end of the campaign.

The black carbon (BC) concentration was measured with an SP2 [Droplet Measurement Technologies, Boulder, CO; *Subramanian et al.*, 2010]. Briefly, particles containing BC absorb energy from an Nd:YAG laser and are heated to the point of incandescence. The incandescence is measured and correlated to the particle's BC mass using BC proxies; the results presented here are based on an Acheson Aquadag®-based calibration. In addition, the concentrations of CO (Teledyne Technologies Inc., Thousand Oaks, CA; model M300EU), CO_2 and CH_4 (Picarro Inc., Santa Clara, CA; model 1301G-M), and O_3 (Thermo Scientific, Waltham, MA; model 49i) were measured.

2.2.4. WRF-Chem and Air Mass Classification

The WRF-Chem model was used to determine periods of urban plumes from T0 to T1. Details on the operation of the model are given by *Fast et al.* [2012]. Briefly, the model was run to forecast the spatial and temporal variations of CO emitted by 20 anthropogenic sources. The spatial distribution of these sources includes regions from the San Francisco Bay Area up to the Sierra Nevada foothills, and from the Sacramento Valley to Southern California. Urban plumes were determined as periods during which CO emitted in the Sacramento region contributed to more than 30% of the total anthropogenic CO at T1. In total, 23 periods of urban plumes were

identified during this study, brought by southwesterly wind favorable to the transport of pollutants from Sacramento to Cool. Eight of these periods were characterized by an air mass transported directly from Sacramento to Cool following a straight path, while during twelve other periods the air mass was transported either to the north or to the south of T1 before being redirected to T1. The remaining three periods consisted of recirculation of aged plumes over the foothills. A second modeling system, the North American Mesoscale (NAM), identified three periods (June 10-13, June 16-17, June 20-21) during which the meteorology was characterized by the passage of mid-tropospheric troughs over California, resulting in a shift of the wind direction from the southwest to the northwest. Therefore, during these eight days, urban plumes were transported to the southeast of Sacramento while the T1 site was influenced by clean air masses coming from the northwest, reducing considerably the concentration of pollutants at T1. Finally, another air mass was brought to the T1 site during the night, when the decrease of the temperature reversed the wind direction and favored downslope flows from the western Sierra Nevada back to the Sacramento Valley. These different periods determined by model predictions and given by *Fast et al.* [2012] were slightly refined in the present study using wind data recorded at T1 and the results of the PMF analysis, which identified among others an oxygenated organic aerosol (OOA) component resulting from urban transport. The periods are marked in Fig. 2-5.

2.3. Results and Discussions

2.3.1. Overview of Submicron Aerosol characteristics

2.3.1.1.Concentrations and chemical composition of submicron aerosols

The particle mass concentration was low at T1, varied between 0.4 and 13.8 µg m^{-3} and the average over the entire study was 3.0 µg m^{-3} (Table 2-1). The chemical composition was dominated by organics, which on average accounted for 80% of the total particle mass. The other components included sulfate (9.9%), ammonium (4.5%), nitrate (3.6%), and BC (1.6%). The chloride concentrations measured by the HR-ToF-AMS were mostly below detection limit during the present study. Similar PM$_1$ composition and loading were determined during the BEARPEX 2007 field campaign at the Blodgett Forest, which is located 35 km to the northeast (i.e., downwind) of the site of this study [*Farmer et al.*, 2011; *Worton et al.*, 2011]. While forest fires may occur in the region during summer [*Worton et al.*, 2011] we found no indication of wildfires based on the time series of Org 60 (mainly the $C_2H_4O_2^+$ ion) and Org 73 ($C_3H_5O_2^+$), two key tracers of biomass burning in AMS mass spectra [*A. C. Aiken et al.*, 2010; *M. Rami Alfarra et al.*, 2007]. In addition, the potassium signal recorded by the HR-ToF-AMS and the gas phase acetonitrile measured by the PTR/MS (Fig. 2-2f) remained low during the entire study, further confirming the lack of biomass burning influence at T1.

The AMS and SMPS agreed very well throughout this study (Fig. 2-5). The slope of the linear regression (1.42) corresponds to the average particle density throughout the study, and is consistent with results obtained with a single particle laser ablation time-of-flight mass spectrometer deployed at the T0 site [*Vaden et al.*, 2011]. We estimated the density of organics at 1.33 g cm^{-3} by subtracting the contribution of the other chemical species, using the known densities for ammonium sulfate (1.78 g cm^{-3}), ammonium nitrate (1.72 g cm^{-3}) and ammonium chloride (1.53 g cm^{-3}), and a density of 1.8 g cm^{-3} for BC based on values recommended by *Bond and Bergstrom* [2006]. We also predicted the density of organics (ρ_{org}) using the average O/C

Figure 2-7. *Time series of (a) AMS total mass + BC and SMPS volume concentrations, (b) concentrations of organics (left y-axis), sulfate, nitrate, ammonium, chloride, and BC (right y-axis), (c) percentage contribution of the species to the total PM$_1$ mass, and (d) particle number size distribution by the SMPS. BC data is not available before 6/3/2010, so PM$_1$ concentrations before this date correspond to the sum of NR-PM$_1$ (AMS species). Shaded regions indicate 23 periods of urban plumes transported from T0 to T1 (orange) and 3 periods subjected to influences from northwesterly wind (green). The remaining periods correspond mainly to downslope flows from the Sierra Nevada to the foothills.*
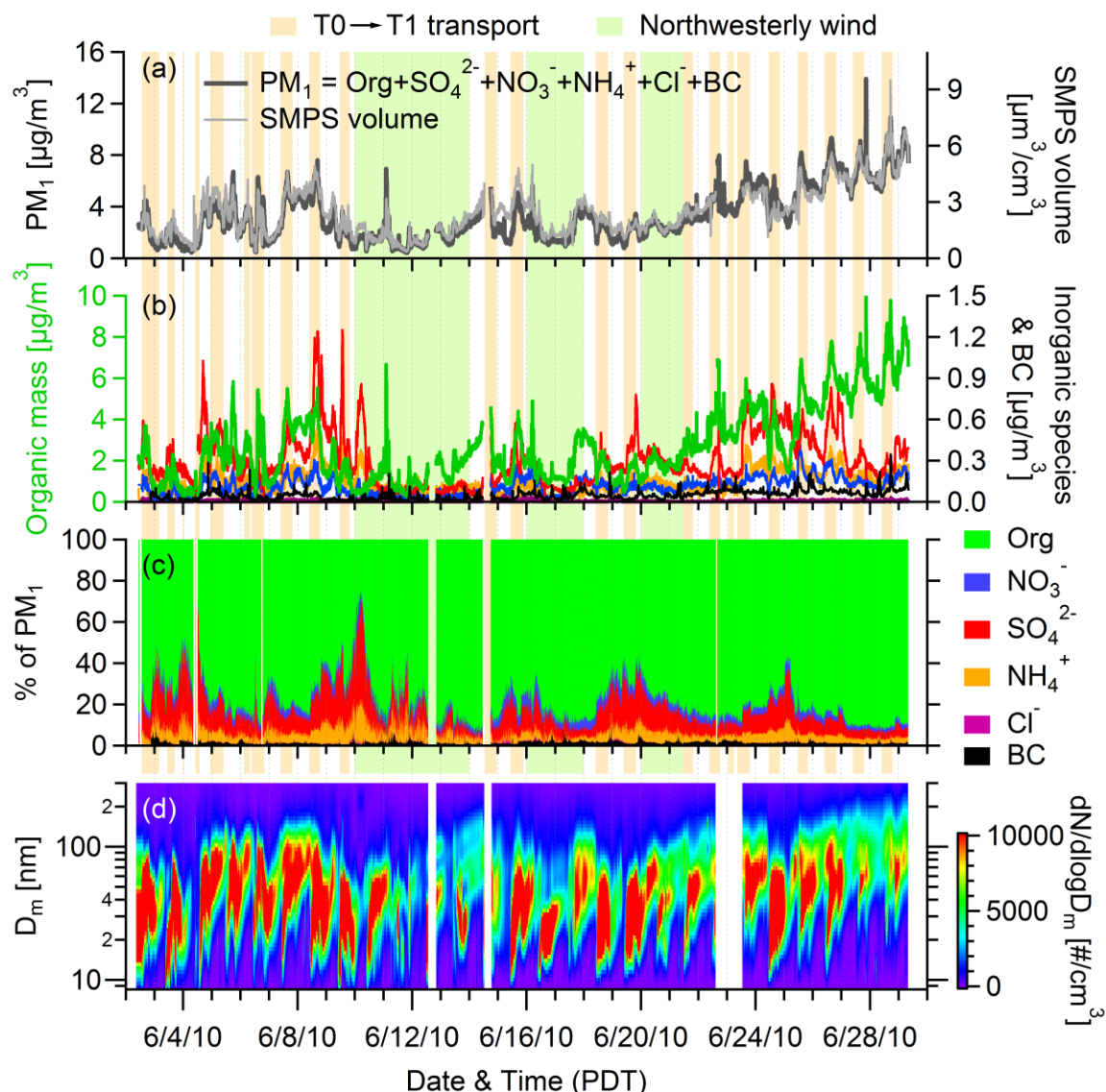
and H/C ratios based on the formula reported in *Kuwata et al.* [2012]:

$$\rho_{org} = [12 + 1 \cdot (H/C) + 16 \cdot (O/C)] / [7 + 5 \cdot (H/C) + 4.15 \cdot (O/C)] \tag{1}$$

in which ρ_{org} is in g cm^{-3}, H/C and O/C are the average values (1.38 and 0.44, respectively) of this study. The ρ_{org} predicted with this method is 1.30 g cm^{-3}, very close to the value of 1.33 obtained based on comparison of particulate mass to volume.

Submicrometer particles appeared to be bulk neutralized at T1, as shown in the scatter plot of the measured NH$_4^+$ concentration vs. the predicted NH$_4^+$ (NH$_4^+_{predicted}$) concentration assuming anions being fully neutralized by NH$_4^+$ (Fig. 2-5):

$$NH_4^+{}_{predicted} = (2 \cdot 18/96 \cdot m_{SO4}) + (18/62 \cdot m_{NO3}) + (18/35.5 \cdot m_{Cl}) \qquad (2)$$

where m_{SO4}, m_{NO3}, and m_{Cl} denote the mass concentrations (in µg m^{-3}) of the species and the denominators correspond to their molecular weights. This equation and its application to inferring particle acidity were discussed in detail by *Zhang et al.* [2007a]. The slope is very close to 1 (Fig. 2-5), suggesting that sulfate was present in the form of ammonium sulfate $(NH_4)_2SO_4$ at T1. Neutralized particles were observed at the Blodgett Forest as well [*Farmer et al.*, 2011]. These results are consistent with the presence of large agricultural regions and thus abundant ammonia emissions in the Sacramento Valley [*Clausnitzer and Singer*, 1996].

Figure 2-8. Scatterplots of (a) organics vs. sulfate, (b) organics vs. nitrate, (c) sum of the main MSA ions vs. sulfate, and (d) fraction of organics vs. PM$_1$ mass. All the scatterplots are colored by air mass types. The data fitting was performed using the orthogonal distance regression (ODR).
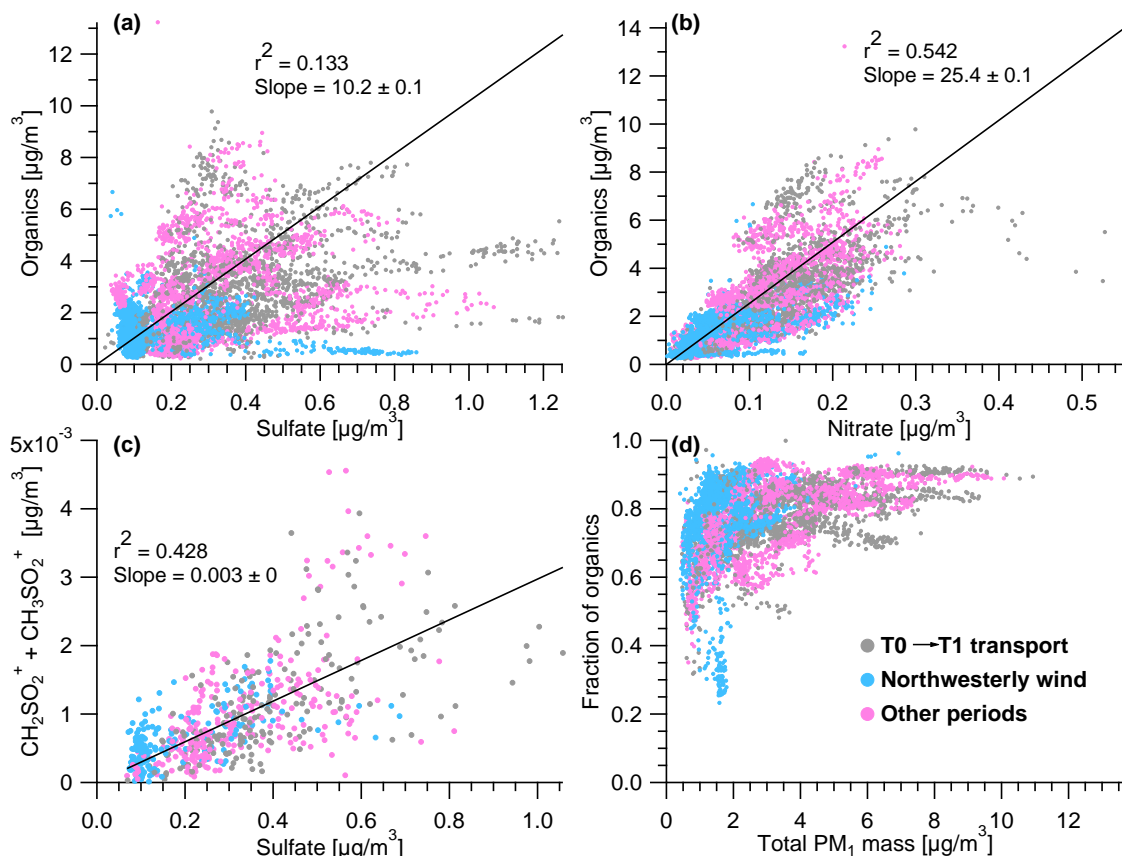
Nitrate accounted for a minor fraction of the particle mass (3.6%; average = 0.11 µg m^{-3}) at T1. 94% of the nitrate signal was contributed by two ions, NO^+ (*m/z* 30) and NO_2^+ (*m/z* 46). In this study, we noticed a much higher slope of NO^+ vs. NO_2^+ in ambient particles than in pure NH_4NO_3 used for the IE calibrations (6.8 vs. 1.7), indicating that an important part of the nitrate signal was not due to ammonium nitrate but possibly corresponded to organonitrates or metal nitrates [*Farmer et al.*, 2010]. The NO^+/NO_2^+ ratio can vary dramatically, depending on the nitrate compound. For example, *Farmer et al.* [2010] report a NO^+/NO_2^+ ratio of 1.5 for The mass concentration of organics was NH_4NO_3 and an average of 3.5 for various organonitrate standards (min: 1.8, max: 4.5), while *Rollins et al.* [2010] measured a NO^+/NO_2^+ ratio in the range 0.99-5.3 for laboratory-generated organonitrates and mentioned that this ratio can increase up to 29 for sodium nitrate. Moreover, Shilling et al. (in preparation) found NO^+/NO_2^+ ratios up

to 8.8 for organic nitrates generated from trimethylbenzene. In this study, the presence of organonitrates was supported by the fact that 16 ions from the $C_xH_yO_zN_p^+$ family were observed in high resolution mass spectra, since organonitrates are reported as a source for these fragments [*Farmer et al.*, 2010; *Rollins et al.*, 2010]. Moreover, organics and nitrate were correlated during this study ($r^2 = 0.54$; Fig. 8), which could arise if a significant fraction of the nitrate signal corresponded to organonitrates. However, metal nitrates (such as sodium nitrate or potassium nitrate) could have been present as well, given that the NO^+/NO_2^+ ratios observed for ambient aerosols were higher than most of the organonitrates previously measured [*Farmer et al.*, 2010; *Rollins et al.*, 2010; Shilling et al., in preparation].

Organosulfates likely existed as well, given that we detected 11 ions from the $C_xH_yS_nO_z^+$ ($x{\geq}1$, $y{\geq}1$, $n{\geq}1$, $z{\geq}0$) family. Three of them ($CH_2SO_2^+$, $CH_3SO_2^+$ and $CH_4SO_3^+$) were unambiguously quantified as they are well separated from adjacent ions in high resolution mass spectra [*Ge et al.*, 2012]. These three ions correlated well with each other ($r^2 > 0.5$) and their signal intensity ratios in T1 aerosols ($CH_2SO_2^+/CH_3SO_2^+ = 0.32$; $CH_4SO_3^+/CH_3SO_2^+ = 0.32$) were close to those observed in the HR-ToF-AMS mass spectrum of pure methanesulfonic acid [MSA; *Ge et al.*, 2012], indicating the presence of mesylate ($CH_3SO_3^-$ - a salt of MSA) in PM_1. However, the total concentration of ions from the $C_xH_yS_nO_z^+$ family was only 2 ng m^{-3}, suggesting very limited contributions of organosulfates to the SOA and sulfate concentrations at T1. The close molar equivalent balance between the anions (= sulfate + nitrate + chloride) and ammonium further supports that the observed sulfate signal corresponded mainly to $(NH_4)_2SO_4$.

2.3.1.2. Size distribution of submicron aerosols

The average size distribution of total PM_1 mass showed a broad mode extending from 60 to 600 nm in D_{va} (Fig. 2-9a). While PM_1 were dominated by organics in the entire size range, larger particles (> 300 nm) had a relatively larger contribution (~25%) of ammonium sulfate compared to smaller particles (< 20%) since these two species had very different size distributions (Fig. 2-96a). Sulfate showed a bimodal distribution with a prominent droplet accumulation mode at ~ 400 nm in D_{va} and a smaller condensation mode at ~ 150 nm (Fig. 2-9b). In contrast, both organics and nitrate showed a broad distribution that peaks at 150-200 nm (D_{va}). The observation of nitrate in the same size mode as organics was probably because of the contribution of organonitrates to nitrate signals.

The different size distributions of organics and sulfate and the poor correlation between their concentrations ($r^2 = 0.13$; Fig. 2-8a) suggest major differences in their sources and processes. The prominent droplet mode of sulfate indicates an important influence of aqueous phase reactions on sulfate production. Indeed, the droplet mode particles are too large to be reached by gas-to-particle partitioning of low volatility compounds under typical atmospheric conditions [*John et al.*, 1990; *Meng and Seinfeld*, 1994], whereas the growth of particles from the condensation mode (< 200 nm in D_{va}) to the droplet mode (400-1000 nm in D_{va}) by coagulation would be too slow with the low aerosol concentrations of the present field campaign. Previous studies have shown that chemical reactions in aqueous phases (i.e., fog and cloud droplets and aerosol phase water) usually add much more mass in the droplet mode than in smaller particles and that aqueous-phase sulfate formation is an important process in the atmosphere [*Ervens et al.*, 2011, and references therein]. In addition, as shown in Fig. 2-8c, sulfate correlated well with $CH_2SO_2^+$ and $CH_3SO_2^+$, two HR-ToF-AMS ions likely representing MSA or its salts [*Ge et al.*, 2012]. MSA is mainly produced by the oxidation of dimethyl sulfide

Figure 2-9. (a) *Average size distributions of the AMS total mass and percentage contribution of aerosol species to total mass, (b) average size distributions of aerosol species, and (c) average size distributions of organic aerosol signals at m/z 43 and m/z 44.*
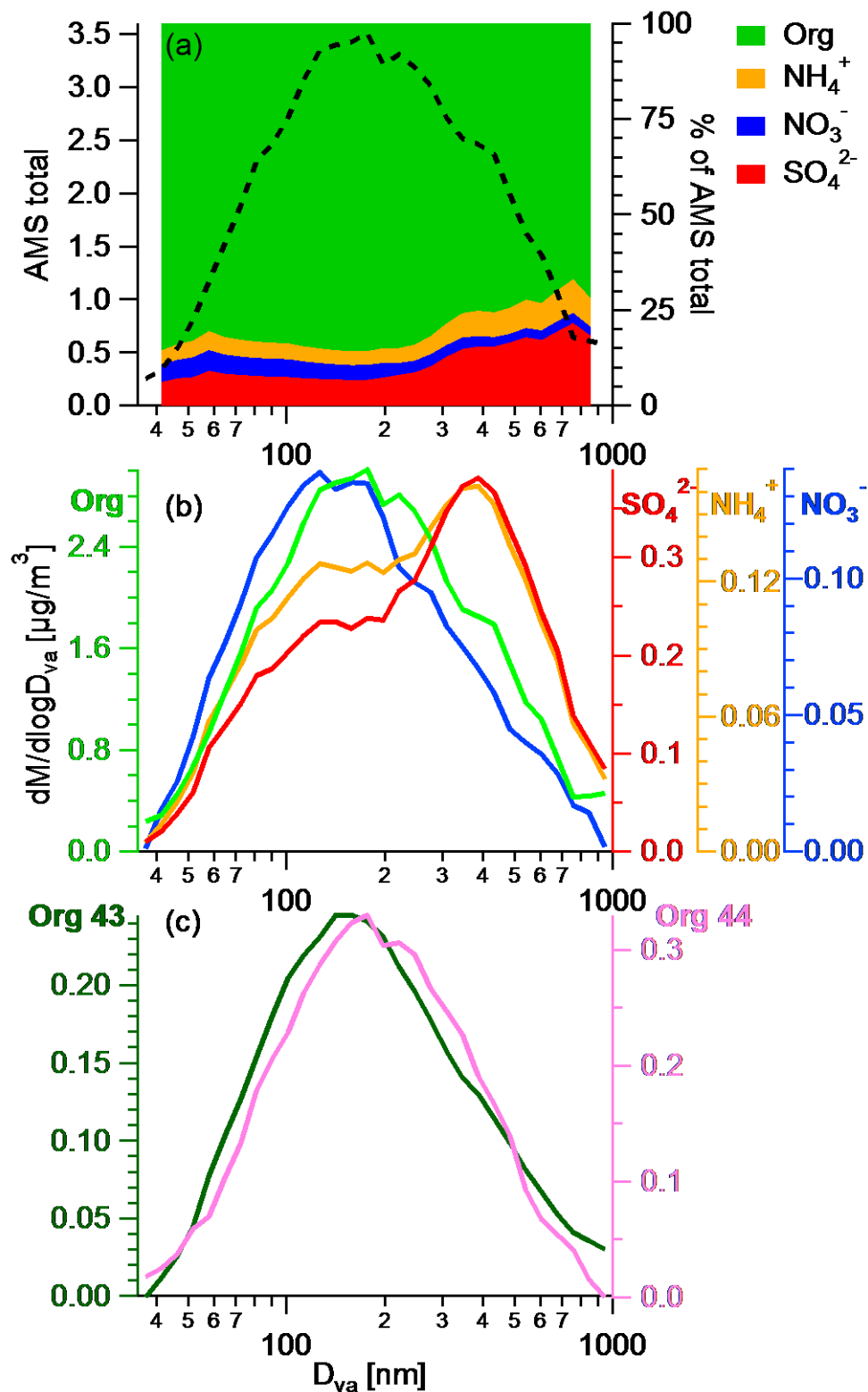
emitted from oceanic sources and its formation is enhanced by aqueous phase processing [*Barnes et al.*, 2006]. For these reasons, we deduce that a large fraction of the droplet mode sulfate particles observed during this study likely originated from the San Francisco Bay Area, where the five oil refineries along San Pablo Bay and the Carquinez Straits (Fig. 2-1a) are the largest SO2 sources in northern California and where regular morning fogs and low clouds may have promoted aqueous phase reactions. This hypothesis is supported by the meteorological data recorded at Oakland North by the California Air Resources Board (http://www.arb.ca.gov/aqmis2/metselect.php). Oakland is located on the east of the San Francisco Bay, very close to the oil refineries (Fig. 2-1a). The RH at Oakland was frequently close to 100% during the night and in the morning in June 2010 (Fig. 2-10), confirming the frequent occurrence of fogs and low clouds, thus aqueous-phase processing of aerosol particles, in the region.

Figure 2-10. *Time series of relative humidity and precipitation recorded at Oakland North (data from the California Air Resources Board) and the T1 site (**a**). Diurnal pattern of relative humidity at Oakland and the T1 site (**b**).*
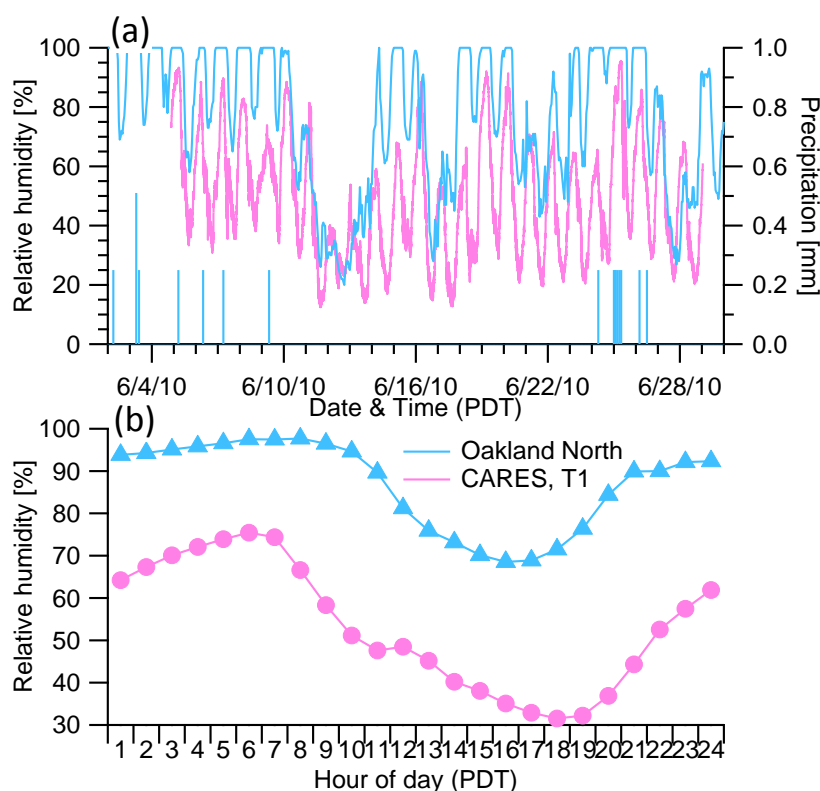
In contrast, the organic size distribution was dominated by a condensation mode (Fig. 2-9b). In addition, the average size distributions of *m/z's* 43 and 44, which are the two most abundant fragment peaks in the mass spectra of OA at T1, were very similar (Fig. 2-9c). Both *m/z*'s were mainly contributed by oxygenated organic ions. The $C_2H_3O^+$ ion, which is commonly associated with aldehydes or ketones [*Ng et al.*, 2011a], represented 86% of the signal at *m/z* 43 (Org43). The CO_2^+ ion, which is associated with carboxylic acids [*Mohammed Rami Alfarra*, 2004; *Takegawa et al.*, 2007], accounted for 96% of the organic signal at *m/z* 44 (Org44). These results indicate that condensation of low volatility oxygenated species formed from gas-phase reactions was the major formation mechanism for particulate organics at T1.

2.3.1.3. Temporal and diurnal variations and implications of aerosol sources and processes at T1

The concentration, chemical composition and size distribution of PM_1 varied dynamically throughout this study (Fig. 2-5), revealing the influences of various sources and processes. Organics were the dominant species during the entire study, except during periods of very low PM_1 loading (< 1 μg m^{-3}) when the mass fraction of sulfate increased to up to 50% of total PM_1. The fact that sulfate dominated aerosol composition in clean air masses, which was mainly associated with northwesterly flow, suggests a regional source of this species. This is consistent with the larger size distribution of sulfate compared to that of organics (Fig. 2-11, right panel).

Figure 2-11. *Diurnal patterns (left panel) and diurnal size distributions (right panel) of **(a)** organics, **(b)** sulfate, **(c)** Org 43, **(d)** Org 44, **(e)** AMS total mass, **(f)** particle number, and **(g)** volume concentrations. Box plots: whiskers correspond to the 10ᵗʰ and 90ᵗʰ percentile, boxes to the 25ᵗʰ and 75ᵗʰ percentile, the horizontal marks in the boxes to the median, and the colored crosses to the mean.*
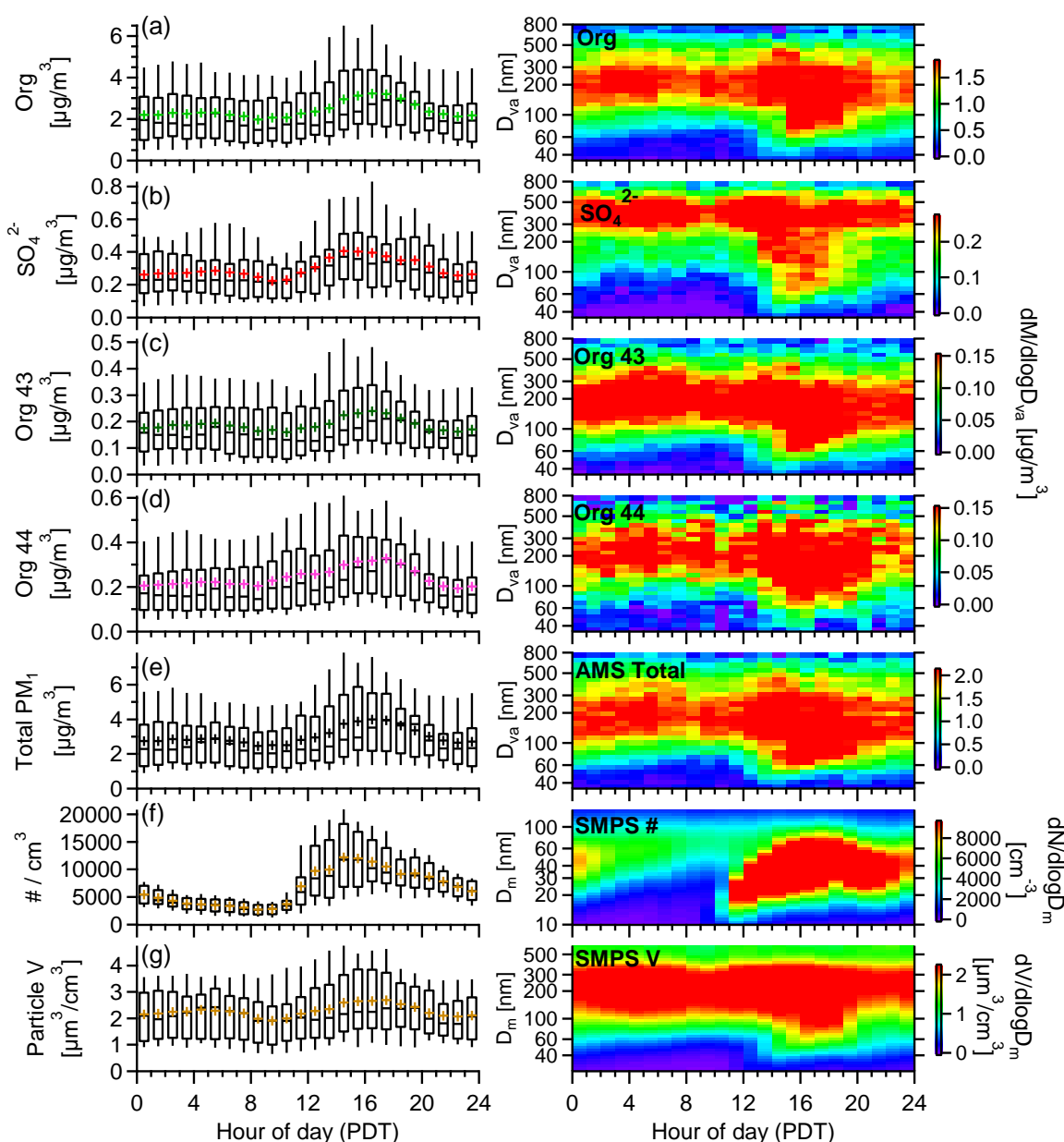
On the other hand, periods with high PM$_1$ loading were associated with high mass fraction of oxidized organics, indicating that episodes of aerosol pollution over the Sierra Nevada foothills were mainly driven by SOA formation. A gradual increase of particle concentration from 1.5 to 11 µg m^{-3} was observed between June 20 and June 28, 2010. The increase was mainly contributed by organics and was accompanied with sharp increases in isoprene concentrations, especially during the last 4 days of the campaign. Since both maximum O$_3$ mixing ratios (in the range 70-80 ppb) and highest daily average temperature also occurred during those days, the increase of aerosol concentration was likely due to more intense chemical processing of aerosol and gas phase pollutants in the region.

The concentrations and size distributions of the chemical species in PM$_1$ all showed strong diurnal variations (Fig. 2-11), which were mainly driven by the very consistent wind patterns as well as the formation of secondary aerosols. Specifically, organics, sulfate, and particle number concentrations all began to increase at ~ 10:00 and peaked between 15:00-17:00. This time period corresponds to the downwind transport from Sacramento to Cool (i.e., T0 to T1 transport) coupled to photochemical oxidation. Indeed, using a Lagrangian particle dispersion model system, *Fast et al.* [2012] determined that the transport times between Sacramento and Cool range between 2 - 8 hours on days with southwesterly winds and that the peak surface concentrations of air pollutants at Cool on average occur around 17:00 PDT in June. Furthermore, the diurnal profile of ozone mixing ratio at T1 demonstrated a peak between 16:00 - 17:00 (Fig. 2-12) because of southwesterly winds that transported ozone produced in Sacramento over the Sierra coupled with additional daytime photochemical production downwind of Sacramento. Similarly, the daytime increase of organics lasted till ~ 17:00 as well, contributed by the transport and subsequent oxidation of VOC precursors emitted from both anthropogenic (from the Sacramento area) and biogenic (from the vegetation between Sacramento and the foothills) sources. The increase of sulfate (mainly in particles smaller than 200 nm in D_{va}) in the afternoon can be explained by the transport of SO$_2$ from upwind sources, e.g., the refineries located in the Bay Area, coupled with photochemical oxidation and condensation of low volatility products.

Figure 2-12. *Diurnal patterns of O$_3$, organics and sulfate. Box plots for O$_3$: whiskers correspond to the 10th and 90th percentile, boxes to the 25th and 75th percentile, the horizontal marks in the boxes to the median, and the black crosses to the mean. Data for organics and sulfate correspond to the mean.*
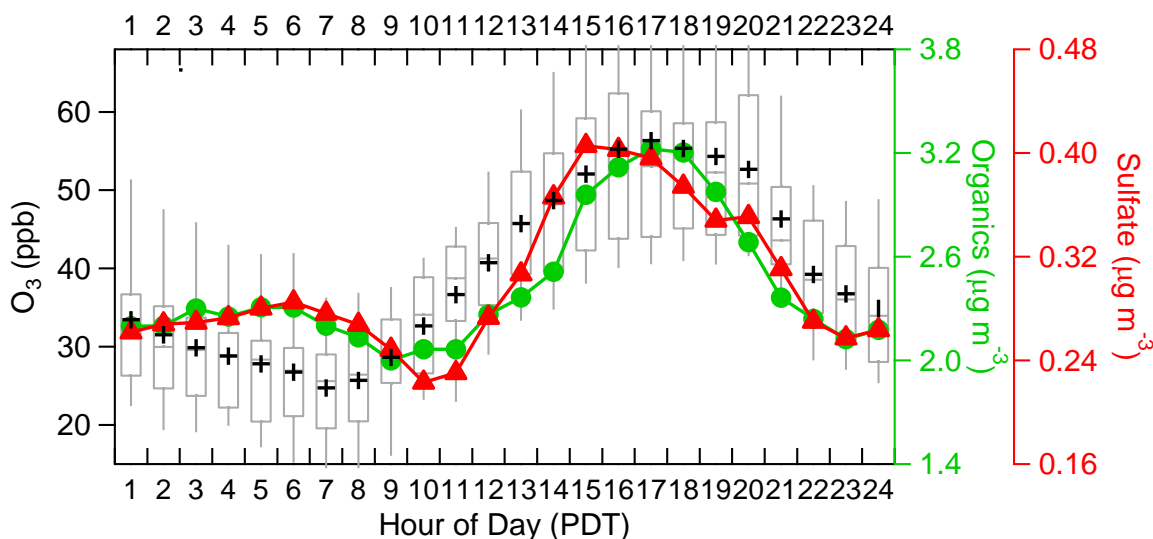
A slight increase of organics and sulfate, primarily in particles smaller than 300 nm (D_{va}), occurred at night, starting around 22:00 (Fig. 2-13). This time corresponds to nocturnal downslope flows, when a part of the polluted air transported to the Sierra Nevada during the day came back to the foothills. Model simulations coupled with observations made during CARES indeed showed that the nighttime recirculation could transport aged trace gases and aerosols from the western slopes of the Sierra Nevada back over Sacramento [*Fast et al.*, 2012]. In addition, a decrease of the boundary layer height, thus less dilution, together with continued reactions of biogenic VOCs with the nighttime residual ozone (20 - 35 ppb on average) and other oxidants (e.g., nitrate radical) might have played a role in the increase of SOA species as well.

Figure 2-13. *Diurnal patterns of organics (**a**) and sulfate (**b**) in the size range 35-200 nm, 200-300 nm and 300-1000 nm (in D_{va}). Data correspond to the mean.*
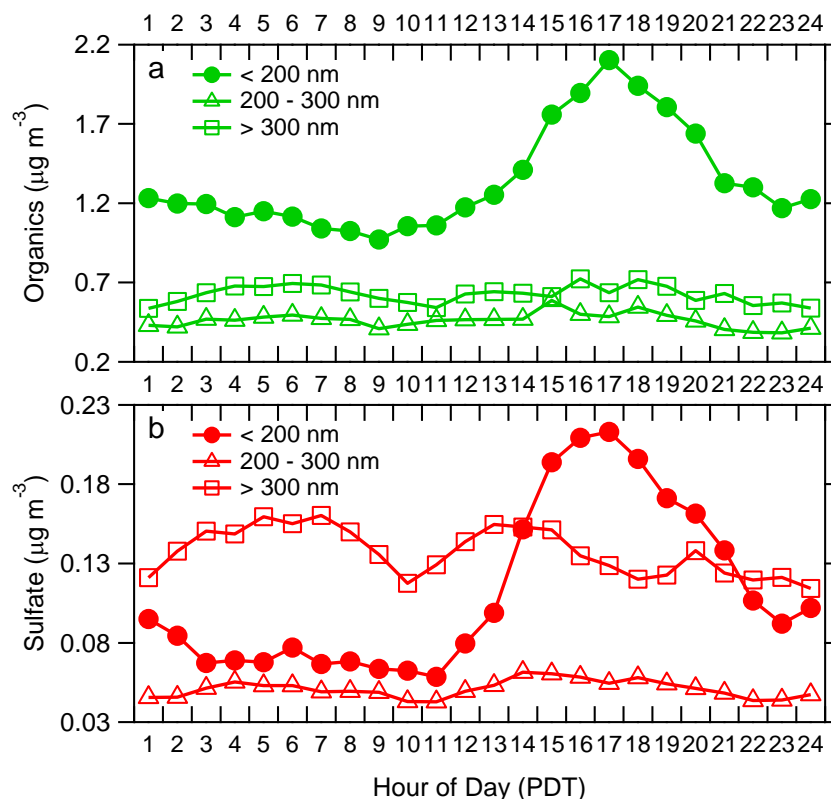
New particle formation (NPF) and growth events occurred almost every day during this study and were frequently observed in the Sierra Nevada [*Creamean et al.*, 2011; *Lunden et al.*, 2006]. In this study, the particle number concentration with sizes of 8-858 nm showed a sharp increase between ~ 9:00 (2800 particles/cm^3) and 15:00 (12100 particles/cm^3), accompanied by the simultaneous increases of organics and sulfate. However, the smallest size measured by our SMPS was 8 nm in mobility diameter (D_m) whereas new particles formed by nucleation have generally 1 nm diameter [*Holmes*, 2007]. Given that the growth rate of new particles was on average ~5 nm/hour during this study, a lag time of 1-2 hours is necessary between the formation and the growth of the new particles to a detectable size, and the onset of nucleation should have occurred earlier. Moreover, an additional lag of several hours is necessary for new particles to grow to sizes detectable by the AMS (minimum 35 nm in D_{va}, corresponding to ~ 25 nm in D_m assuming spherical particles with a density of 1.4 g cm^{-3}). An increase of the organics and sulfate

concentrations in ultrafine particles was observed between 11:00 and 16:00 (Fig. 2-11, right panel). The average increase of the mass concentration of organics (~ 1.1 µg m^{-3}) was ~ 6.5 times higher than that of sulfate (~ 0.17 µg m^{-3}) between 10:00 - 17:00, indicating that organics played a more important role in new particle growth than sulfate did. We notice that the mass concentrations of both Org 43 (mainly $C_2H_3O^+$) and Org 44 (mainly CO_2^+) in the ultrafine mode increased during this period (Fig. 2-11c & 2-11d). Similarly, increases of Org 43 and 44 in the ultrafine mode were observed during the growth of new particles at Pittsburgh [*Zhang et al.*, 2005a; *Zhang et al.*, 2004] and in a Finnish Forest [*J. D. Allan et al.*, 2006]. Since the total increase of these two fragments alone (0.2 µg m^{-3}) is as much as the increase of sulfate during the same period, oxidized organics appear to have played important roles in growing new particles in the Sierra Nevada foothills. A complete description and the determination of the conditions allowing the formation of new particles and their subsequent growth and the evolution of particle chemistry are presented in Section 3.

2.3.1.4. Chemical properties of organics

Organics, which dominated PM$_1$ composition at T1, were overall oxidized with average O/C = 0.44 (range 0.06-0.75) and H/C = 1.38 (range 1.01-2.09). The nominal formula of organics at T1 during CARES was $C_1H_{1.38}N_{0.004}O_{0.44}$, which corresponds to an average organic mass-to-carbon (OM/OC) ratio of 1.7 (range 1.19-2.15). As shown in Fig. 2-14a, the average organic mass spectrum was dominated by four oxygenated ions: CO_2^+ (*m/z* 44), CO^+ (*m/z* 28), $C_2H_3O^+$ (*m/z* 43), and CHO^+ (*m/z* 29). In addition, 55% of the signal at *m/z* 57 was contributed by an oxygenated ion – $C_3H_5O^+$. $C_4H_9^+$, which is a dominant ion at *m/z* 57 in POA from fossil fuel combustion [*Mohr et al.*, 2009] and has been used as an AMS tracer ion for HOA [e.g., *Zhang et al.*, 2005c], accounts for 45% of the *m/z* 57 and only 0.44% of the total organic signal, due to minor influence of primary emissions at T1.

The elemental ratios (O/C and H/C) of the organics show strong diurnal patterns (Fig. 2-14b-2-14d). O/C increased from 0.43 to 0.52 between 7:00 and 12:00 while H/C decreased simultaneously (Fig. 2-14b & 2-14c). Given that the observed increases of O/C coincided with the increases of Org 43, Org 44, and total organics mass in particles smaller than 300 nm (Fig. 2-11c & 2-11d), daytime formation and condensation of low volatility and oxidized organics onto the surface of pre-exiting particles appeared to be an important mechanism controlling organic aerosol composition and loading in the Sierra foothills region. The slight decrease of O/C and increase of H/C between 21:00 - 22:00 were likely due to the emissions of primary hydrocarbon-like organic particles from local sources. Compared to OA observed at Whistler Mountain, a forested site in western Canada, the average O/C ratio of this study was much lower (0.44 vs. 0.83 [*Y. Sun et al.*, 2009]. A major reason is that Whistler peak is a frequent receptor of highly aged aerosols associated with trans-Pacific dust events and regional plumes [*McKendry et al.*, 2008; *Y. Sun et al.*, 2009]. In addition, aqueous-phase processing of aerosols in clouds, which could increase the O/C of organics [*Ervens et al.*, 2011], is likely an important process given the frequent cloud cover over Whistler peak [*Y. Sun et al.*, 2009]. In contrast, since the weather during CARES was mostly dry with sunny skies [*Fast et al.*, 2012] the formation of SOA was primarily driven by gas-phase reactions and condensation of low volatility species. This conclusion is supported by the observation of a dominant condensation mode in the size distribution of organics throughout the entire study. Overall, the O/C values observed at T1 suggest that organic particles over the Sierra foothill were less aged, comprising of SOA formed in urban plume during transport or locally from biogenic VOCs.

*Figure 2-14. (**a**) Average high resolution mass spectrum of organics colored by ion category, along with a pie chart with the contribution of each ion category to the total signal. Diurnal patterns of (**b**) oxygen-to-carbon (O/C) ratio, (**c**) hydrogen-to-carbon (H/C) ratio, and (**d**) organic mass-to-carbon (OM/OC) ratio of organics. The $C_xH_yS_nO_z^+$ family is not shown in the pie chart due to its very small contribution (average = 0.09%). Box plots: whiskers correspond to the 10th and 90th percentile, boxes to the 25th and 75th percentile, the horizontal marks in the boxes to the median, and the colored crosses to the mean.*
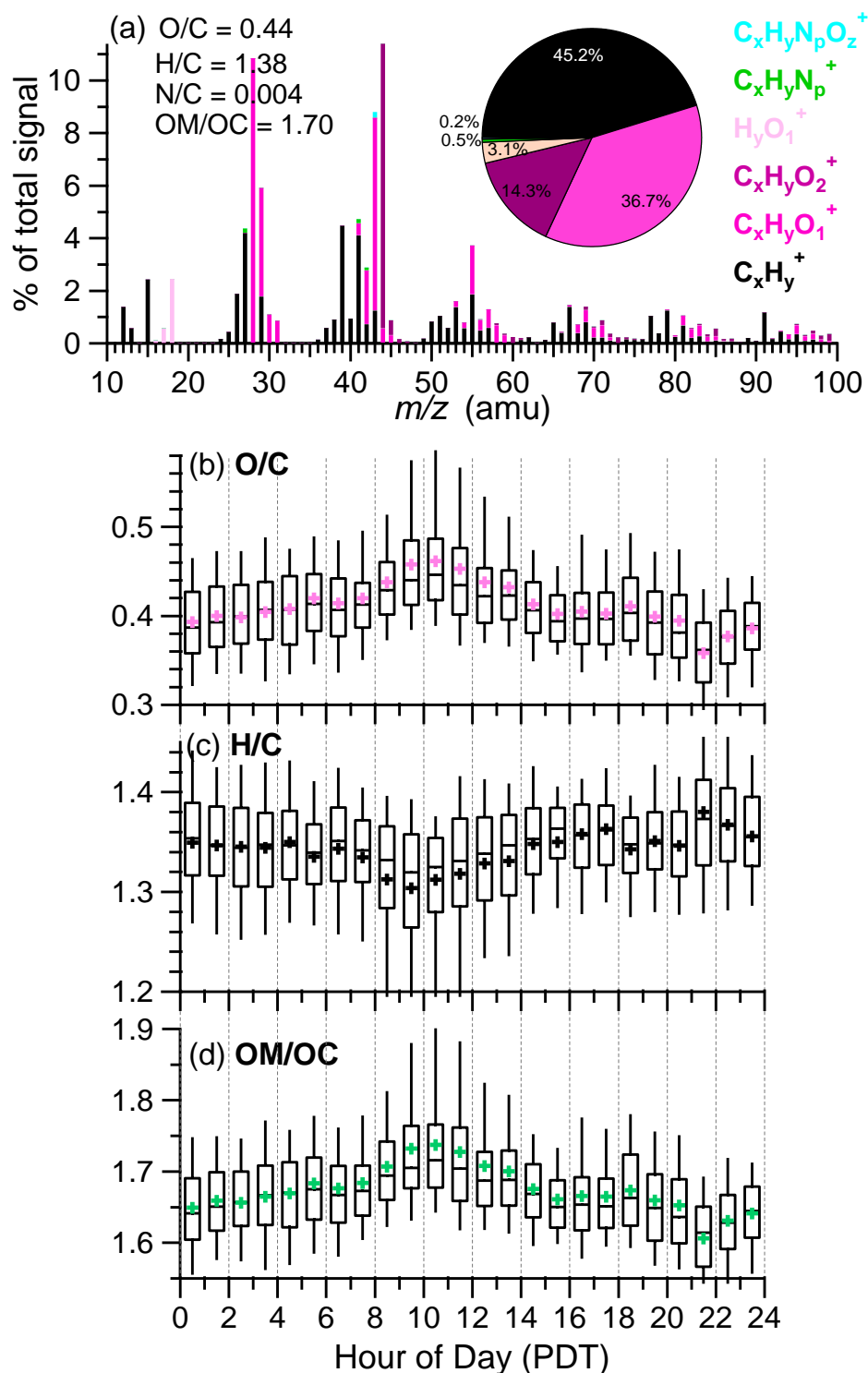
2.3.2. Organic Aerosol Factors and Discussions on the Sources and Processes Affecting OA Composition

Three distinct OA factors were identified for this study via PMF analysis of the high resolution mass spectra of organics. These include two oxygenated OA factors, one more oxidized (O/C = 0.54) than the other (O/C = 0.42), and a hydrocarbon-like OA (HOA, O/C = 0.08). A number of previous studies identified more than one OOA factors at various locations [e.g., *J. L. Jimenez et al.*, 2009; *Lanz et al.*, 2010; *Ng et al.*, 2010b; *Q Zhang et al.*, 2011, and references therein]. Based on correlations with sulfate and ammonium nitrate, OOAs are usually named based on their inferred volatilities, e.g., LV-OOA (low volatility) and SV-OOA (semi-volatile) [*J. L. Jimenez et al.*, 2009]. However, *Hildebrandt et al.* [2010] identified two OOA factors with similar volatility but different O/C at a remote coastal site in Greece. For the present study, our preliminary analysis of the thermodenuder data indicates that both OOAs were more volatile than sulfate and that they showed somewhat different volatility profiles. But the differences did not appear statistically significant due to relatively noisy data. We thus use the terms of "more oxidized" (MO-OOA) and "less oxidized" OOA (LO-OOA) in the forthcoming discussions.

2.3.2.1. More oxidized OOA (MO-OOA) and association with biogenic emissions

As shown in Fig. 2-15a, the mass spectrum of MO-OOA is dominated by oxygenated fragments (i.e., ions from the $C_xH_yO_1^+$ and $C_xH_yO_2^+$ families). *m/z* 43 (97.4% is $C_2H_3O^+$) and *m/z* 44 (97.3% is CO_2^+) were the largest peaks. The O/C ratio (0.54) in MO-OOA falls between the average values observed in the SV-OOA (0.35±0.14) and LV-OOA (0.73±0.14) factors identified in worldwide datasets [*J. L. Jimenez et al.*, 2009; *Ng et al.*, 2010b]. The O/C ratio and the mass spectrum of MO-OOA are similar to those of biogenic SOA (BSOA) acquired from chamber studies and ambient environments. A few prominent ions measured in BSOA, such as $C_2H_3O^+$ (*m/z* 43) and $C_3H_6O^+$ (*m/z* 58) [*Chen et al.*, 2009; *Kiendler-Scharr et al.*, 2009b; *Slowik et al.*, 2010], are also enhanced in MO-OOA, accounting for 12% and 1.1%, respectively, of the total signal. In addition, the signal of CHO^+ (*m/z* 29) is clearly enhanced in the MO-OOA spectrum compared to that in the average OOA mass spectrum of different field campaigns [*Ng et al.*, 2011b], but in similar abundance as it is in the spectra of α-pinene and isoprene SOAs from smog chamber experiments [*M. R. Alfarra et al.*, 2006; *Chhabra et al.*, 2010; *Shilling et al.*, 2009], BSOAs from plant chamber experiments [*Kiendler-Scharr et al.*, 2009b], and ambient OOAs influenced by biogenic emissions [*Chen et al.*, 2009; *Kiendler-Scharr et al.*, 2009b; *Slowik et al.*, 2010]. Note that previous studies have reported significant signals at *m/z* 29 in the spectra of biomass burning particles [*Ng et al.*, 2011b]. However, in the absence of signals at *m/z* 60 ($C_2H_4O_2^+$) and 73 ($C_3H_5O_2^+$), which correspond to the two fragments of levoglucosan usually used as tracers for biomass burning, the signal at *m/z* 29 cannot be associated to biomass burning in this study. As shown in Fig. S7, the agreements between the mass spectra of our MO-OOA vs. biogenic SOA identified at Chebogue Point (r^2 = 0.95) and from plant chamber experiments (r^2 = 0.97; Kiendler-Scharr et al., 2009) are especially high. Since the AMS ionizes molecules with 70 eV electrons, the mass spectrum it generates for an ensemble aerosol should reflect its bulk chemical composition [*M R Canagaratna et al.*, 2007; *McLafferty and Turecek*, 1993]. The observed mass spectral similarities thus suggest a compositional resemblance between MO-OOA and biogenic SOA.

Figure 2-15. *High-resolution mass spectra (colored by ion category) and elemental ratios of the OA factors (**a-c**). Average contribution of ion categories to the total signal of the OA factors (**d**), and average contribution of OA factors to the three main ion categories (**e**). Time series (**f, g, h**) and diurnal patterns (**i, j, k**) of OA factors and tracer compounds, along with their correlation coefficients (r^2). Grey box plots for OA factors (i, j, k): whiskers correspond to the 10th and 90th percentile, boxes to the 25th and 75th percentile, the horizontal marks in the boxes to the median, and the colored solid circles to the mean. Colored markers for tracer compounds (i, j, k) correspond to the mean.*
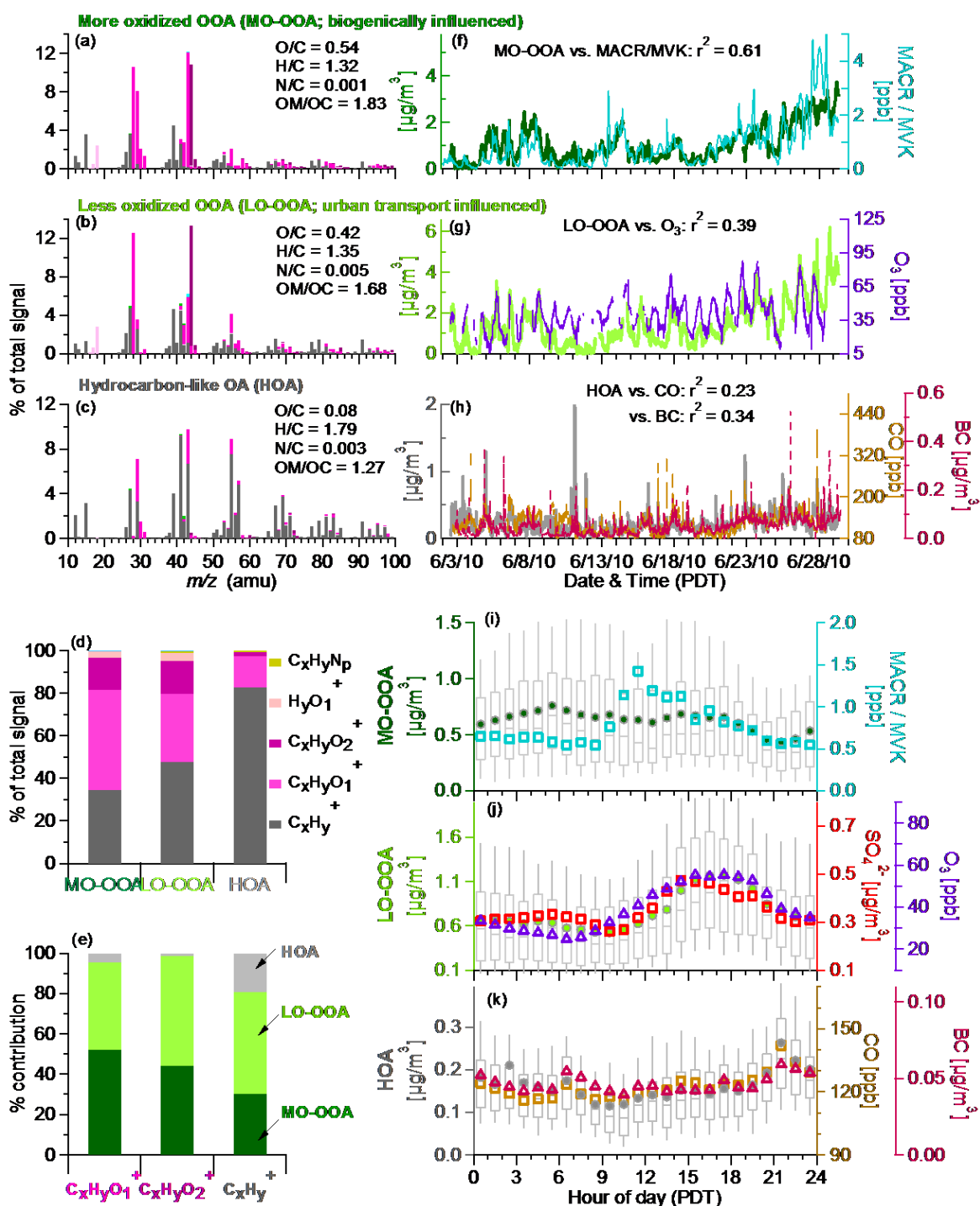
Figure 2-16. *Scatterplots of (**a**) MACR+MVK vs. MO-OOA, (**b**) O₃ vs. LO-OOA, (**c**) black carbon vs. HOA, and (**d**) CO vs. HOA. All the scatterplots are colored by time and the data fittings were performed using the orthogonal distance regression (ODR).*
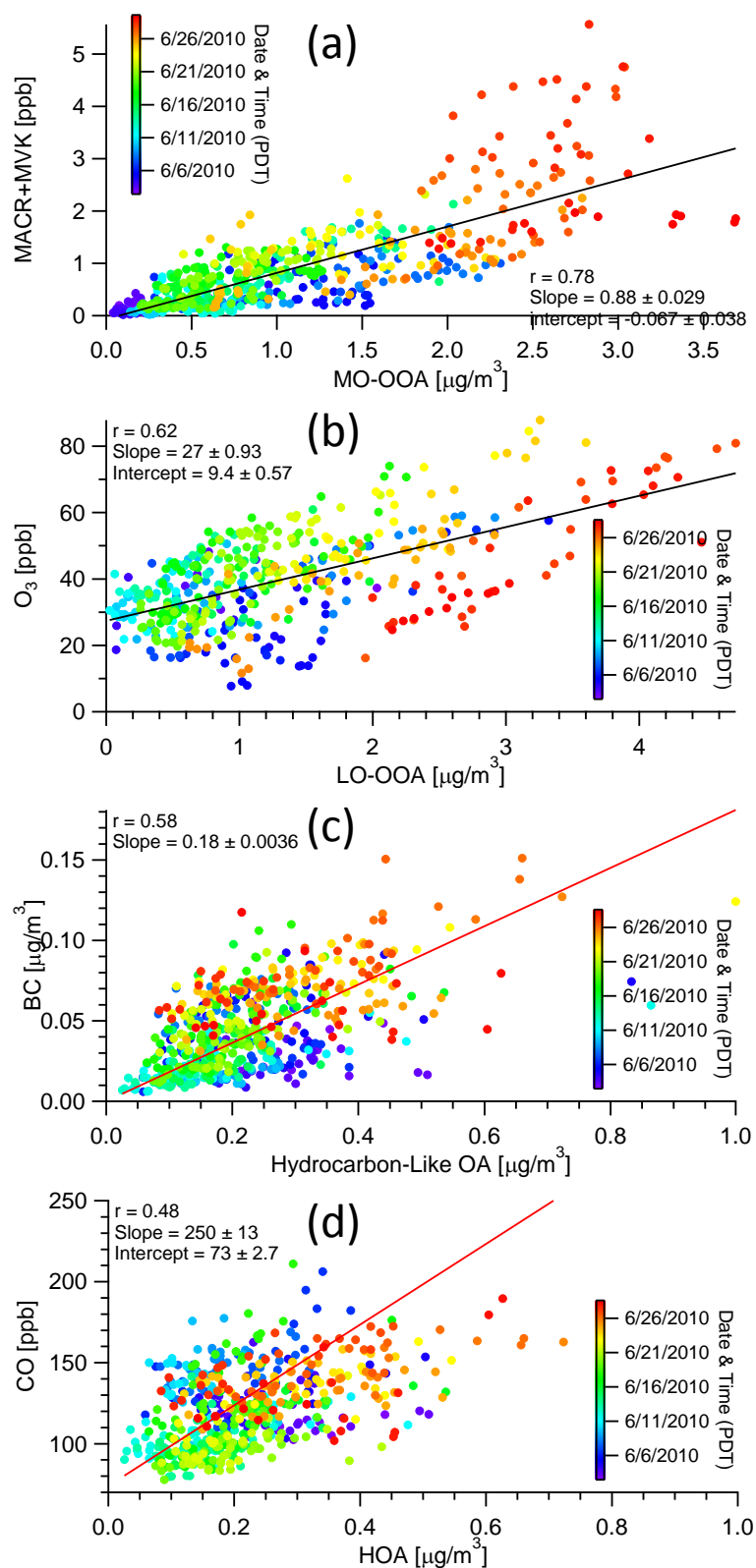
Another support for associating MO-OOA with BSOA is the temporal variation profiles of aerosol and gaseous species observed during this study. MO-OOA showed very weak correlation with primary emission tracers for anthropogenic sources (e.g., BC, CO, benzene, toluene, and aromatic hydrocarbon derivatives; $r^2 < 0.2$). It, however, correlated moderately with biogenic VOCs (isoprene and monoterpenes; r^2 of 0.3-0.4) and fairly well with two isoprene oxidation products – methacrolein (MACR) and methyl vinyl ketone (MVK) ($r^2 = 0.61$; Fig. 2-16a). The covariance between MO-OOA and MACR/MVK was particularly high during several periods in the first three weeks of the study (Fig. 2-15f). Both MO-OOA and MACR/MVK increased during last week of the campaign due to enhanced photochemical processing, but the increase of MACR/MVK was much greater (Fig. 2-15f), weakening the overall linear relationship between them (Fig. 2-16a). MO-OOA also correlated well with two long-lived oxygenated VOCs – acetone ($r^2 = 0.73$) and methanol ($r^2 = 0.61$). According to previous reports vegetation is a main source of atmospheric methanol [*Jacob et al.*, 2005] whereas acetone is generated in part through atmospheric oxidation of precursor hydrocarbons in addition to plant emissions [*Jacob et al.*, 2002]. During this study, these two VOCs covaried tightly ($r^2 = 0.87$; Fig. 2-17), which was also the case during two previous field campaigns at the Blodgett Forest [*Schade and Goldstein*, 2001; 2006]. The strong correlation suggests that both compounds were mainly associated with biogenic sources at the Sierra foothills. All these results corroborate the notion that MO-OOA was associated with photochemical processing of biogenic precursors.

Figure 2-17. *Scatterplot of methanol vs. acetone, colored by air mass types. The data fitting was performed using the orthogonal distance regression (ODR).*
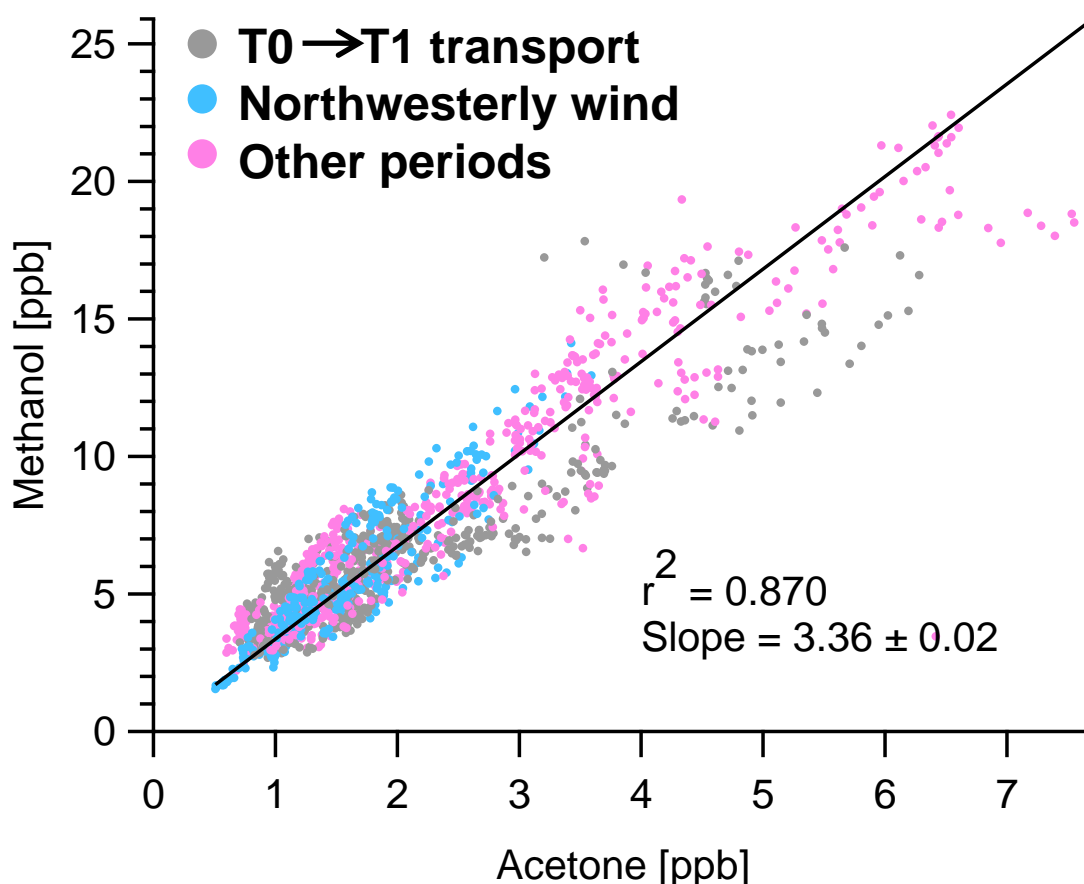
Despite positive correlation, MO-OOA and MACR/MVK had quite different diurnal patterns (Fig. 2-15i). MACR/MVK increased sharply in the morning and declined shortly past noon, whereas the diurnal profile of MO-OOA was relatively flat but showed two small increases in the early afternoon (peak around 14:00) and at night from 22:00 to 5:00 (Fig. 2-15i). The daytime increase happened during the strong midday emission of isoprene from the surrounding deciduous forest due to elevated temperature and light intensity [*Sharkey et al.*, 1996], coupled with the simultaneous peaking of photochemical oxidants (e.g., OH). The nighttime increase likely corresponded to the nocturnal downslope winds which transport air masses over the Sierra Mountains back to the foothills [*Fast et al.*, 2012]. Indeed, a close look at the time series of the PTR/MS data (Fig. 2-2) reveals that amongst all the VOCs recorded at T1, only monoterpenes showed an important increase during the night. In fact, the concentrations of monoterpenes reached a peak between 5:00 and 6:00 and decreased very fast during the day. This behavior may arise because 1) pine trees which emit monoterpenes grow mostly on the east of the T1 site, at higher elevations of the Sierra Nevada and 2) the regular nocturnal downslope flows bring emissions in the Sierras back to the foothills [*Fast et al.*, 2012]. The fast daytime decrease of monoterpenes may be due to the high reactivity of these compounds as well as the scarcity of pine trees to the southwest of T1. In addition, the peaking of MO-OOA later than the peaking of MACR/MVK is consistent with the facts that MACR and MVK are the first generation oxidation products of isoprene and that they undergo further reactions to produce SOA. This explanation is confirmed by previous chamber experiments on isoprene photooxidation, in which the production of SOA was found to occur at the same time as the oxidation of the primary oxidation products (e.g., MACR+MVK) and the increase of SOA continued for several hours after MACR/MVK reached maximum [*Holzinger et al.*, 2007b; *Lee et al.*, 2006]. It is also important to point out that since the formation of MVK and MACR from isoprene oxidation occurs on a time scale of several hours [*Apel et al.*, 2002], the fact that MO-OOA covaried with them suggests that a large fraction of the biogenic SOA over the Sierra foothills was relatively fresh with an average photochemical age of several hours.

2.3.2.2. Less oxidized OOA (LO-OOA) and association with anthropogenic emissions

Similar to MO-OOA, oxygenated fragments dominate the LO-OOA mass spectrum, in which m/z 44 (94% is CO_2^+) is the most abundant peak. However, the $C_xH_y^+$ ions are more important in LO-OOA (Fig. 2-15b), accounting for 48% of the total signal (vs. 35% in MO-OOA; Fig. 2-15d). It was observed previously that when organic particles become more oxidized, f_{44} (the fraction of total mass spectral signal at m/z 44) and O/C increase together [*A. C. Aiken et al.*, 2008; *Ng et al.*, 2010b]. However, in the present study, despite larger f_{44} in LO-OOA than in MO-OOA, the O/C in LO-OOA is lower than in MO-OOA (0.42 vs. 0.54; Fig. 2-15a & 2-15b). This divergence was because the O/C ratio depends not only on the relative abundance of the m/z 44 fragment (mostly CO_2^+) but also on hundreds of other ions containing carbon and oxygen. Thus, f_{44} alone is unable to predict the O/C value accurately if ions other than CO_2^+ contribute substantially to overall O/C [*Chhabra et al.*, 2010]. Indeed, CHO^+ (m/z 29) accounts for 7.6% of the total signal in the MO-OOA spectrum, compared to 1.0% in LO-OOA. The large CHO^+ peak increases the O/C of MO-OOA. Meanwhile, a bigger fraction of $C_xH_y^+$ in LO-OOA decreases its O/C.

The mass spectral differences between LO-OOA and MO-OOA (Fig. 2-15a & 2-15b) imply significant differences in their chemical compositions. A main spectral difference is

highlighted in Fig. 2-18, which shows f_{44} vs. f_{43} for the three OA factors and ambient data acquired during this study. f_{44} and f_{43} denote the fractions of the total signal at *m/z* 44 and *m/z* 43 in a mass spectrum. This triangle plot, first presented by *Ng et al.* [2010b], is a practical way of classifying OOA factors identified in different atmospheric environments. Factors with different levels of oxidation fall in different regions of the triangle plot. The more oxidized, low volatility OOAs usually fall in the upper part of the triangle, whereas the less oxidized semivolatile OOAs fall in the lower part. The region corresponding to SV-OOA is broad, which indicates that fresher OOAs may have more variable mass spectra, depending on their sources and processes. The upper part of the triangle is much thinner, suggesting that SOA composition tends to become more similar after ageing and long oxidation processes [*Ng et al.*, 2010b].

Figure 2-18. Triangle plot (f_{44} vs. f_{43}) with ambient data (colored by time) and OA factors determined via PMF analysis of the high resolution organic mass spectra. The triangle region was determined by Ng et al. [2010b] and corresponds to region where ambient OOA factors from different datasets fall. Dark red star points correspond to OOA factors previously published and reporting biogenic influences [J. D. Allan et al., 2006; L. D. Cottrell et al., 2008; Kiendler-Scharr et al., 2009b; Raatikainen et al., 2010; Slowik et al., 2010; Y. Sun et al., 2009; Williams et al., 2007].
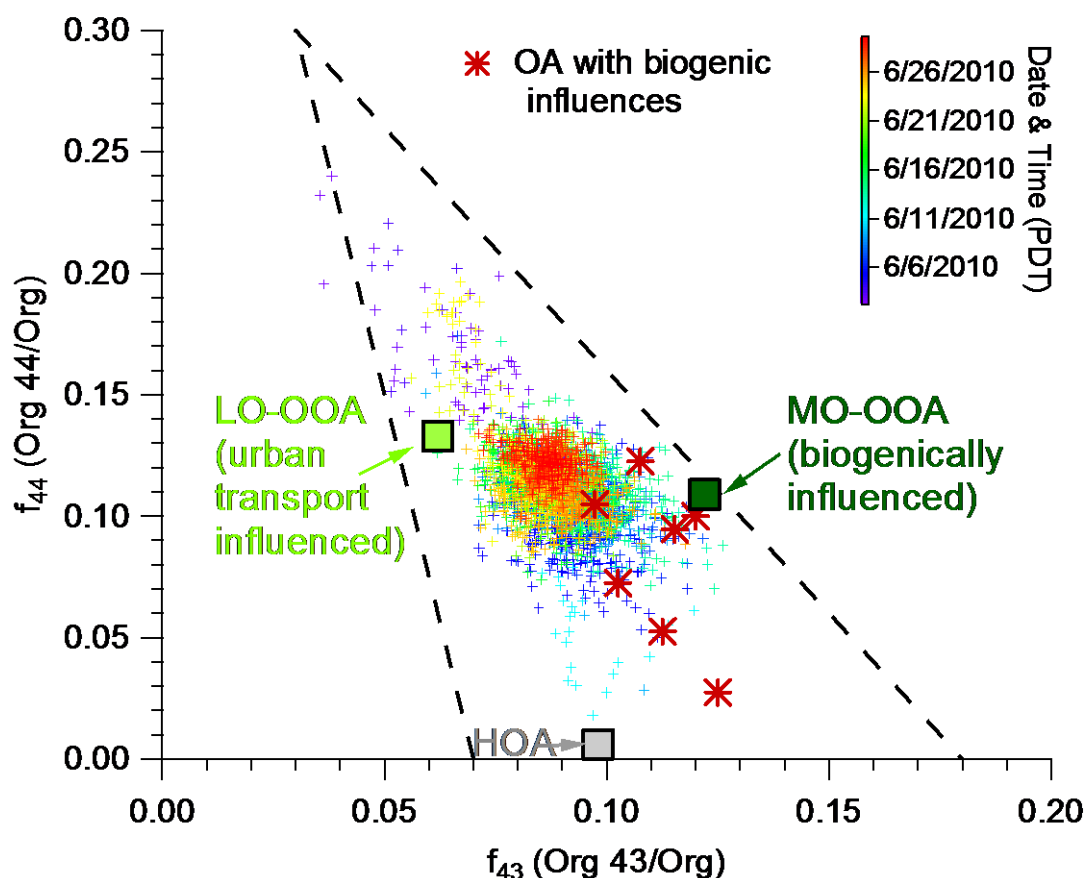
Both OOAs of this study reside in the middle region of the triangle where the less oxidized SV-OOAs and the more aged LV-OOAs overlap (Fig. 2-18). However, LO-OOA lies near the left side of the triangle whereas MO-OOA lies near the right side. Most interestingly, the f_{43} (0.12) and the f_{44}/f_{43} ratio (0.9) of MO-OOA are within the range of the corresponding values observed for ambient OOAs influenced significantly by biogenic emissions [*J. D. Allan et al.*,

2006; *Chen et al.*, 2009; *L. D. Cottrell et al.*, 2008; *Kiendler-Scharr et al.*, 2009b; *Raatikainen et al.*, 2010; *Slowik et al.*, 2010; *Y. Sun et al.*, 2009]. These observations reinforce our arguments that the MO-OOA factor of this study represents biogenic SOA. However, it is important to note that the "position" of an OOA factor in the triangle plot is not a reliable indicator for its sources. For example, the mass spectra of chamber SOAs generated from anthropogenic hydrocarbons were found to be highly variable [*Chhabra et al.*, 2011; *Lambe et al.*, 2011]. While SOAs from alkanes, polycyclic aromatic hydrocarbons (PAHs), and lubricating oil generally lie on the left region of the triangle plot, closer to LO-OOA than to MO-OOA, SOAs produced from diesel fuel, m-xylene, and toluene lie on the right side of triangle [*Chhabra et al.*, 2011; *Lambe et al.*, 2011], overlapping with SOAs from biogenic precursors and MO-OOA. Nevertheless, given the very low mixing ratios of aromatic VOCs (e.g., average concentration of benzene + toluene was 0.12 ppb; Fig. 2-2), especially compared to the very high concentrations of isoprene (1.2 ppb) observed during this study, it is unlikely that aromatic compounds contributed significantly to SOA production over the Sierra foothills.

In addition to mass spectral differences, the temporal profiles of LO-OOA and MO-OOA were different from each other as well, suggesting that they were influenced by different emission sources or atmospheric processes. LO-OOA correlated positively with ozone ($r^2 = 0.39$; Fig. 2-15g & 2-16) and both showed a prominent diurnal cycle (Fig. 2-15j). In contrast, there was almost no correlation between MO-OOA and O_3 ($r^2 = 0.05$) and their diurnal patterns were obviously different. Herndon et al. (2008) observed a strong correlation between OOA and odd oxygen ($O_x = O_3 + NO_2$) in photochemically processed urban plumes from Mexico City. This observation was made at a downwind site free of local emission sources and meteorological transport was found responsible for the correlation between OOA and O_3 [*Herndon et al.*, 2008; *Wood et al.*, 2010]. For the present study, due to the lack of NO_2 data, we did not use odd oxygen but just O_3. Nevertheless, our findings are very similar to those from Mexico City. As shown in Fig. 2-15g, LO-OOA correlated with ozone particularly well between 10:00 and 18:00 when photochemical processing was intense. The correlation between LO-OOA and O_3 over the entire study appeared only moderate ($r^2 = 0.39$; Fig. 2-15g) though, mainly because the linear relationships between them varied considerably from day to day (Fig. 2-16). The strong correlation between LO-OOA and O_3 – a secondary photochemical oxidant – during daytime indicates that LO-OOA corresponded to photochemically produced SOA. The strong correlation also means that LO-OOA and O_3 were formed on similar timescales, indicating that LO-OOA was relatively fresh, likely less than 8 h in photochemical age. A similar conclusion was reached about the OOA that correlated with O_x in emission plumes from Mexico City [*Wood et al.*, 2010]. The relatively low O/C (0.42) of LO-OOA is also consistent with its being relatively fresh.

The diurnal profiles of LO-OOA, O_3, and sulfate were similar, showing strong increases between 10:00 to 18:00 (Fig. 2-15j). This time period corresponded to southwesterly upslope winds that regularly transport urban emissions from Sacramento over the foothills of the Sierra Nevada [*Fast et al.*, 2012]. In addition, the trends of LO-OOA, O_3, and sulfate mirrored the daytime evolution patterns of aerosol number and size distributions, which were attributed to meteorological transport coupled to photochemical processing. These results, together with the mass spectral features of LO-OOA (e.g., high contribution of ions from the $C_xH_y^+$ family), indicated that LO-OOA corresponded to SOA photochemically produced in urban plumes that were transported to the Sierra foothills by southwesterly wind [*Fast et al.*, 2012].

2.3.2.3. HOA and association with local traffic emissions

The HOA mass spectrum (Fig. 2-15c) shows characteristic signals of $C_4H_9^+$ (*m/z* 57), $C_4H_7^+$ (*m/z* 55), and hydrocarbon ion series increasing at 14 (CH_2) mass unit intervals (i.e., $C_nH_{2n-1}^+$ and $C_nH_{2n+1}^+$). $C_xH_y^+$ ions account for 83% of the total signal in HOA (Fig. 2-15d). The larger $C_nH_{2n+1}^+$ (n > 2) ions are mostly contributed by HOA, thus correlate tightly with HOA but poorly with the two OOAs. A similar behavior was observed in a summer study in New York City where the HOA factor was proven a surrogate for traffic-related POA [*Sun et al.*, 2011]. HOA is clearly separated from the two OOAs on the triangle plot (Fig. 2-18), indicating their chemical differences. However since the HOA spectrum also shows a major peak at *m/z* 43 (mostly $C_3H_7^+$), a second triangle plot corresponding to f_{CO2} (CO_2^+/total organic ratio) vs. f_{C2H3O} ($C_2H_3O^+$/total organic ratio) is given in Fig. 2-19 to distinguish OA factors better. The mass spectrum pattern as well as the elemental ratios (O/C = 0.08, H/C = 1.79) of the HOA factor identified in this study are consistent with the HOA factors representative of traffic emission determined in urban areas [*A. C. Aiken et al.*, 2009a; *J. D. Allan et al.*, 2010b; *Ng et al.*, 2011b; *Sun et al.*, 2011; e.g., *Zhang et al.*, 2005a].

Figure 2-19. *Triangle plot (f_{CO2} vs. f_{C2H3O}) with ambient data (colored by time) and OA components. The triangle region has been determined by Ng et al. [2010b] and corresponds to region where ambient OOA components from different datasets fall. Red star points correspond to OOA components previously published and reporting biogenic influences [J. D. Allan et al., 2006; L. D. Cottrell et al., 2008; Raatikainen et al., 2010; Slowik et al., 2010; Y. Sun et al., 2009; Williams et al., 2007].*
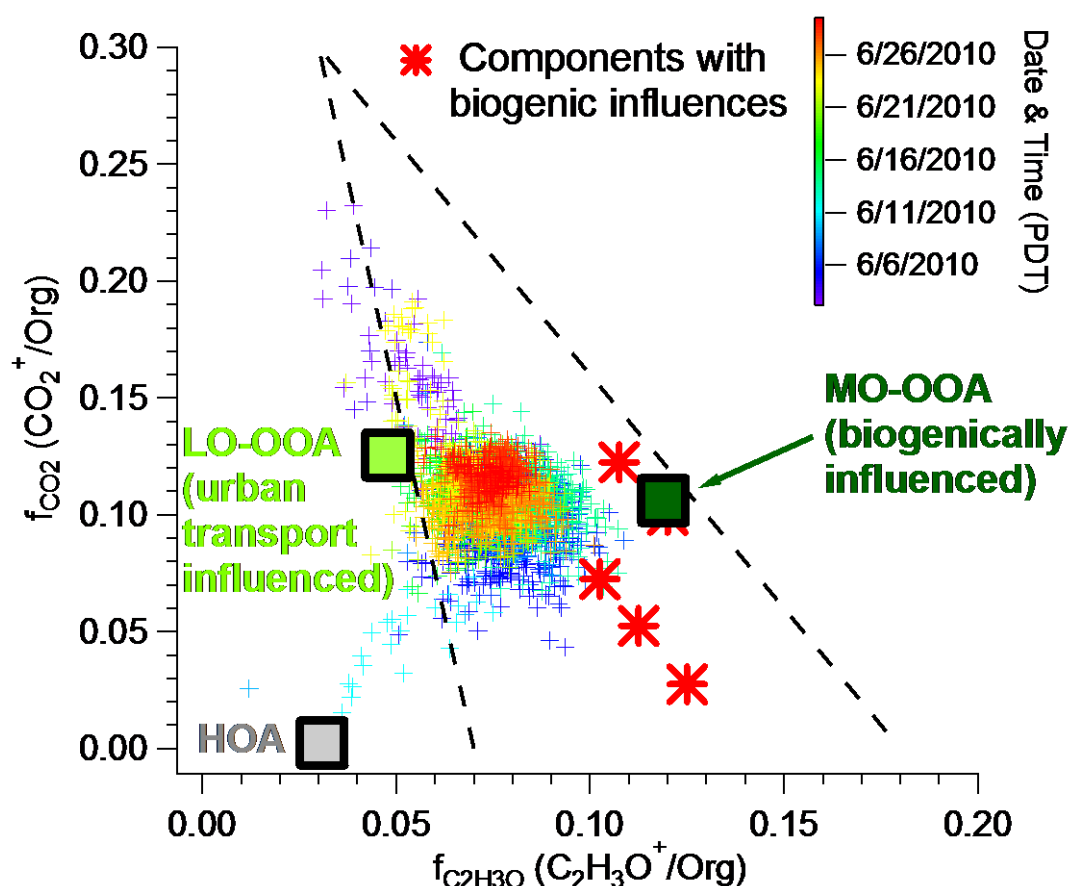
Table 2-1. *Summary of the average concentrations and % of total PM$_1$ or VOCs during the entire study and in the three air masses as marked on Fig. 2-5*

	Entire study		T0→T1 transport		Northwesterly wind		Other periods	
	[μg/m^3]	[% of PM$_1$]	[μg/m^3]	[% of PM$_1$]	[μg/m^3]	[% of PM$_1$]	[μg/m^3]	[% of PM$_1$]
Organics	2.4	80.4	3.1	80	1.4	79	2.6	81
MO-OOA	0.97	40[a]	1.1	36[a]	0.63	44[a]	1.1	42[a]
LO-OOA	1.2	51[a]	1.8	57[a]	0.61	43[a]	1.3	50[a]
HOA	0.22	9.0[a]	0.22	7.2[a]	0.19	13[a]	0.23	8.6[a]
Sulfate	0.30	9.9	0.39	10	0.18	10	0.31	9.6
Nitrate	0.11	3.6	0.13	3.5	0.070	4.0	0.12	3.5
Ammonium	0.13	4.5	0.17	4.4	0.091	5.2	0.14	4.3
Chloride	0.002	0.1	<DL[b]	0.1	<DL[b]	0.0	<DL[b]	0.1
Black Carbon	0.07	1.6	0.054	1.4	0.032	1.8	0.053	1.6
Total PM$_1$[c]	3.0		3.9		1.8		3.3	
	[ppb]	[% of VOC]	[ppb]	[% of VOC]	[ppb]	[% of VOC]	[ppb]	[% of VOC]
Photo-oxidation products[d]	7.6	82	8.3	81	5.6	79	7.9	83
Biogenic VOCs[e]	1.5	16	1.7	17	1.3	18	1.4	14
Aromatic VOCs[f]	0.23	2.4	0.19	1.8	0.19	2.7	0.27	2.8
Total VOCs	9.3		10.2		7.1		9.6	

[a] % of total organics

[b] Detection limit

[c] Total PM$_1$ = Org + SO$_4^{2-}$ + NO$_3^-$ + NH$_4^+$ + Cl$^-$ + BC

[d] Photo-oxidation products = acetaldehyde + acetic acid + methacrolein + methyl vinyl ketone + methyl ethyl ketone + formaldehyde + acetone

[e] Biogenic VOCs = isoprene + monoterpenes + 2-methyl-3-buten-2-ol + methyl chavicol

[f] Aromatic VOCs = benzene + C2-benzenes + C3-benzenes + C4-benzenes + toluene

The average concentration of HOA was 0.22 μg m^{-3}, which accounted for 9% of total OA mass over the entire campaign (Table 2-1). The sporadic spikes in HOA (Fig. 11h & 11k) were probably due to local traffic around the sampling site. Note that because of low concentrations, the HOA and BC data were noisy, and the correlations between HOA and primary combustion tracers (BC and CO) appeared to be relatively low (r^2 = 0.34 and 0.23, respectively; Fig. 2-15h, 2-16g, and 2-16h). For the same reason, the correlation between CO and BC was low during this study as well (r^2 = 0.31). Similar observation was made at a rural site impacted by urban outflow where the correlations between HOA, BC, and CO were degraded because of noisy data [*Zhang et al.*, 2007c]. Note that oxidation of biogenic VOCs was unlikely a significant source of CO at T1. According to a previous study at Blodgett forest, oxidation of biogenic VOCs was estimated to contribute only up to 5 ppb of CO during summertime over the Sierra foothills (Worton et al., 2011). In addition, biomass burning was found negligible during this study as well. These results indicate that emissions related to transport were likely the main sources of HOA, CO, and BC at T1. Indeed, the diurnal patterns of these three species were very similar and all showed small increases between 6:00-7:00 and 21:00-22:00, probably due to local traffic near the sampling site (Fig. 2-15k). Furthermore, the average ratio of HOA/CO (after subtracting a background of 80 ppb) was determined at ~ 5 μg/m^3/ppm, which is very close to the HOA to CO emission ratios observed in urban plumes [*Zhang et al.*, 2005a]. These results, as well as its mass spectral

pattern, indicate that the HOA factor determined in this study mainly represented POA emitted from transport related sources.

2.3.3. Influence of Anthropogenic Emissions on SOA Formation

During this study, the average concentrations of LO-OOA and MO-OOA were 1.2 µg m^{-3} and 0.97 µg m^{-3}, respectively (Table 2-1), which together accounted for 91% of the total organic mass and 72% of the PM$_1$ mass (Table 2-1). Similarly, organics were found predominantly oxygenated during the BEARPEX 2007 field campaign [*Worton et al.*, 2011], suggesting that SOA is a dominant aerosol component over the higher elevations of the Sierra Nevada as well. These observations indicate that SOA formation from both biogenic and anthropogenic precursors plays important roles controlling the loading, composition, and possibly climate-relevant properties of aerosols over the Sacramento and west Sierra Nevada region. Here, we compared aerosol concentrations, compositions, and size distributions during periods of urban plumes to those dominated by biogenic emissions (Table 2-1 and Fig. 2-20) to study the influence of anthropogenic emissions from Sacramento on the formation of SOA at the Sierra foothills, Details on the classification of the three types of air masses (T0→T1 transport, northwesterly wind periods, and other periods) are given in section 2.2.4. The average particle mass concentration was more than two times higher in urban plumes (3.9 µg m^{-3}) than in background air (i.e., during the northwesterly wind period; 1.8 µg m^{-3}). The mass distributions of two OOAs were consistent with different wind patterns, with urban plumes dominated by LO-OOA (i.e., urban transport SOA) and the northwesterly wind periods dominated by MO-OOA (i.e., biogenic SOA). The other periods were also dominated by the LO-OOA, likely because these periods correspond mainly to nocturnal downslope flows, which brought back a part of the polluted air from the Sierra Nevada to the foothills. The average size distributions of organics and sulfate showed a significant difference between the three types of air masses – the presence of a mode smaller than 150 nm in D_{va} (Fig. 2-20). This mode grew conspicuously in the sulfate size distribution during the T0 to T1 transport periods (Fig. 2-20b). It was also visible, but with lower intensity and larger mode size, during the downslope wind periods. This mode was barely noticeable during the northwesterly wind periods. The strong enhancement of small mode particles in the urban transport air mass was associated with the frequent occurrence of new particle growth events during which the formation and condensation of H$_2$SO$_4$ and SOA species led to the growth of newly formed particles.

SOA formation in different air masses can be investigated using the ΔOA/ΔCO ratio to take into account of the dilution effect of primary emissions. ΔOA and ΔCO correspond to the organic aerosol and CO concentrations above their respective background levels, and were determined for the three air masses separately based on the averages of the lowest 5% data. ΔOA was 0.3 µg m^{-3} in each air mass, while ΔCO was 85 (T0→T1 transport), 80 (northwesterly wind periods) and 90 (other periods) ppb respectively. Fig. 2-21 shows the relationships between ΔOA and ΔCO during the entire campaign, as well as for different air masses and periods with different concentrations of biogenic VOCs. ΔOA and ΔCO were weakly correlated during this study (r^2 = 0.22; Fig. 2-21a), while the correlation was found to be much higher during a recent field campaign performed at the Blodgett Forest [r2 = 0.79; *Worton et al.*, 2011]. The ratio of ΔOA to ΔCO varied between 5-196 µg/m^3/ppm (Fig. 2-21a), indicating large variations in SOA formation rates. The minimum value of this study (5 µg/m^3/ppm) was very close to the HOA/CO (4 µg/m^3/ppm) ratio observed at an urban location – Pittsburgh [*Zhang et al.*, 2005a], consistent with influence from primary combustion emissions.

*Figure 2-20. Comparison of the average size distributions of (**a**) organics, (**b**) sulfate and (**c**) particle number concentration between the three air mass categories as marked on Fig. 2.*
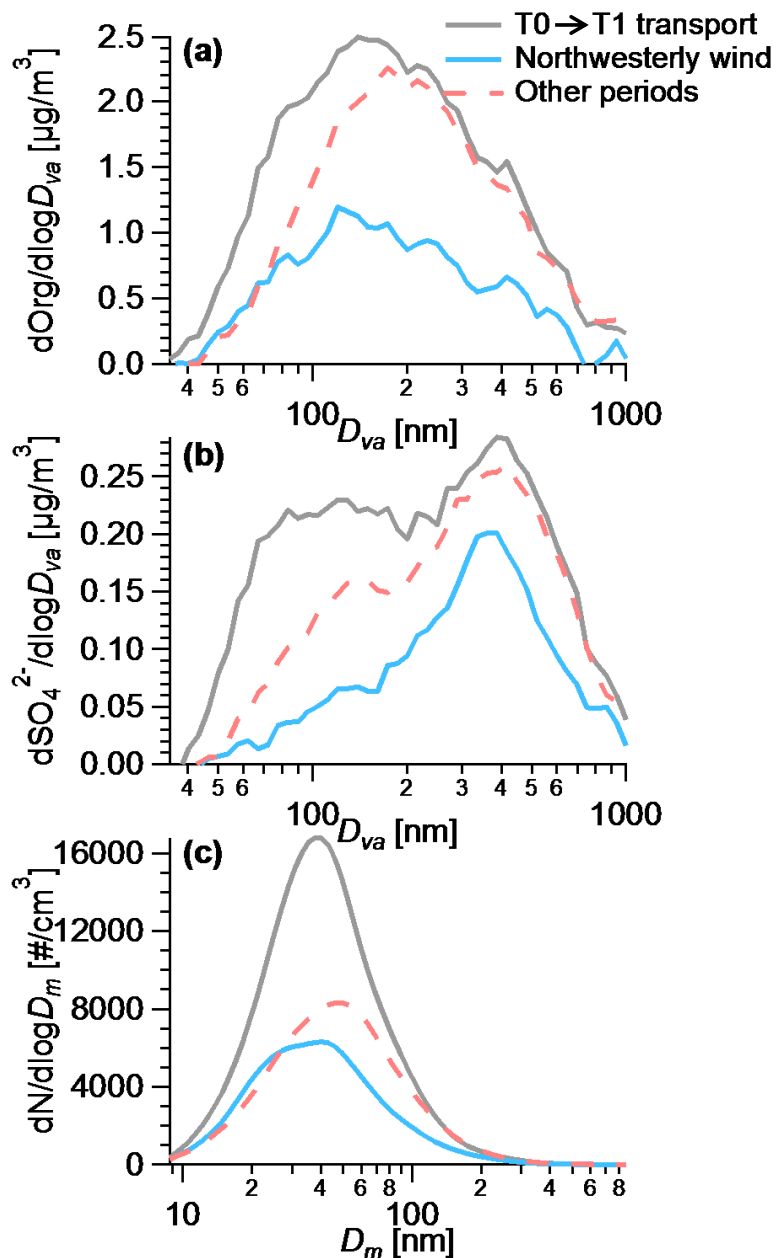
The diurnal pattern of $\Delta OA/\Delta CO$ showed a gradual increase between 10:00 (50 $\mu g/m^3$/ppm) and 17:00 (72 $\mu g/m^3$/ppm; Fig. 2-21b). This time period corresponded to the urban plume from T0 to T1. The diurnal pattern of $\Delta OA/\Delta CO$ showed another gradual increase between 23:00 (41 $\mu g/m^3$/ppm) and 3:00 (61 $\mu g/m^3$/ppm). This period corresponded to nocturnal downslope winds which brought a part of the polluted air back from the Sierra Mountains to the foothills. The increase of $\Delta OA/\Delta CO$ during this period (20 $\mu g/m^3$/ppm) was comparable to that during the daytime transport events (22 $\mu g/m^3$/ppm). These results indicate that SOA formation was enhanced at T1 during periods when the site was more strongly influenced by anthropogenic emissions.

Figure 2-21. (a) Scatterplot of organics vs. CO, colored by the sum of biogenic VOCs (= isoprene + monoterpenes + 2-methyl-3-buten-2-ol [MBO] + methyl chavicol). (b) Diurnal pattern of ΔOA/ΔCO. Scatterplot of ΔOA/ΔCO during three air mass types as marked on Fig. 2: (c) T0 to T1 transport, (d) northwesterly wind and (e) other periods. In (c), (d), and (e), the data points are classified into periods of high (> 2 ppb) or low (< 0.7 ppb) mixing ratios of biogenic VOCs. Box plots: whiskers correspond to the 10th and 90th percentile, boxes to the 25th and 75th percentile, the horizontal marks in the boxes to the median, and the colored crosses to the mean. The data fitting (c, d, e) was performed using the orthogonal distance regression (ODR).
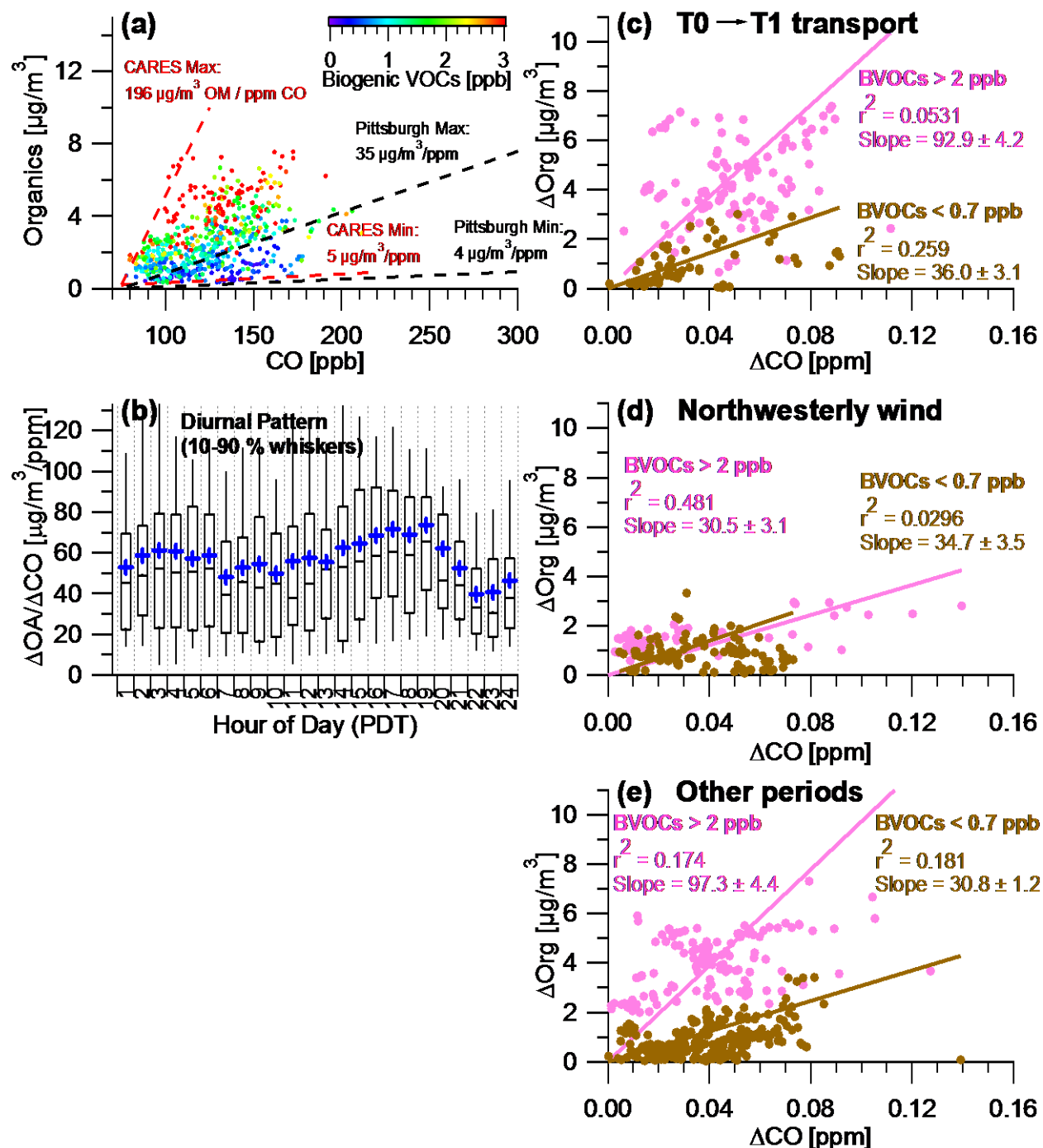
An important parameter in the comparison between different air masses is the photochemical age. Unfortunately, we were not able to determine this parameter with the data acquired at T1. Gas phase toluene and benzene data were too noisy because of low concentrations. Since NO_x was not measured at T1 the NO_x/NO_y ratio could not be used either. *J A de Gouw et al.* [2008] derived an equation that relates $\Delta OC/\Delta CO$ (the increase of organic carbon mass relative to the increase of CO) to the photochemical age (Δt in hour) based on ambient measurements in the northeastern US in summer:

$$\Delta OC/\Delta CO = 5.3 \times \exp(-0.00677 \times \Delta t) + 57 \times (\exp(-0.00677 \times \Delta t) - \exp(-0.0384 \times \Delta t)) \quad (3)$$

Using the $\Delta OA/\Delta CO$ and OM/OC values from this study, we determined that the average $\Delta OC/\Delta CO$ during this study was 21 $\mu gC/m^3/ppm$. The average ratios for different air masses were 25 $\mu gC/m^3/ppm$ (T0 to T1 transport), 17 $\mu gC/m^3/ppm$ (northwesterly wind), and 21 $\mu gC/m^3/ppm$ (other periods). According to Eqn. 3, the $\Delta OC/\Delta CO$ for periods of urban transport would correspond to a photochemical age of $\sim$ 16 hours, much longer than the time needed for particles to be transported from T0 to T1. The T0 $\rightarrow$ T1 transport time was estimated at 2-8 hours based on model predictions [*Fast et al.*, 2012] as well as comparisons of observations at T1 and T0, e.g., the time delays between the onset of the new particle growth events and the peaking times of pollutants. This is also in agreement with *Dillon et al.* [2002], who determined that the Sacramento urban plume takes on average 5 hours to reach the Blodgett Forest. Apparently, the relationship derived from the northeastern US does not apply to the Sacramento Valley Air Basin, where the type and concentration of precursors, meteorological conditions, and concentrations of oxidants are vastly different.

As shown in Fig. 2-21c-e, the slope of ΔOA vs. ΔCO depends strongly on the amount of biogenic VOCs present during these periods, suggesting that the enhancement of SOA formation due to anthropogenic influences is also dependent on the amount of biogenic VOCs available. To calculate the sum of biogenic VOCs, we took into account of isoprene, monoterpenes, MBO and methyl chavicol, knowing that isoprene was by far the most abundant biogenic VOC measured during this study (82% of the total biogenic VOCs in average). Note that the temporal variations of the different biogenic VOCs are very different (Fig. 2-2), isoprene being dominant during the day while monoterpenes were higher during the night and obviously transported during the downslope flows from the Sierra Nevada to the foothills. During the transport periods from T0 to T1 (Fig. 2-21c), the slope of ΔOA vs. ΔCO increased by a factor of 3 when the sum of biogenic VOCs was higher than 2 ppb, compared to periods when the mixing ratio was lower than 0.7 ppb (93 vs. 36 $\mu g/m^3/ppm$). This change in SOA mass relative to CO was approximately the same as that during the downslope flows (97 $\mu g/m^3/ppm$; Fig. 2-21e) when anthropogenic influences were still present, but was much higher than during the northwesterly wind periods (31 $\mu g/m^3/ppm$; Fig. 2-21d) dominated by biogenic SOAs. In summary, these results suggest that the SOA formation was enhanced when anthropogenic influences increased at Cool, but only if significant amounts of biogenic precursors were present. The observations from this study also support the hypothesis that the interaction between anthropogenic and biogenic precursors enhances the SOA formation [*J. A. de Gouw et al.*, 2005; *L. I. Kleinman et al.*, 2008a; *R. Volkamer et al.*, 2006; *Weber et al.*, 2007].

2.4. Conclusions

An HR-ToF-AMS and an SMPS were deployed at Cool, CA, the T1 rural site of the CARES field campaign in June 2010 to characterize the mass concentration, chemical composition and size distributions of submicrometer aerosols. The sampling site was located at

the foothills of the Sierra Nevada Mountains, where biogenic emissions from forests are periodically mixed with urban outflow transported by consistent southwest winds from Sacramento. The average mass loading during the entire campaign was 3.0 µg m^{-3}, with organics (80% of the total PM$_1$ mass) being the dominant component followed by sulfate (9.9%), ammonium (4.5%), nitrate (3.6%), black carbon (1.6%), and chloride (0.1%). The amount of ammonium appeared to be in charge balance with observed anions (sum of SO$_4^{2-}$ + NO$_3^-$ + Cl$^-$), indicating that sulfate was mainly present in the form of (NH$_4$)$_2$SO$_4$. The average size distribution indicated that sulfate was mainly present in the accumulation mode (D_{va} 200-600 nm) whereas organics showed broader distributions peaking at smaller sizes. New particle formation and growth events were observed almost every day with the SMPS. Our results showed that organics and, to a lesser extent, sulfate played key roles in the new particle growth. Three OA factors were identified by PMF analysis of the high resolution mass spectra, including two distinct OOA factors (91% of total organics) and an HOA (9%). The more oxidized MO-OOA (O/C = 0.54) was found to represent biogenically influenced SOA, while the less oxidized LO-OOA (O/C = 0.42) corresponded to anthropogenically influenced SOA mainly formed in the air mass transported from the Sacramento area. The HOA factor corresponded to primary emissions from local sources. The diurnal variation patterns of LO-OOA, ozone, and sulfate were very similar and all showed substantial daytime increases consistent with impacts from urban transport. However, the time series of LO-OOA and sulfate were poorly correlated, indicating different source regions of their precursor species and different formation mechanisms. For instance, the prominent droplet mode of sulfate and the tight correlation between sulfate and MSA indicate a significant influence of aqueous-phase reactions on sulfate production. A large fraction of this droplet mode may come from the San Francisco Bay Area, where oil refineries are the largest SO$_2$ sources identified in northern California and where aqueous reactions would have been promoted by fogs and low clouds during morning hours around the Bay Area. The good correlations observed between MO-OOA and first generation isoprene photooxidation products (MVK and MACR) and between LO-OOA and ozone suggest that both SOA types were relatively fresh, which were consistent with their relatively low O/C ratios.

23 periods of urban plumes from T0 (Sacramento) to T1 (Cool) were identified using the WRF-Chem model. The average chemical composition of aerosols was overall similar in different air masses. PM$_1$ mass loading, however, was more than twice higher during the T0 to T1 transport periods than during northwesterly wind periods (3.9 vs. 1.8 µg/m^3). In addition, a second mode of sulfate in small sizes (D_{va} 100-150 nm) became conspicuous during the T0 to T1 transport periods, due to the frequent occurrence of new particle growth events in urban plumes. This mode was less obvious in air masses dominated by biogenic SOAs and almost disappeared during northwesterly wind periods. ΔOA/ΔCO, an indicator for SOA production, varied in the range of 5-196 µg/m^3/ppm during this study. Enhanced SOA formation was observed when urban emissions from Sacramento arrived at T1 and interacted with biogenic precursors. Moreover, the largest SOA formation was observed in urban plumes mixed with a high concentration of biogenic VOCs. For example, in air masses influenced by urban emissions, ΔOA/ΔCO values were on average above 90 µg/m^3/ppm in the presence of high biogenic VOCs (> 2 ppb), compared to 36 µg/m^3/ppm at low biogenic VOCs (< 0.7 ppb). The average ΔOA/ΔCO was 30 - 35 µg/m^3/ppm in air masses dominated by biogenic SOA with little anthropogenic influence (i.e., during the northwesterly wind periods).

3. CHEMISTRY OF REGIONAL NEW PARTICLE EVENTS IN SACRAMENTO VALLEY AIRBASIN

3.1. Introduction

New particle formation and growth processes are an important source of ultrafine particles in both clean and polluted environments. A large number of studies reported the observations of intensive new particle events at various locations, including urban areas [*Ahlm et al.*, 2012; e.g., *Brock et al.*, 2003; *Dunn et al.*, 2004; *Stanier et al.*, 2004; *Wu et al.*, 2007; *Zhang et al.*, 2004], remote sites [*Creamean et al.*, 2011; *Pikridas et al.*, 2012; *Vakkari et al.*, 2011; e.g., *Weber et al.*, 1999], forested locations [e.g., *J. D. Allan et al.*, 2006; *Han et al.*, 2013; *Pierce et al.*, 2012], coastal sites [*Liu et al.*, 2008; *Modini et al.*, 2009; e.g., *O'Dowd et al.*, 2002; *Wen et al.*, 2006], and polar regions [*Asmi et al.*, 2010; e.g., *Komppula et al.*, 2003; *Koponen et al.*, 2003]. These events significantly affect the number concentrations and size distributions of particles in the atmosphere with important implications on human health and climate [*Bryan R. Bzdek and Johnston*, 2010; *Kerminen et al.*, 2012; *Spracklen et al.*, 2006]. However, despite frequent observations, the chemical processes underlying the formation and growth of new particles remain poorly understood.

New particle events occur in two steps, i.e., the formation of nuclei, followed by the growth of the stable clusters to larger sizes by condensation of low-volatility compounds and coagulation. For ambient measurements, the evolution of the number-based particle size distribution is a main criterion for identifying the onset of new particle events. Scanning mobility particle sizer (SMPS) is the most widely used instrument to determine the particle size distribution and number concentration during these events. The evolution of the chemical composition of ultrafine particles during new particle formation and growth is another piece of critical information needed for understanding this process. For that purpose, aerosol mass spectrometer (AMS) [*Ahlm et al.*, 2012; *J. D. Allan et al.*, 2006; *Creamean et al.*, 2011; e.g., *Zhang et al.*, 2004; *L. D. Ziemba et al.*, 2010], chemical ionization mass spectrometer (CIMS) [e.g., *Dunn et al.*, 2004; *Jokinen et al.*, 2012; *James N. Smith et al.*, 2005; *J. N. Smith et al.*, 2008; *James N. Smith et al.*, 2010], nano aerosol mass spectrometer (NAMS) [e.g., *B. R. Bzdek et al.*, 2011; *Bryan R. Bzdek et al.*, 2012], and atmospheric pressure ionization time-of-flight (APi-TOF) mass spectrometer [*Kulmala et al.*, 2013; *Lehtipalo et al.*, 2011] have been successfully deployed in the field to study the chemical processes underlying atmospheric new particle events.

An important finding from previous studies is that organics and sulfate are usually involved in the growth of new particles up to sizes where they can act as cloud condensation nuclei (CCN). The contribution of these two species to particle growth depends on the concentrations of the precursors and meteorological conditions. For example, at urban or industrial locations where the SO_2 mixing ratio is high, sulfate is an important contributor to the growth of new particles [*Brock et al.*, 2003; *Bryan R. Bzdek et al.*, 2012; *Yue et al.*, 2010; *Zhang et al.*, 2004]. At rural and remote locations, however, the growth of new particles was found to be almost exclusively driven by organics [*Ahlm et al.*, 2012; *Laaksonen et al.*, 2008; *Pierce et al.*, 2012; *J. N. Smith et al.*, 2008; *L. D. Ziemba et al.*, 2010]. In addition, it was found that in Pittsburgh, USA, despite high ambient SO_2 concentrations, H_2SO_4 contributes mainly to the early stage of the new particle growth, while the growth up to CCN sizes is mainly driven by

secondary organic aerosols (SOA), especially during late morning and afternoon when photochemistry is more intense [*Zhang et al.*, 2005a; *Zhang et al.*, 2004].

SOA is a major component of fine particles globally [*J. L. Jimenez et al.*, 2009; *Zhang et al.*, 2007c]. Understanding its roles in new particle formation and growth is important for addressing aerosols' effects on climate and human health. Recent studies found significantly enhanced SOA formation rates in mixed biogenic and anthropogenic emissions [*J. A. de Gouw et al.*, 2005; *L. I. Kleinman et al.*, 2008a; *A. Setyan et al.*, 2012; *Shilling et al.*, 2013; *R. Volkamer et al.*, 2006]. However, there is little known about the influence of the interactions of organic species from biogenic and anthropogenic sources on new particle growth. The Sacramento Valley in California is a place of choice to study this process. The Sacramento metropolitan area lies in the Central Valley to the north of the San Joaquin River Delta and to the southwest of the forested Sierra Nevada Mountains. The wind in this region is characterized by a very regular pattern, especially in summer [*Fast et al.*, 2012]. Indeed, during the day, a southwesterly wind usually brings air masses from the San Francisco Bay to the Sacramento metropolitan area and pushes northeast to the Sierra Nevada Mountains [*Dillon et al.*, 2002], promoting the transport of urban plumes from Sacramento to forested regions where biogenic emissions are intense.

The U.S. Department of Energy (DOE) sponsored Carbonaceous Aerosols and Radiative Effects Study (CARES) that took place in the Sacramento Valley in June 2010 was designed to take advantage of this regular wind pattern to better understand the life-cycle processes and radiative properties of carbonaceous aerosols in a region influenced by both anthropogenic and biogenic emissions [*Zaveri et al.*, 2012b]. Within the framework of CARES, a wide range of instruments were deployed between June 2 and 28, 2010 at two ground sites located in Sacramento (T0, urban site) and Cool, CA at the foothills of the Sierra Nevada Mountains (T1, rural site), respectively, to measure aerosol chemical composition, size distribution, and optical and hygroscopic properties, as well as trace gases and meteorological data [*Zaveri et al.*, 2012b]. One of the major observations during CARES was that particles were dominated by organics in this region, and that the formation of SOA was enhanced when anthropogenic emissions from the Sacramento metropolitan area and the Bay Area were transported to the foothills and mixed with biogenic emissions [*A. Setyan et al.*, 2012; *Shilling et al.*, 2013].

During CARES, new particle growth events were observed almost daily at both the T0 and T1 sites. Similarly, previous studies conducted at the University of California Blodgett Forest Research Station, approximately 75 km to the northeast of Sacramento and 35 km to the northeast of the T1 site, also reported the frequent occurrence of NPE [*Creamean et al.*, 2011; *Lunden et al.*, 2006]. In their study conducted from May to September 2002, *Lunden et al.* [2006] found that the oxidation products of reactive biogenic compounds accounted for a significant portion of the particle growth. The study of *Creamean et al.* [2011], which took place in early spring of 2009, found that sulfate and amines participated in the growth of new particles and that long-range transport of SO_2 from Asia seemed to contribute to faster growth. These findings indicate that new particle formation and growth are important processes in Northern California and that it is important to better understand the regional characteristics and the chemistry underlying these processes. For these reasons, a main aim of the present paper is to examine the evolution characteristics of new particles at the T0 and T1 sites during CARES, with a focus on the size-resolved particle chemical composition based on HR-ToF-AMS measurements at T1.

3.2. Experimental

3.2.1. Sampling Site and Instrumentation

The T0 sampling site was located on the campus of the American River College in Sacramento (38° 39′ 01″ N, 121° 20′ 49″ W, 30 m above sea level) and the T1 site was located on the campus of the Northside School at Cool (38° 52′ 16″ N, 121° 01′ 22″ W, 450 m above sea level). Sacramento is the capital of California, with 480,000 inhabitants in the city and 2.5 million people living in the metropolitan area. Cool is a small town (2500 inhabitants) surrounded by very large forested areas, and located ~40 km northeast of Sacramento at the Sierra Nevada foothills.

Chemical composition and size distribution of non-refractory submicron aerosols (NR-PM$_1$) were analyzed using an Aerodyne HR-AMS [*M R Canagaratna et al.*, 2007; *DeCarlo et al.*, 2006b]. A detailed discussion on its operation at T1 during the present study was presented in *A. Setyan et al.* [2012]. Briefly, the HR-AMS was equipped with an aerodynamic lens allowing the transmission of particles in the range ~30-1500 nm (in vacuum aerodynamic diameter, D_{va}). The instrument was operated alternatively in V- and W-mode every 2.5 min. In V-mode, data was recorded in mass spectrum (MS) mode and particle time-of-flight (PToF) mode. The MS mode was used to obtain average mass spectra and determine the concentration of the species in submicrometer particles without size information. In the PToF mode, average mass spectra were acquired for 92 size bins covering 30-1500 nm (D_{va}), allowing the determination of the size-resolved chemical composition. W-mode data was recorded exclusively in MS mode.

The particle number size distribution was measured with an SMPS. The instrument used at T1 consists of a Hauke-type differential mobility analyzer (DMA) and a condensation particle counter (CPC; TSI Inc., Shoreview, MN; model 3772) [*A. Setyan et al.*, 2012]. The SMPS was set to measure particles in the range 8-858 nm (in mobility diameter, D_m), divided into 70 logarithmically distributed size bins. SMPS data has been corrected to take into account the DMA-CPC lag time, bipolar charge distribution, CPC efficiency, and diffusion loss. The SMPS deployed at T0 was a commercial instrument (TSI Inc.; model?) and measured particles in the range 12-737 nm (in D_m) divided into 115 size bins. Diffusion loss correction was applied after the data inversion. All dates and times reported in this paper are in Pacific Daylight Time (PDT = UTC – 7 hr), which was the local time during this study.

3.2.2. Data Analysis

Particle number concentration and size distribution have been used to identify new particle events in the atmosphere. However, given that the new particles formed by nucleation have generally a diameter in the size range 1-3 nm, smaller than the smallest size measured by our SMPS's, we were not able to observe the new particle formation themselves during the present study, but only the growth of the newly formed particles into particles of larger sizes. For this reason, we will not use the terms "nucleation" or "new particle formation" in the forthcoming discussion, but rather "new particle growth". Each day for which complete SMPS data was available was classified as new particle event (NPE) if the particle number concentration in the size range 12-20 nm increased by more than 800 particles/cm^3, and if this increase was accompanied by the increase of the mode during the following hours. These two conditions allowed us to distinguish NPE from primary emissions from vehicles, which also produce small particles but are usually observed as occasional spikes in the time series of the particle number concentration in the range 12-20 nm. In addition, each growth event was

considered as "strong" if the increase of the particle number concentration in the range 12-20 nm was higher than 1500 particles/cm^3, and "weak" if the increase was lower than this threshold. A summary of the new particle growth events observed during this study is provided in Table 3-1.

Table 3-1. *Summary of the characteristics of new particle growth events observed at Sacramento (T0) and Cool (T1) in northern California.*

Day	T0 Growth rate nm/hr	ΔN #/cm^3/hr	NPE Event	T1 Growth rate nm/hr	ΔN #/cm^3/hr	ΔOrg $_{40\text{-}120\,nm}$ µg/m^3/hr	ΔSO$_4^{2-}$ $_{40\text{-}120\,nm}$ µg/m^3/hr	Wind	NPE Event
6/2/2010	Incomplete SMPS data		N/A[a]	Incomplete SMPS data		0.75	0.10	T0→T1[b]	N/A
6/3/2010	10.5	6.12E+03	strong	4.1	2.56E+03	0.98	0.32	T0→T1	strong
6/4/2010	5.4	6.80E+03	strong	12.5	6.14E+03	Incomplete PToF data		T0→T1	strong
6/5/2010	10.9	9.57E+03	strong	9.3	1.07E+03	No PToF data		T0→T1	weak
6/6/2010	12.1	7.40E+03	strong	8.8	2.98E+03	Incomplete PToF data		T0→T1	weak
6/7/2010	10.1	6.40E+03	strong	7.6	5.86E+03	0.28	0.063	T0→T1	strong
6/8/2010	4.1	5.64E+03	strong	7.7	4.19E+03	0.35	0.075	T0→T1	strong
6/9/2010	7.3	1.21E+04	strong	6.1	6.92E+03	0.49	0.075	T0→T1	strong
6/10/2010	6.5	7.76E+03	weak	4.2	4.31E+03	0.19	0.0	NW	weak
6/11/2010	7.1	2.48E+03	weak	-[c]	-	-	-	NW	no NPG
6/12/2010	-	-	no NPG	Incomplete data				NW	N/A
6/13/2010	-	-	no NPG	-	-	-	-	NW	no NPG
6/14/2010	4.6	1.26E+04	strong	Incomplete data				T0→T1	N/A
6/15/2010	4.4	6.75E+03	strong	3.8	4.52E+03	0.27	0.095	T0→T1	strong
6/16/2010	2.5	4.50E+03	strong	3.6	1.59E+03	-	-	NW	weak
6/17/2010	-	-	no NPG	2.9	2.28E+03	0.19	0.0	NW	weak
6/18/2010	6.7	3.56E+04	strong	4.3	5.30E+03	0.32	0.032	T0→T1	strong
6/19/2010	3.4	2.60E+04	strong	5.9	5.20E+03	0.19	0.041	T0→T1	weak
6/20/2010	4.1	8.69E+03	strong	4.4	2.04E+03	-	-	NW	weak
6/21/2010	5.2	4.19E+03	weak	9.5	1.96E+03	0.17	0.0	NW	weak
6/22/2010	7.6	1.51E+04	strong	Incomplete SMPS data		0.10	0.0	T0→T1	N/A
6/23/2010	11.1	7.28E+03	weak	Incomplete SMPS data		0.17	0.060	T0→T1	N/A
6/24/2010	6.4	7.11E+03	strong	7.6	8.28E+03	0.64	0.13	T0→T1	strong
6/25/2010	8.0	4.07E+03	strong	4.7	3.15E+03	0.31	0.0	T0→T1	weak
6/26/2010	7.7	9.13E+03	strong	5.3	1.81E+03	0.27	0.11	T0→T1	weak
6/27/2010	9.3	5.25E+03	strong	5.6	1.34E+03	0.11	0.0	T0→T1	weak
6/28/2010			undefined[d]			-	-	T0→T1	undefined
mean	7.1	9.57E+03		6.2	3.76E+03	0.34	0.06		
std dev	2.7	7.62E+03		2.5	2.09E+03	0.24	0.08		
median	6.9	7.20E+03		5.6	3.15E+03	0.27	0.06		
min	2.5	2.48E+03		2.9	1.07E+03	0.10	0.0		
max	12.1	3.56E+04		12.5	8.28E+03	0.98	0.32		

[a] "N/A" stands for not applicable

[b] "T0 → T1" stands for T0 to T1 transport periods

[c] "-" means that no increase was observed

[d] "undefined" means that the SMPS data did not allow to determine whether a growth event took place or not, because of a change in the wind direction during the day.

The mode(s) of each size distribution recorded during this study have been determined with a multiple peak fitting tool available in Igor Pro 6.2.2.2 (WaveMetrics Inc., Lake Oswego, OR). The growth rate (GR), which corresponds to the increase of the mode of newly formed particles per time unit (nm/hr), has been calculated for each individual growth event as GR =

ΔD_m / Δt, in which ΔD_m is the difference of the mode between the beginning of the growth and the period when the growth significantly slows down, and Δt is the duration of the growth.

3.3. Results and Discussions

3.3.1. Evolution of Particle Number Distributions during Regional New Particle Events

The SMPSs were fully operational during 26 days at T0, and 22 days at T1, from June 2 – 29, 2010. The time series of the particle number size distributions show that new particle events frequently occurred at both sites (Fig. 3-1), indicating that these events occurred on a regional scale. A total of 19 NPE were identified at T1 (86% of the time; Table 3-1), eight of which were considered as "strong" and eleven as "weak". Most of the events (14 in total) occurred during periods of southwesterly wind that transported urban plumes to the T1 site (i.e., T0 → T1), except for 5 events which occurred during northwesterly wind periods (Table 3-1). In addition, all 8 strong NPE occurred during the T0 → T1 periods (Table 3-1). At T0, 22 new particle events were identified, 18 of which were considered as "strong" and only four events were "weak".

Figure 3-1. *Time series of (**a, d**) wind direction colored by wind speed, (**b, e**) solar radiation, temperature and relative humidity, and (**c, f**) particle size distributions at the T0 and T1 sites.*
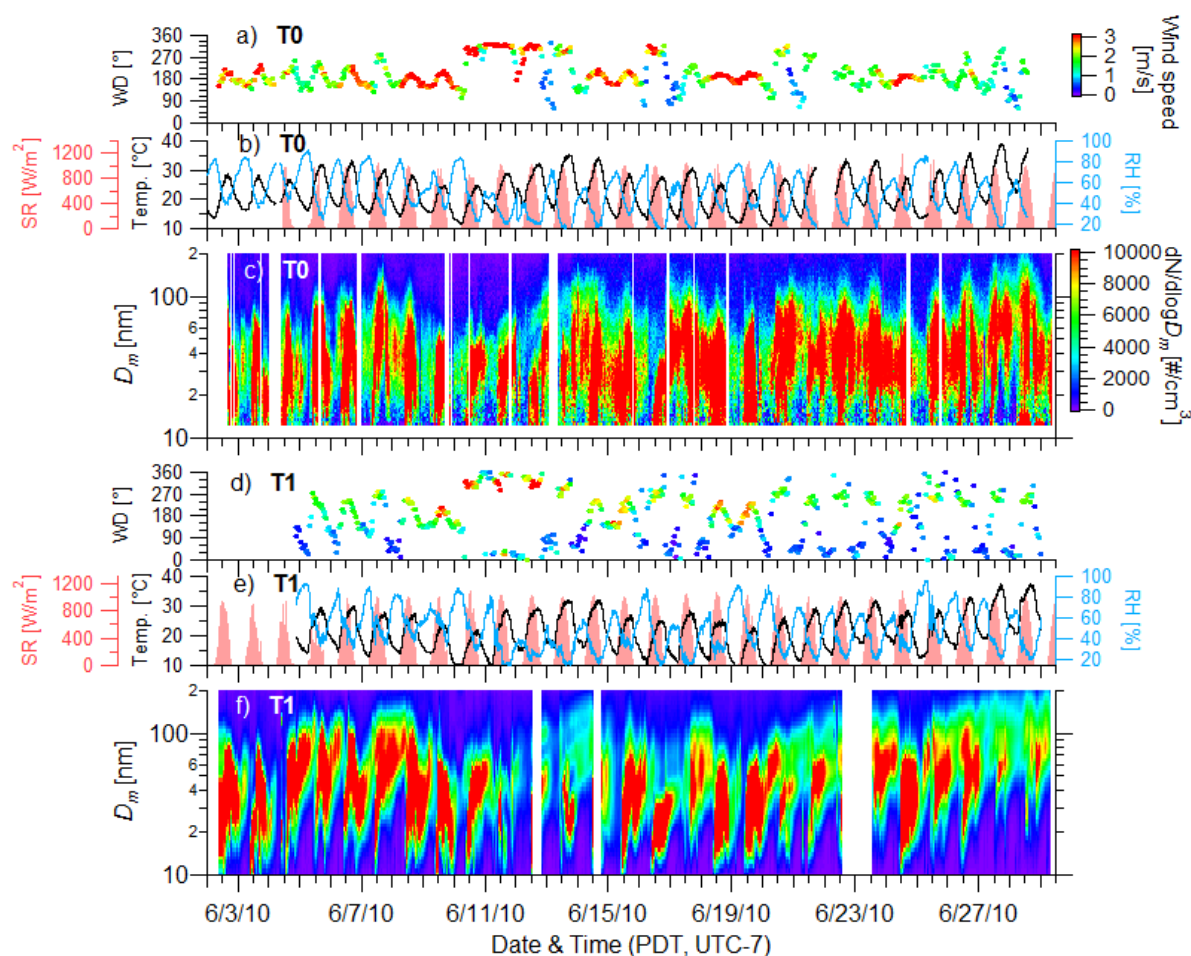
Generally, the increase of the particle number concentration during these events was higher at T0 than at T1 (average 9.57E3 vs. 3.76E3 #/cm^3/hr; Table 3-1). The average ($\pm$ 1σ)

growth rate of new particles was also higher at T0 (7.1 ± 2.7 nm/hr) compared to at T1 (6.2 ± 2.5 nm/hr). The occurrence of relatively stronger and faster NPE at T0 is likely due to the proximity of emission sources of precursor species and a higher anthropogenic influence. Indeed, the frequency as well as the growth rates observed during the present study were much higher than those reported by *Lunden et al.* [2006] at ~35 km northeast of T1 (frequency = 30% of the time, average growth rate = 3.8 ± 1.9 nm/hr). The lower frequency might be related to the fact that their site was subject to relatively lesser anthropogenic influences from urban areas to the southwest (e.g., Sacramento and the San Francisco Bay Area).

During the present study, all growth events began in the morning, with the appearance of a nucleation mode observed with the SMPS between 9:00 and 12:00. Then the growth of these particles lasted several hours, and the modes reached their maximum in the afternoon, usually after 15:00. The modes at the end of the growth in general peaked between 40-50 nm, but for several cases, the mode did not reach 35 nm, especially for the weakest events or when a change in the wind direction was observed during the day (Fig. 3-1).

Figure 3-2. Time evolution of the particle size distributions at the (a) T0 and (b) T1 sites on June 26, along with the hourly averaged wind direction (length of the arrows is proportional to the wind speed) for each site. Time series of (c) NR-PM$_1$ species and BC, and (d) three different OA factors.
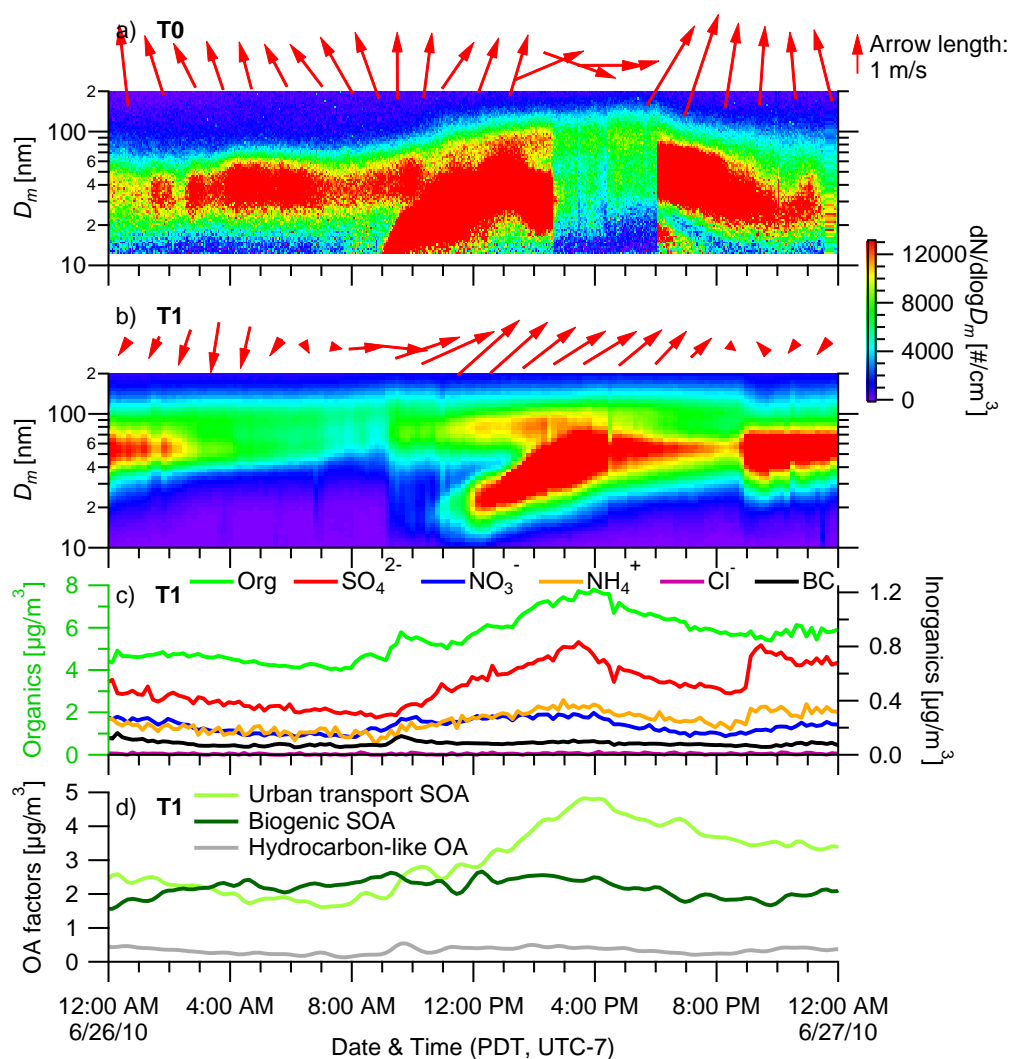
An important observation of the present study is that NPE began at T1 a few hours later than at T0, especially during days characterized with daytime T0 → T1 transport. A typical example of this phenomenon occurred on June 26 (Fig. 3-2 and 3-3). According to *Fast et al.* [2012], a T0 to T1 transport occurred that day. Particles smaller than 20 nm (in D_m) began to increase slightly before 9:00 at T0 (Fig. 3-2a), and a nucleation mode appeared at the same time (Fig. 3-3). Then, during the following hours, the mode increased slowly up to ~50 nm (in D_m), due to agglomeration and condensation of low-volatility compounds onto the surface of these

Figure 3-3. Comparisons of the average particle number size distributions for each hour at T0 and T1 during June 26.
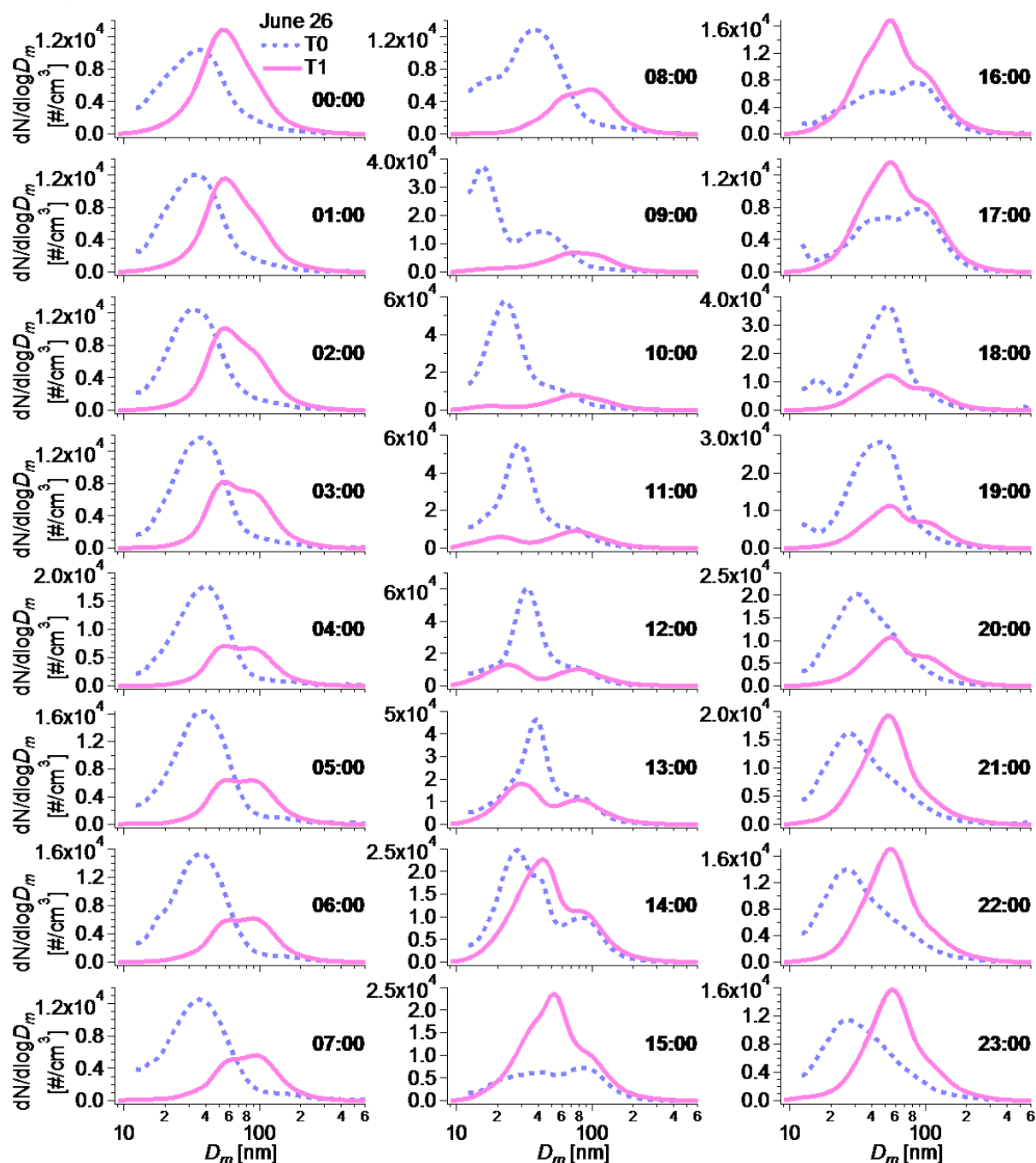
new particles. Thus, as shown in Fig. 3-2a, the evolution of the particle number size distribution shows a "banana shape", which is a typical observation with the SMPS for the formation of new particles followed by their growth. At T1, the same phenomenon occurred at ~11:00, i.e., 2 hours after T0 (Fig. 3-2b). This time delay is consistent with the wind direction and speed data recorded at T1 which indicate the sampling of air masses transported from the T0 direction. Another evidence for this pseudo Lagrangian sampling is the observation of a sudden change in wind direction at ~14:30 at T0 that brought in a very clean air mass associated with a sharp decrease of particle number concentration that lasted for ~3.5 hours (Fig. 3-2a). Particle concentration at T0 increased again at ~18:00 after a shift of the wind direction back to southwesterly. A mirrored decrease of particle concentration, although less dramatically, was observed at 16:30 at T1, ~2 hours after the clean air mass event at T0 (Fig. 3-2b). The increase of particle concentration occurred at T1 around 21:00, ~3 hours after the increase occurred at T1, consistent with gradually decreasing wind speed from 16:30 to 21:00. The wind direction at T1 remained southwesterly during the entire afternoon (Fig. 3-2b).

This time delay between T0 and T1 was also observed during the other events, and this is confirmed by the diurnal evolution profiles of the size distributions at both sites (Fig. 3-4a and 3-4c). These observations indicate that new particle growth generally occurred during T0 → T1 transport promoted by the daytime southwesterly wind and that the new particle growth events were generally more intense at T0 compared to at T1. Wind rose plot during NPE (Fig. 3-5g) confirms that these events usually occurred when the wind was coming from the southwest, which corresponds to the location of the Sacramento metropolitan area. On the other hand, when NPE was not observed, the wind was coming mainly from the northwest and the west (Fig. 3-5h), bringing air masses dominated by biogenic emissions [A. *Setyan et al.*, 2012], thus reducing anthropogenic influences at T1.

Figure 3-4. *Diurnal size distributions of the particle number concentration at the (a, b) T0 and (c, d) T1 sites during NPE days (left panel) and non-NPE days (right panel). Black crosses correspond to the modes fitted by log-normal distributions.*
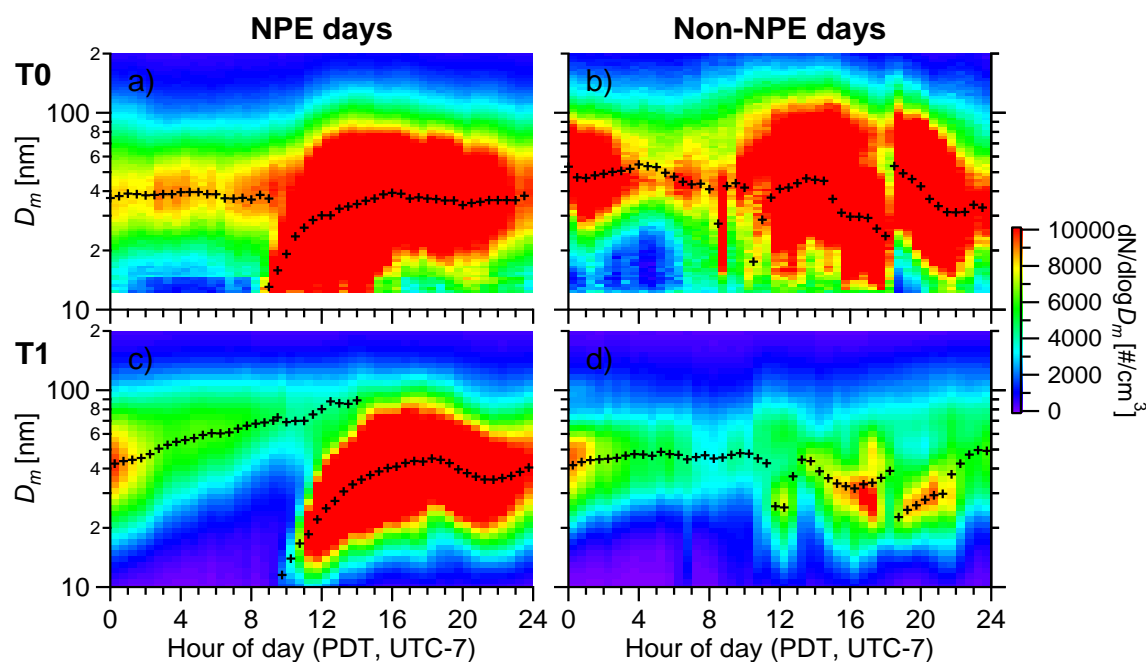
Figure 3-5. Diurnal size distributions of (*a, b*) Org, (*c, d*) SO$_4^{2-}$, and (*e, f*) particle volume concentrations, and (*g, h*) daytime wind rose plots (8:00-20:00 PDT) for NPE days (left panel) and non-NPE days (right panel).
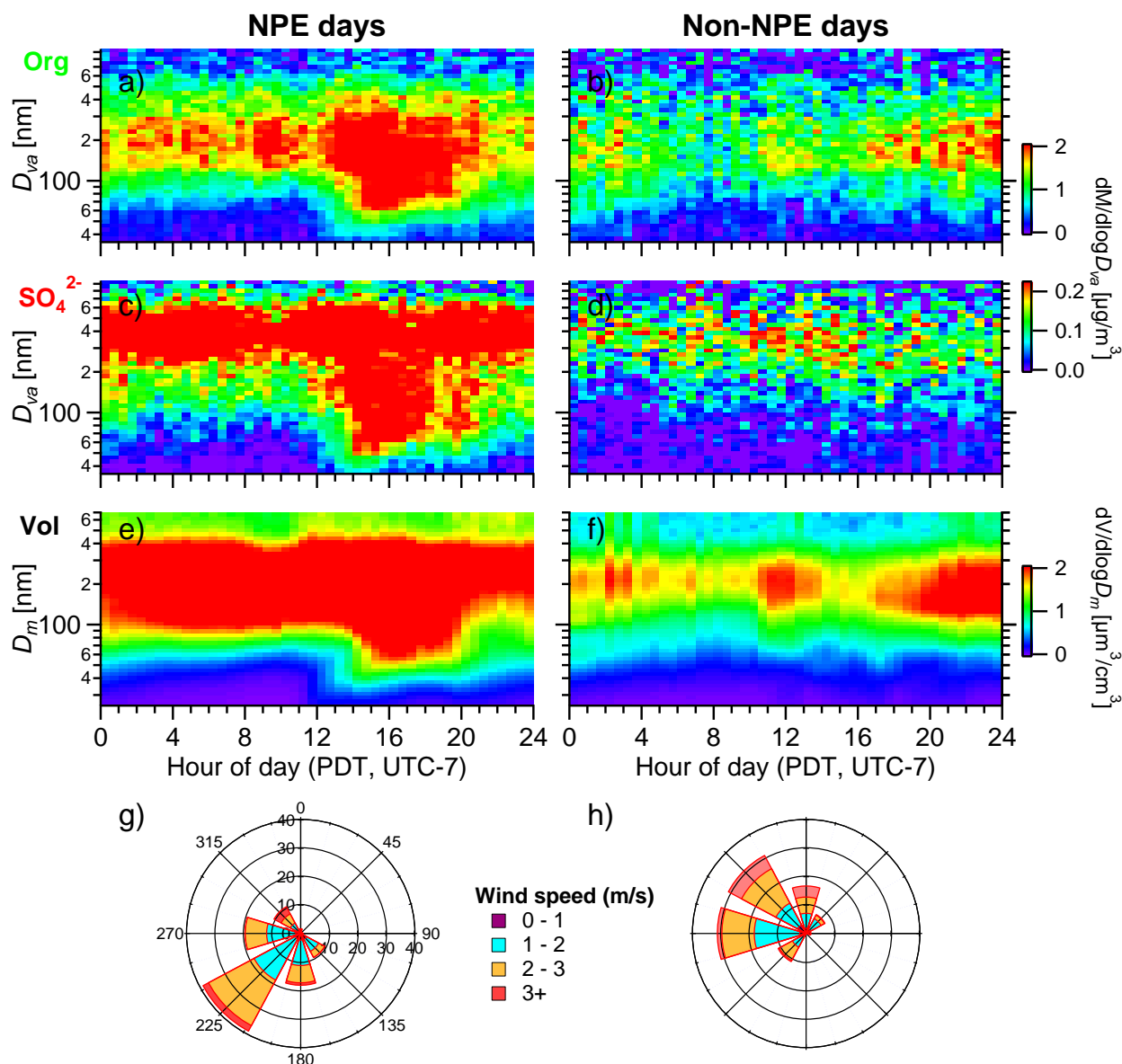
It is interesting to notice that the evolution of the size distributions and concentrations during the evening and the night is not similar at T0 and T1. Indeed, at T0, particle concentration remains almost constant between 23:00 and 8:00, while the mode is centered at ~35-40 nm (in D_m) during this period (Fig. 3-4a). On the contrary, particle concentration decreases gradually at T1 during night, while the mode increases from 35 nm (at 21:00) up to 90 nm (at 14:00 the following day; Fig. 3-4c). This may be due to the fact that the T0 site was more influenced by nanoparticles from vehicular emissions than the T1 site, due to the proximity of traffic, anthropogenic emissions, and transport from the Bay Area. On the other hand, the T1 site was more influenced by downslope winds during the night, when a change in the wind direction brought down more aged aerosols from the Sierra Nevada to the foothills [*A. Setyan et al.*, 2012].

3.3.2. Evolution of Particle Chemistry during New Particle Growth

The evolution of particle chemistry during NPE at the T1 site was studied in detail with an HR-ToF-AMS. As summarized in Table 3-1, the increase of particle number concentration during the new particle growth events was accompanied by an increase of organics and sulfate in ultrafine particles (40-120 nm in D_{va}). The average (± 1σ) increase of organics in that size range was 0.71 (± 0.29) μg/m^3 while that of sulfate was 0.10 (± 0.11) μg/m^3.

Fig. 3-5 shows the diurnal size distributions of organic matter, sulfate, and particle volume concentrations, along with the wind rose plots during new particle event and non-event days. The growth of new particles was mainly contributed by sulfate and organics (Fig. 3-5a and 3-5c), but the increase of particle mass observed by the AMS occurred after 11:00, later than the increase of number concentration according to the SPMS. This is because the smallest size measured by our SMPS is 8 nm (in D_m), while the transmission through the AMS is significant only for particles larger than 30 nm (in D_{va}) [*J. T. Jayne et al.*, 2000]. Given that particle density at T1 was on average 1.4 during this study [*A. Setyan et al.*, 2012], and assuming that they are spherical, the smallest particles measured by the AMS correspond to ~21 nm in D_m. Thus, the SMPS was the first instrument to detect the growth of new particles, while the HR-ToF-AMS observed the growth 2 or 3 hours later, depending on the growth rate. A similar observation was reported during NPE in Pittsburgh [*Zhang et al.*, 2004]. It is interesting to notice that organics, sulfate, and particle volume exhibit qualitatively the same diurnal size distributions (Fig. 3-5). Indeed, they have a constant mode in larger particles during the entire day, and they increase in ultrafine particles in the afternoon during the growth events.

Figure 3-6. *Diurnal patterns of (a, b) Org and (c, d) SO$_4^{2-}$ in the range 40-120, 120-200 and 200-800 nm (in D$_{va}$) during NPE days (left panel) and non-NPE days (right panel).*
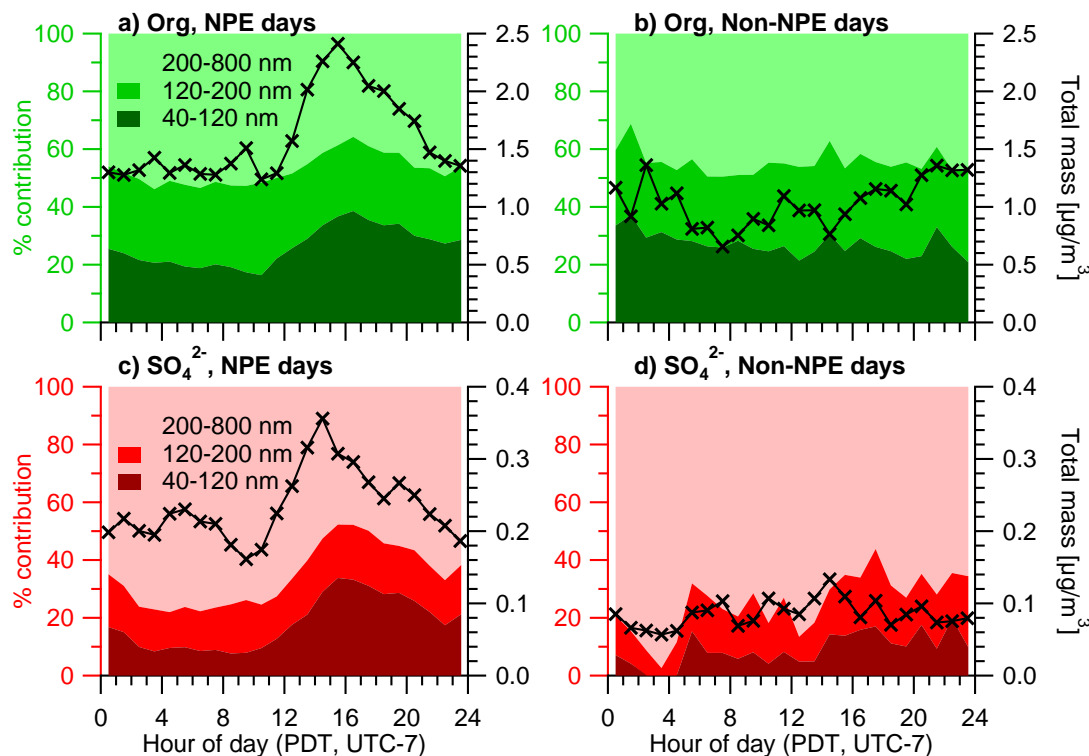
As shown in Fig. 3-6, the diurnal patterns of organics and sulfate in three different size ranges (40-120, 120-200 and 200-800 nm in D_{va}) show that their increase during the afternoon

occurred mainly in ultrafine particles (40-120 nm) while the increases in the rest of the sizes were very moderate during NPE days. In comparison, the diurnal profiles of both species are relatively flat and their concentrations much lower during the non-event days (Fig. 3-6b and 3-6d). Although both organics and sulfate in ultrafine particles increased in the afternoon, the increase of the organic mass in the 40-120 nm particles (average $\pm 1\sigma = 0.71 \pm 0.29$ µg/m^3) was on average 7 times higher than that of sulfate (0.10 ± 0.11 µg/m^3) (Fig. 3-6a and 3-6c). Clearly, the growth of new particles was mainly driven by organics. This is in agreement with previous studies, which also emphasized the key-role of organics in the growth of new particles up to CCN sizes [*Ahlm et al.*, 2012; *Laaksonen et al.*, 2008; *Pierce et al.*, 2012; *J. N. Smith et al.*, 2008; *Y M Zhang et al.*, 2011; *L. D. Ziemba et al.*, 2010]. Moreover, another important observation is the increase of nitrogen-containing ion signals by a factor of 2 during NPE (Fig. 3-7f). These ions are likely

Figure 3-7. *Diurnal patterns of (**a**) Org (40-120 nm), (**b**) SO$_4^{2-}$ (40-120 nm), (**c**) urban transport SOA, (**d**) biogenic SOA, (**e**) particle number (8-15 nm), and (**f**) amine ion during NPE and non-NPE days.*
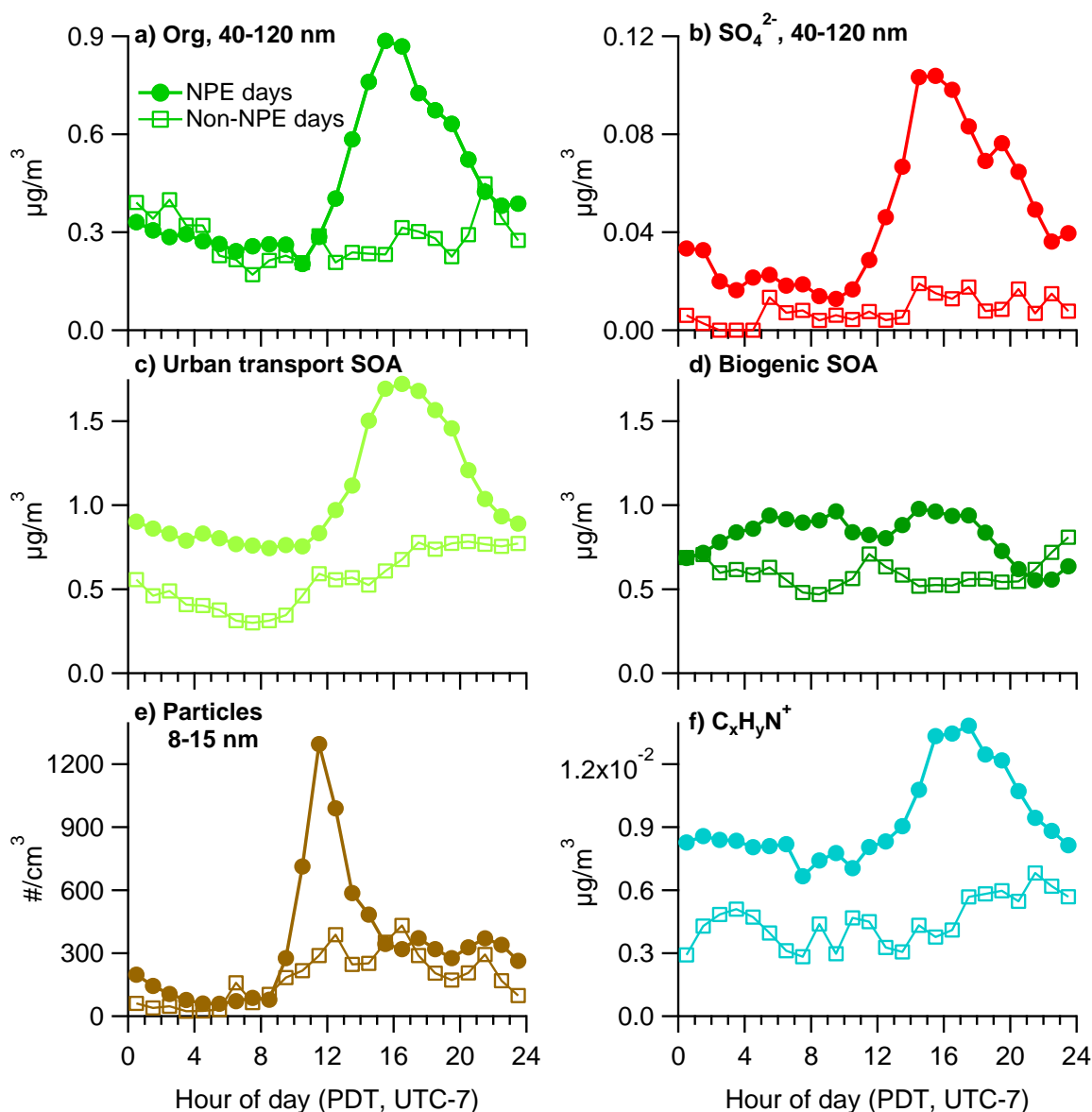
related to the presence of aminium species, suggesting that this class of compounds is involved in the formation and growth of new particles. This is also consistent with previous studies [*B. R. Bzdek et al.*, 2011; *Creamean et al.*, 2011; *Laitinen et al.*, 2011; e.g., *Makela et al.*, 2001; *J. N. Smith et al.*, 2008; *James N. Smith et al.*, 2010].Due to the high contribution of organics to submicron aerosol mass, thus its chemistry, in the region, positive matrix factorization (PMF) analysis was performed on the high resolution mass spectra of the AMS to investigate the sources and processes of organics [*A. Setyan et al.*, 2012]. Briefly, three distinct factors were determined, including a biogenically-influenced SOA (O/C ratio = 0.54, 40% of total organic mass), an anthropogenically-influenced SOA associated with urban plumes (O/C ratio = 0.42, 51%), and a hydrocarbon-like organic aerosol (HOA) mainly associated to local primary emissions (O/C ratio = 0.08, 9%). Details on the determination and validation of these three OA types are given in *A. Setyan et al.* [2012]. As shown in Fig. 3-7, during NPE days, urban transport SOA increased by more than a factor of 2 (from 0.8 to 1.7 $\mu g/m^3$) between 10:00 and 16:00 (Fig. 3-7c), while that of biogenic SOA remained almost constant during that period (Fig. 3-7d). This result underlines the key-role played by the urban plume from Sacramento in the NPE events at Sierra foothills.

Fig. 3-8 shows the evolutions of the size distributions of Org, SO_4^{2-}, organic tracer ions, and particle concentration during daytime. The average size distributions of Org and SO_4^{2-} during NPE days show significant increase of the concentration in the small mode (Fig. 3-8e and 3-8g). Org 43 (mostly $C_2H_3O^+$) and Org 44 (mostly CO_2^+) increased at the same time (Fig. 3-8i and 3-8k). Org 43 is the most important signal in the mass spectrum of the biogenic SOA (Fig. 3-11c), while Org 44 is the most prominent signal in that of the urban transport SOA (Fig. 3-11a). The simultaneous increase of both Org 43 and Org 44 during the growth of new particles suggests that anthropogenic and biogenic emissions influenced the growth. On the other hand, the increases of the concentrations of Org, SO_4^{2-}, Org 43, and Org 44 in the ultrafine size were all negligible during non-event days.

An important parameter to determine was the neutralization of sulfate in the ultrafine mode during NPE. We already know from the mass spectral mode of the AMS that sulfate was fully neutralized in the bulk during the entire study [*A. Setyan et al.*, 2012]. Many previous studies mentioned that sulfate involved in NPE was usually under the form of sulfuric acid, especially during the initial steps of the growth [*Brock et al.*, 2003; *Bryan R. Bzdek et al.*, 2012; *Yue et al.*, 2010; *Zhang et al.*, 2004]. However, northern California contains very large agricultural regions with a lot of sources of ammonia, which could possibly neutralize quickly sulfate in the ultrafine mode. Unfortunately, PToF data of ammonium in unit mass resolution was too noisy and not usable to determine the time evolution of ammonium in ultrafine particles. Therefore, we used PToF data in high resolution, and determined the size distributions of ammonium and sulfate based on those of the NH_3^+ and SO^+, which are the ions of ammonium and sulfate, respectively, with the highest signal-to-noise ratio. Then, we used the scatterplots of NH_3^+ vs. total ammonium and SO^+ vs. total sulfate to reconstruct the size distributions of ammonium and sulfate (details of this data treatment are given in Appendix 3-A).

As show in Fig. 3-9, despite relatively noisy data, the different size distributions suggest that sulfate was fully neutralized by ammonium in the entire size range, including ultrafine particles. Moreover, we did not observe any difference in the sulfate neutralization between NPE and non NPE days or between different times of the day. These results suggest that sulfate in ultrafine particles was under the form of ammonium sulfate and that sulfuric acid was quickly neutralized after condensation.

Figure 3-8. *2-hour averaged size distributions of particle number (**a, b**) and volume (**c, d**), SO$_4^{2-}$ (**e, f**), Org (**g, h**), Org 43 (**i, j**), and Org 44 (**k, l**) during NPE days and non-NPE days between 8:00 and 18:00.*
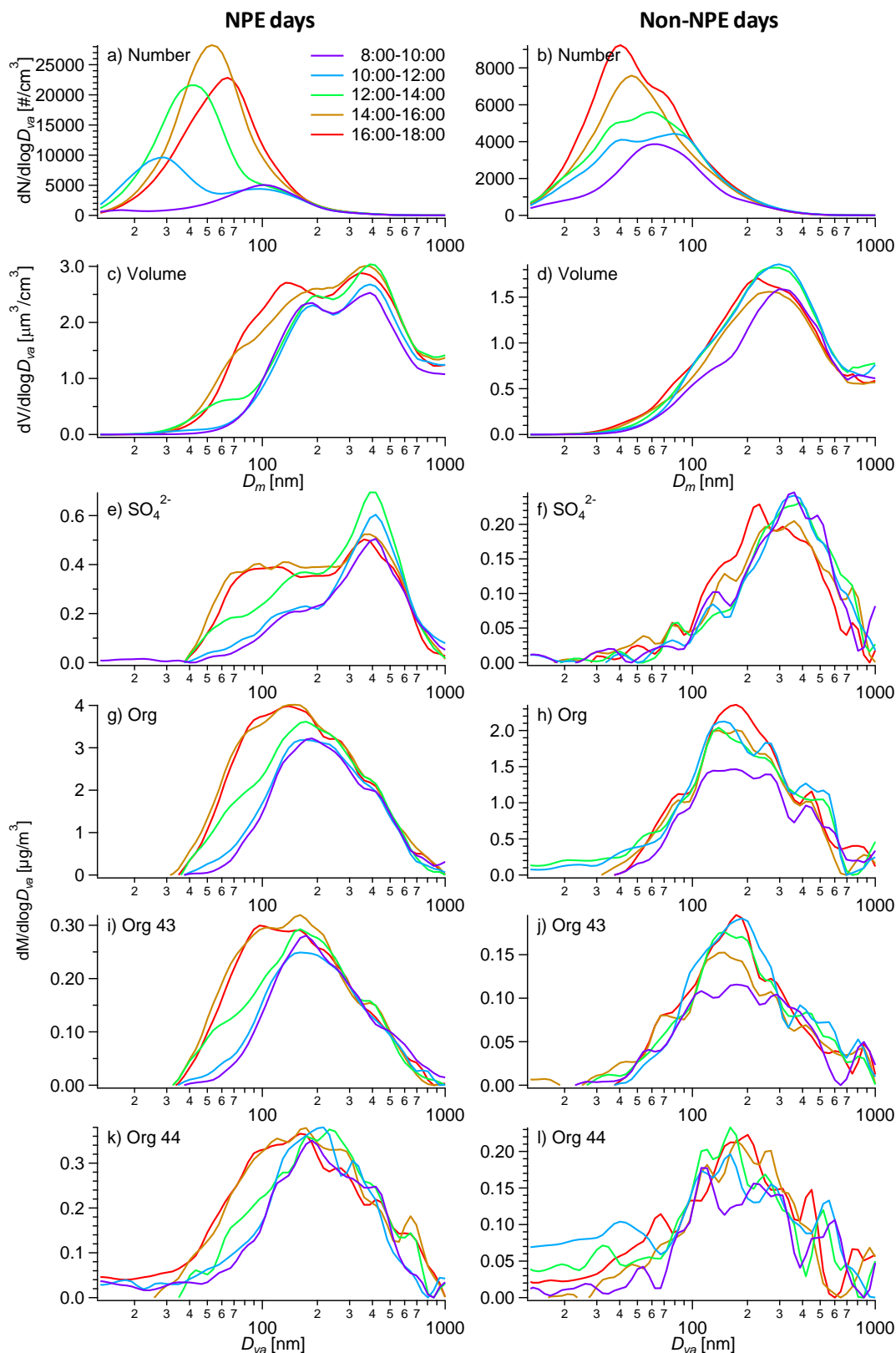
Figure 3-9. *Size distributions of SO_4^{2-}, NH_4^+ and NH_4^+ measured/NH_4^+ predicted ratio between 6:00-7:00 (**a, b**), 10:00-11:00 (**c, d**), 14:00-15:00 (**e, f**), and 18:00-19:00 (**g, h**) during new particle event (NPE; left panels) and non-NPE (right panels) days.*
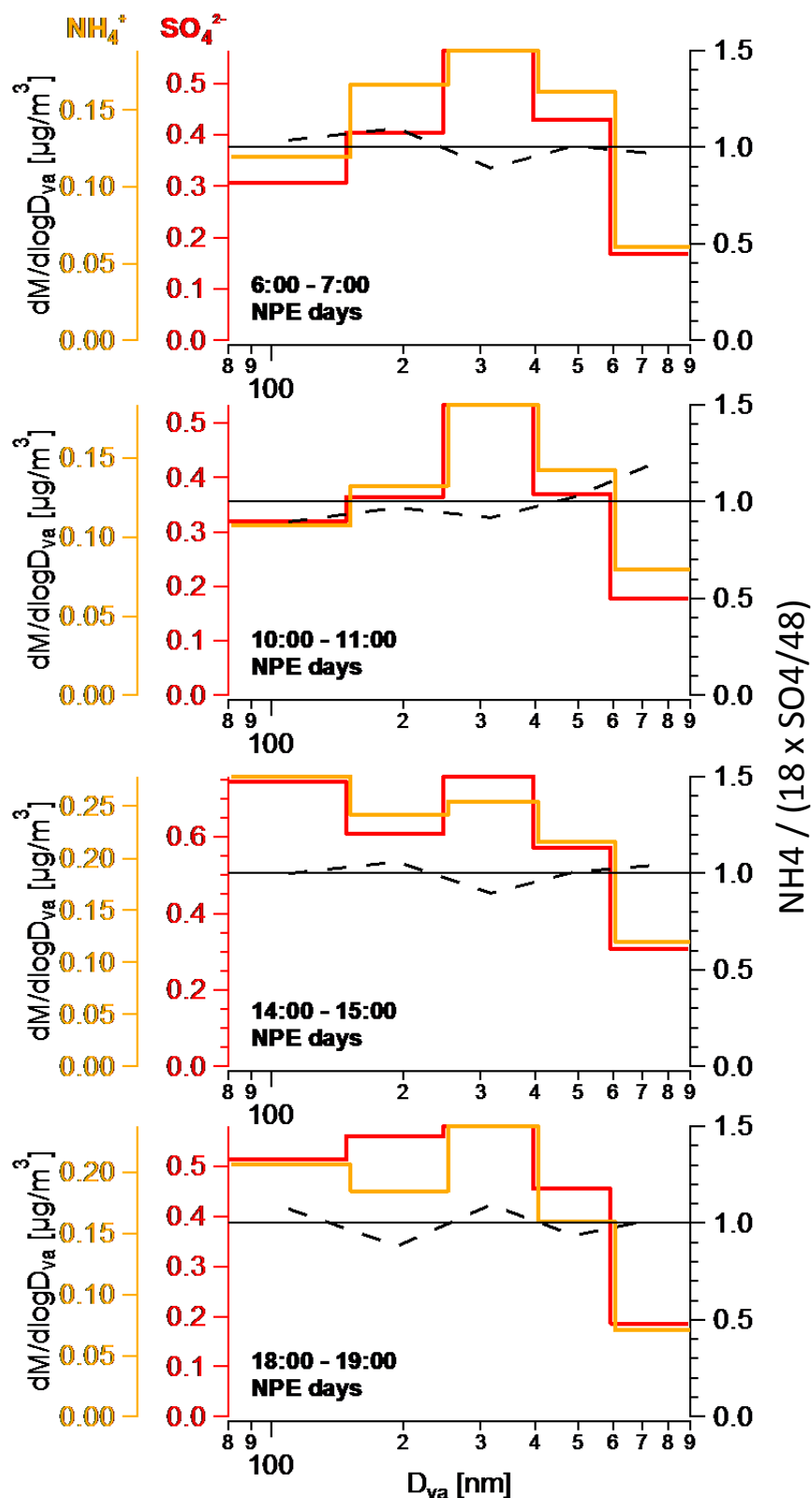
3.3.3. Anthropogenic Influence on New Particle Growth Events

Fig. 3-10, 3-11, and 3-12, and Table 3-2 compare average concentrations and diurnal patterns of VOCs, trace gases (O_3, CO), BC, and meteorological parameters (temperature, relative humidity and solar radiation) during new particle growth event and non-event days. The most important differences between NPE and non-event days were the concentrations of photo-oxidation products (formaldehyde, acetaldehyde, sum of methacrolein and methyl vinyl ketone) and anthropogenic precursors (BC, CO and toluene), which were all much higher during NPE days than during non-event days. Photo-oxidation products were on average ~1.5 times more concentrated on NPE days (formaldehyde: 2.71 ± 1.39 ppb, vs. 1.83 ± 0.81 ppb during non-NPE days; acetaldehyde: 0.97 ± 0.47 ppb, vs. 0.71 ± 0.24 ppb; sum of methacrolein and methyl vinyl ketone: 0.98 ± 0.79 ppb, vs. 0.75 ± 0.50 ppb), which suggests that the condensation of these compounds onto the surface of particles could be an important factor driving the growth of new particles.

*Figure 3-10. (**b**) Average concentrations of VOCs, O_3, CO, BC, NR-PM$_1$ species, and different OA factors between 8:00 and 18:00 (PDT) during NPE and Non-NPE days. (**a**) NPE days / Non-NPE days ratios for the same parameters.*
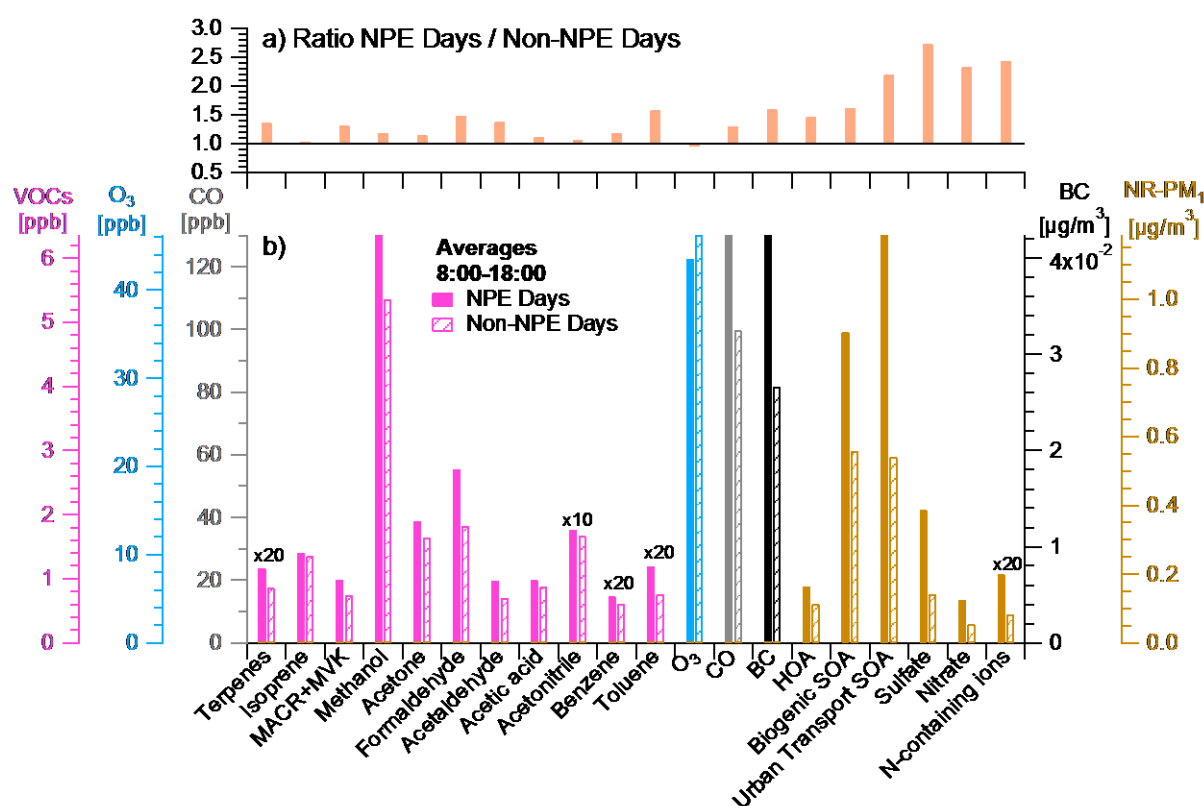
Moreover, the diurnal patterns of these compounds during NPE and non-NPE days (Fig. 3-12) show a clear difference during the afternoon, while these differences are much smaller during nighttime. This result stresses the influence of photochemistry in the formation of new particles. BC (0.042 ± 0.028 µg m^{-3} during NPG days, vs. 0.027 ± 0.017 µg m^{-3} during non-NPE days), CO (130.1 ± 27.0 ppb vs. 99.8 ± 19.8 ppb) and toluene (0.060 ± 0.037 ppb vs. 0.038 ± 0.019 ppb; Table 3-2) were also on average 1.5 times higher on NPE days. The ozone

concentrations, however, are very similar between two types of days (46.2 ± 10.5 ppb during non-NPG vs. 43.5 ± 14.2 ppb). These results point out the importance of the anthropogenic influence on the formation and growth of new particles, most of these events occurring in the urban plume from Sacramento. However, during a study undertaken at the Blodgett Forest, which is located ~35 km on the northeast of the present sampling site and ~75 km downwind from Sacramento, *Lunden et al.* [2006] observed new particle growth events when the degree of anthropogenic influence was significantly reduced.

Figure 3-11. *Diurnal patterns of (**a**) temperature, (**b**) relative humidity, and (**c**) broadband solar radiation during new particle event (NPE) days and non-NPE days.*
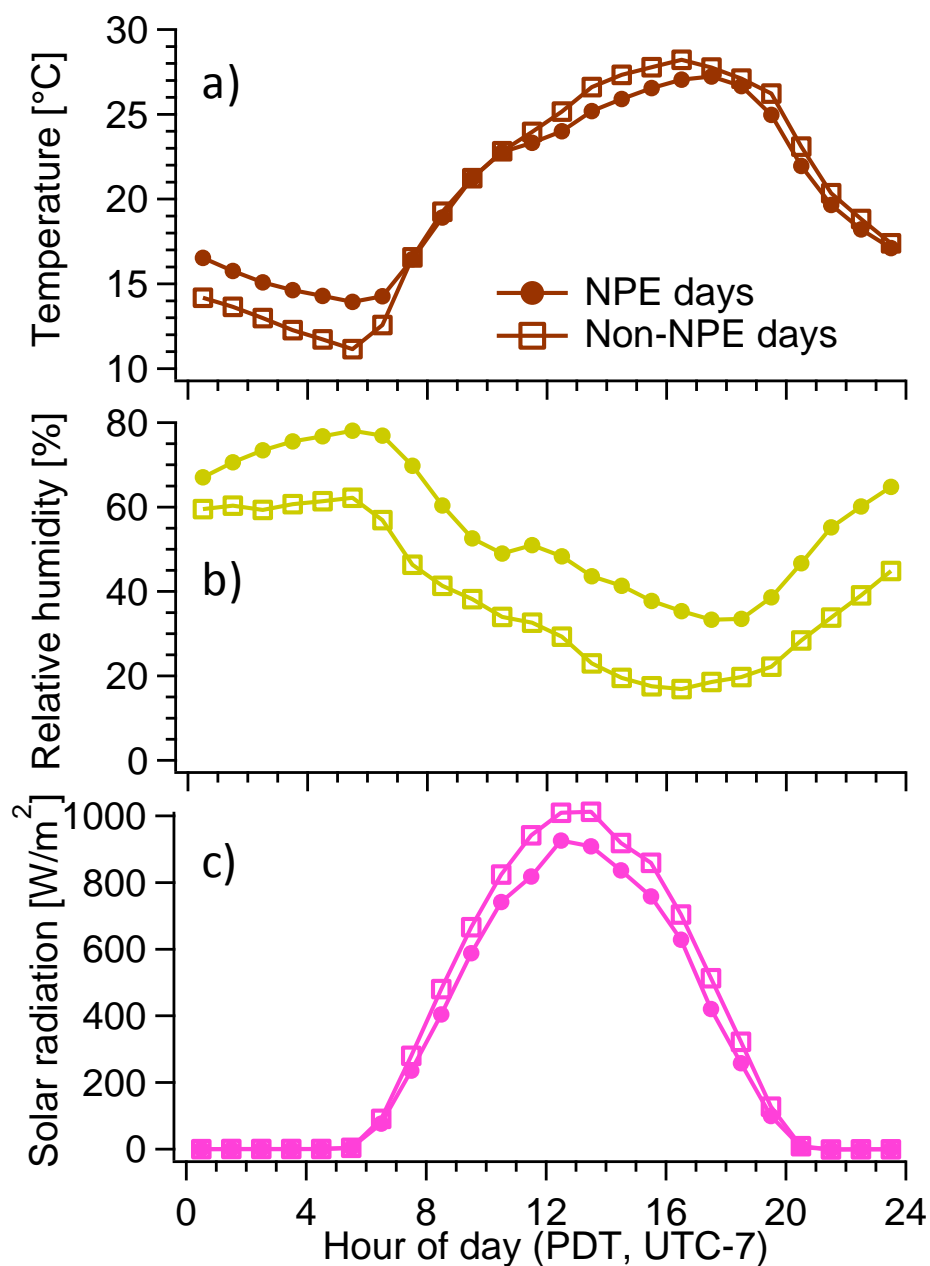
Figure 3-12. *Diurnal patterns of (**a**) isoprene, (**b**) terpenes, (**c**) sum of methacrolein (MACR) and methyl vinyl ketone (MVK), (**d**) formaldehyde, (**e**) acetic acid, (**f**) acetaldehyde, (**g**) benzene, (**h**) toluene, (**i**) black carbon, (**j**) CO, (**k**) O_3, and (**l**) NO_x, during NPE and non-NPE days.*
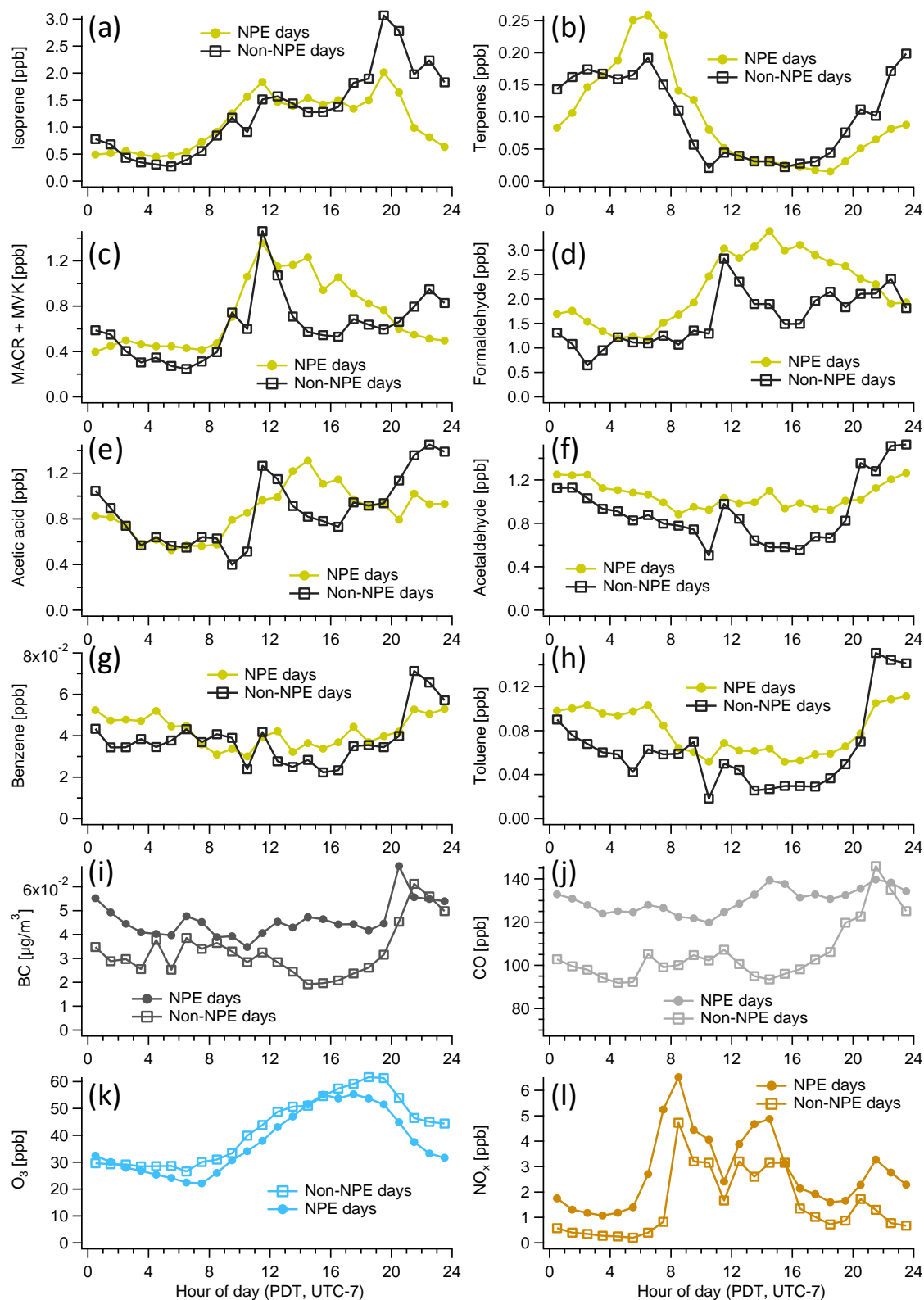
Table 3-2. *Summary of average value ± 1 standard deviation for meteorological parameters, particle phase species, and gaseous species during new particle event (NPE) and non-NPE days at the T1 site between 8:00 and 18:00 PDT.*

Parameter	NPE days	Non-NPE days
Meteorological data		
Temperature (^{o}C)	24.2 ± 4.4	25.0 ± 4.1
Relative humidity (%)	45.3 ± 12.6	27.1 ± 12.1
Solar radiation (W m^{-2})	702.9 ± 246.1	792.7 ± 200.4
Particle phase		
Particle number (# cm^{-3})	9.4E3 ± 6.1E3	4.1E3 ± 1.9E3
Growth rate (nm/hr)	6.2 ± 2.5	-
Biogenic SOA (µg m^{-3})	0.90 ± 0.65	0.56 ± 0.27
Urban transport SOA (µg m^{-3})	1.2 ± 0.90	0.54 ± 0.44
HOA (µg m^{-3})	0.16 ± 0.15	0.11 ± 0.08
SO_4^{2-} (µg m^{-3})	0.39 ± 0.22	0.14 ± 0.10
NO_3^- (µg m^{-3})	0.13 ± 0.08	0.054 ± 0.036
BC (µg m^{-3})	0.042 ± 0.028	0.027 ± 0.017
Trace gases (ppb)		
Terpenes	0.058 ± 0.088	0.043 ± 0.034
Isoprene	1.40 ± 1.02	1.35 ± 0.80
MACR + MVK	0.98 ± 0.79	0.75 ± 0.50
Methanol	6.36 ± 3.12	5.36 ± 1.76
Acetone	1.90 ± 1.09	1.64 ± 0.42
Formaldehyde	2.71 ± 1.39	1.83 ± 0.81
Acetaldehyde	0.97 ± 0.47	0.71 ± 0.24
Acetic acid	0.98 ± 1.10	0.87 ± 0.43
Acetonitrile	0.18 ± 0.03	0.17 ± 0.02
Benzene	0.036 ± 0.029	0.031 ± 0.014
Toluene	0.060 ± 0.037	0.038 ± 0.019
O_3	43.5 ± 14.2	46.2 ± 10.5
CO	130.1 ± 27.0	99.8 ± 19.8

It is interesting to note that the relative humidity (RH) was on average 18% higher the days when new particle growth was observed (45.3 ± 12.6 %) compared to non-event days (27.1 ± 12.1 %). Previous studies, however, found contradictory links between new particle growth events and RH. For example, *Lunden et al.* [2006] and *Charron et al.* [2007] observed growth events when RH was high, while non-event days were characterized by significantly lower RH. In addition, most of the previous studies reported NPE when the RH was low [*Boy and Kulmala*, 2002; *Guo et al.*, 2012; *Hamed et al.*, 2011; *Hamed et al.*, 2007; *Jeong et al.*, 2010]. The exact role of RH in new particle formation and growth is not clearly elucidated yet. According to *Hamed et al.* [2011], who used a combination of field data, theoretical calculations and numerical models, the anticorrelation between RH and new particle growth would simply be due to the fact that solar radiation and photochemistry usually peak at noon when the RH exhibits its lower value. However, this does not seem to have influenced the growth events of the present study, since the weather was sunny during the entire field campaign. The only point is that the

RH was much lower during northwesterly wind periods [*A. Setyan et al.*, 2012], during which we usually did not observe growth events.

Fig. 3-13 shows the average size-resolved mass spectra of organics in the range 40-120 nm (D_{va}) during NPE days and non-event days, along with the mass spectra of biogenic SOA and urban transport SOA reported in Setyan et al. [*A. Setyan et al.*, 2012]. The average mass spectrum of organics before the growth (i.e., between 8:00 and 11:00) has been subtracted in order to remove the influence of particles existing before the start of the growth events. We notice that the mass spectrum of organics in the range 40-120 nm (D_{va}) during the growth is dominated by the signal at m/z 44 (mostly CO_2^+), while that of m/z 43 (mostly $C_2H_3O^+$) is approximately the half of it (Fig. 3-13a). We also notice that the average mass spectrum of organics during the growth is very similar to that of the urban transport SOA (Fig. 3-13a). This is confirmed with the scatterplot of Fig. 3-13b, which shows that the spectrum during the growth is very similar to that of urban transport SOA ($r^2 = 0.95$), while its correlation coefficient towards the mass spectrum of biogenic SOA is lower ($r^2 = 0.87$). On the other hand, the average mass spectrum of organics on non-event days is very similar to that of biogenic SOA, as shown by the scatterplot of Fig. 3-13d. These results, coupled to the higher concentrations of anthropogenic compounds on NPE days suggest that the growth of new particles at the T1 site was mainly driven by the interaction between anthropogenic precursors transported from Sacramento and biogenic emissions.

Figure 3-13. *Average mass spectra of (**a**) urban transport SOA and Org$_{40-120nm}$ (i.e., organics in 40-120 nm particles) during NPE days, and (**c**) biogenic SOA and Org$_{40-120nm}$ during Non-NPE days. Scatterplots that compare the mass spectra of (**b**) urban transport SOA vs. Org$_{40-120nm}$ during NPE days, and (**d**) biogenic SOA vs. Org$_{40-120nm}$ during non-NPE days.*
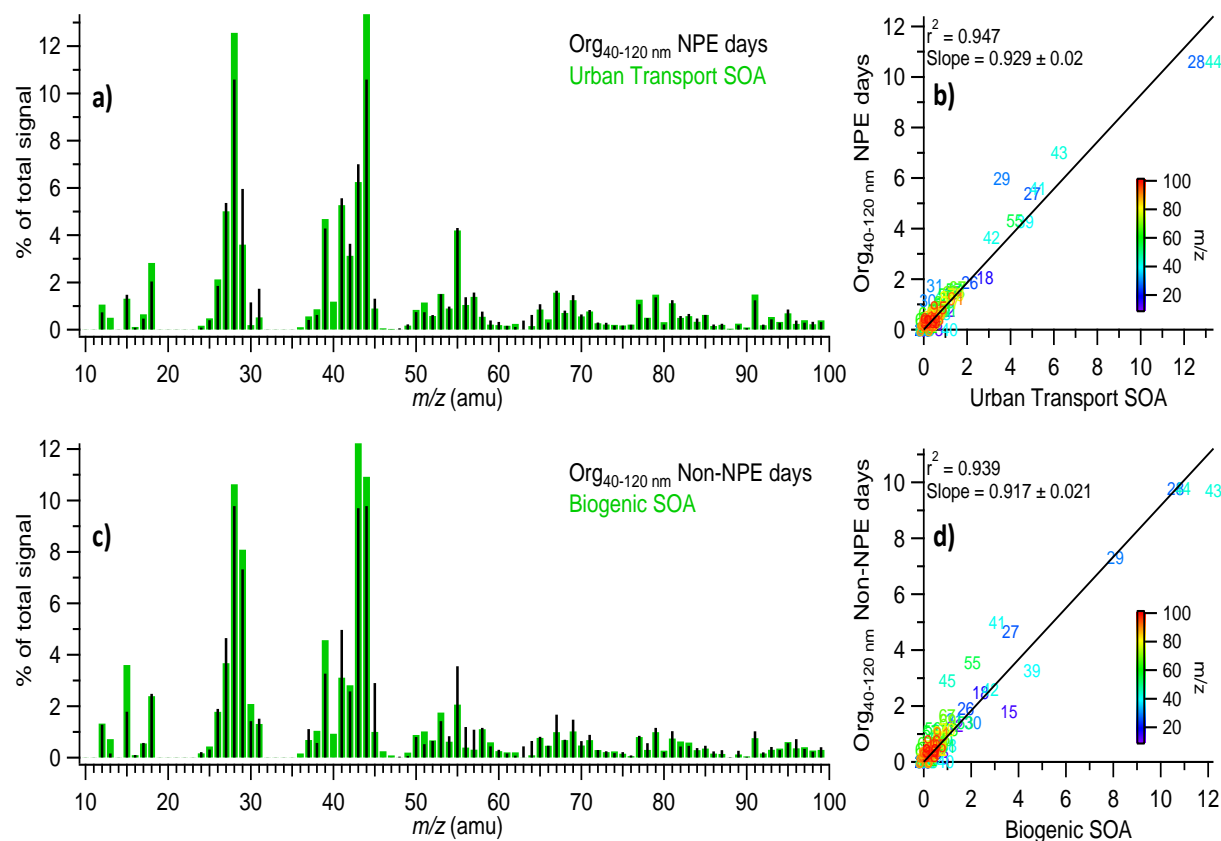
3.4. Conclusions

New particle growth events were frequently observed during the US DOE's CARES campaign in June 2010. Presented here is a description of these events observed with an SMPS deployed at Sacramento (T0, urban site) and Cool (T1, rural site at the Sierra foothills) in northern California. Our results showed that these growth events took place on a regional scale, predominantly during periods of dominant southwestern flow that transports urban plumes and anthropogenic emissions from the Sacramento metropolitan area and the San Francisco Bay Area near Carquinez Strait. Growth rates were on average higher at T0 (7.1 ± 2.7 nm/hr) than at T1 (6.2 ± 2.5 nm/hr), due to higher anthropogenic influences at T0. The evolution of the chemical composition and size distribution of these newly formed particles has been investigated in detail with an HR-ToF-AMS deployed at T1. Our results indicate that the new particle growth was mainly driven by organics, with a small contribution of ammonium sulfate. For example, the average increase of the organic mass in ultrafine particles (40-120 nm in D_{va}, which corresponds to 30-85 nm in physical diameter, assuming no internal voids, sphericity = 1, and density = 1.4 g/cm^3) was 0.7 µg/m^3 during this period, approximately 7 times higher than that of sulfate (0.1 µg/m^3). Our results also indicate that aminium concentration was enhanced during the new particle growth. The size-resolved mass spectra of organics in the size range 40-120 nm (in D_{va}) during the growth events were very similar to the mass spectrum of anthropogenically-influenced SOA from urban plume. In addition, during the new particle growth event days, the concentrations of photo-oxidation products (formaldehyde, acetaldehyde, sum of methacrolein and methyl vinyl ketone) and species representative of urban emissions (e.g., BC, CO and toluene) were on average 1.5 - 2 times higher than during non-event days. These results suggest that new particle growth events were promoted by the interaction between biogenic emissions and transported urban plumes.

3.5. Appendix A – Determination of the Size Distributions of Ammonium and Sulfate Using High Resolution Data

PToF data in AMS is usually used in unit mass resolution to determine size distributions of species. However, during the present study, PToF data of ammonium was too noisy and not usable to determine size distributions for short selected periods. Therefore, in the present case, PToF data has been used in high resolution, in which ammonium fragments had satisfactory signal to noise (S/N) ratios. First, 86 size bins recorded in the PToF mode and covering 40-1400 nm (in D_{va}) have been grouped into 7 different size ranges in order to increase the S/N ratio. Given that the PToF data processed in the PIKA software is without DC markers applied, an eighth size range between 1400-2200 nm has been used as a background signal to subtract the signals of the other size ranges (Fig. 3-A1). Then, for each size range, average high resolution mass spectra have been plotted, and the signals of the ammonium and sulfate fragments having the best S/N ratios have been integrated. For that purpose, we chose NH_3^+ (m/z 17) for ammonium and SO^+ (m/z 48) for sulfate (Fig. 3-A1). The scatterplots of NH_3^+ vs. total ammonium and SO^+ vs. total sulfate (Fig. 3-A2) have then been used to reconstruct the concentrations of ammonium and sulfate for each of the 7 size ranges. Finally, these results have been used to reconstruct size distributions of the two species in Hz, and converted to µg/m^3 by scaling the size distributions to the concentrations of these species in MS mode.

***Figure 3-A1.*** *Average high resolution mass spectra between 14:00-15:00 during NPE days for particles in the range 250-400 nm (**a, b**), 1400-2200 nm (**c, d**), and top MS minus bottom MS (**e, f**).*
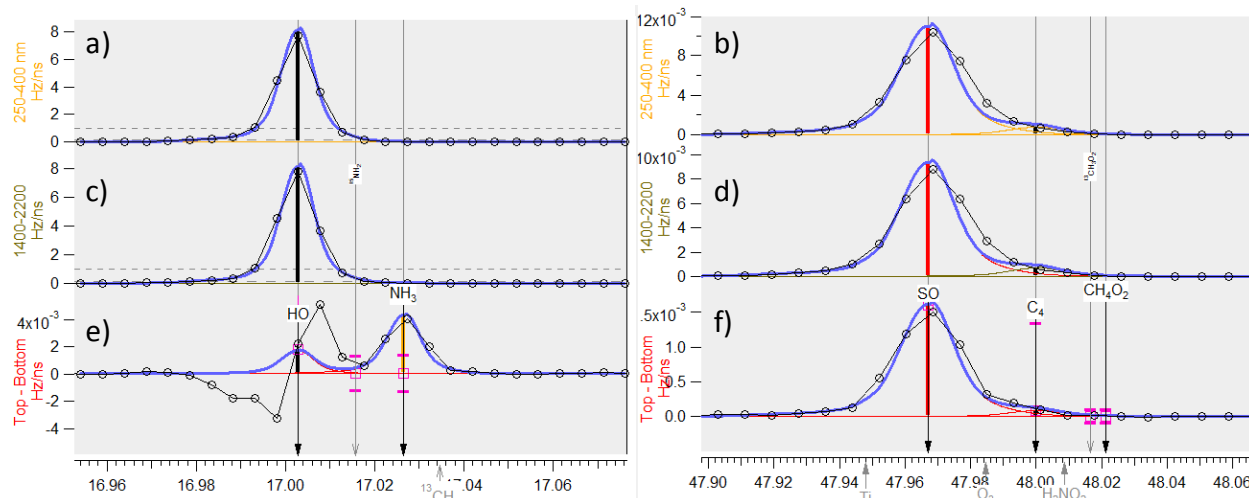
Figure 3-A2. *Scatterplots of (**a**) NH_3^+ vs. total ammonium, and (**b**) SO^+ vs. total sulfate. The data fitting was performed using the orthogonal distance regression (ODR).*
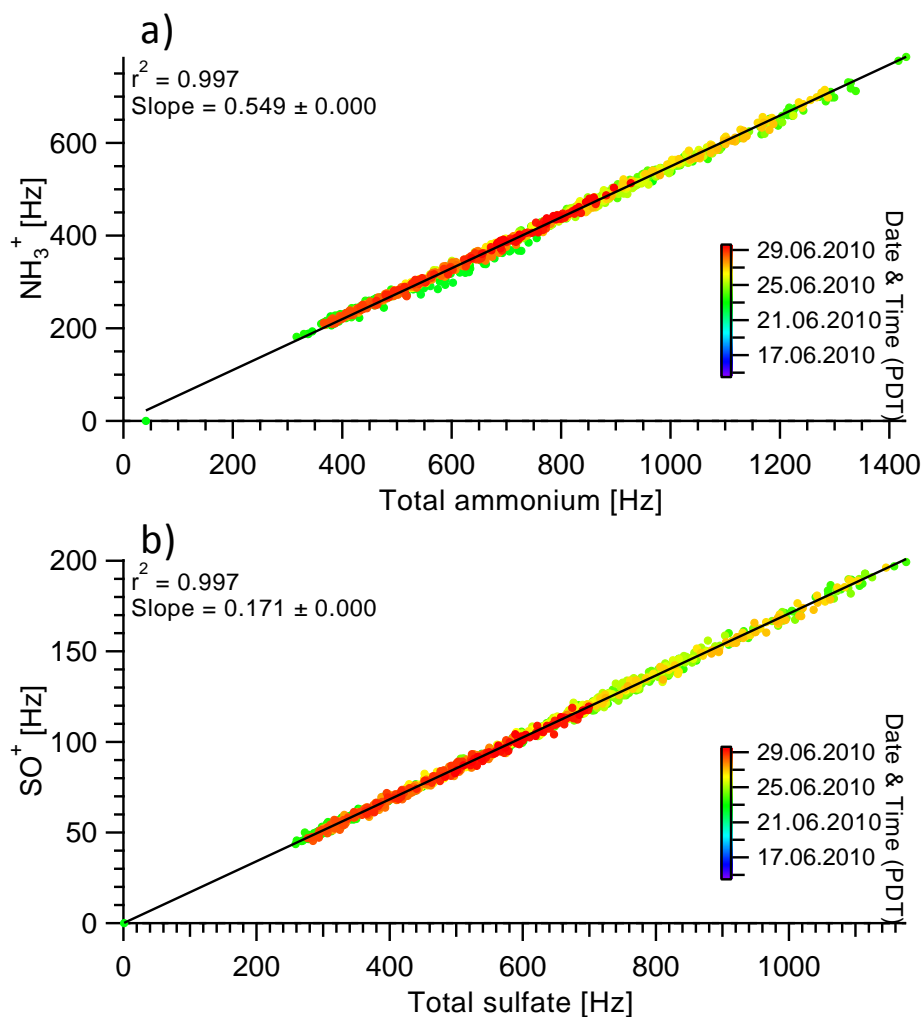
4. SUMMARY AND CONCLUSIONS

The US DOE's Carbonaceous Aerosol Radiative Study (CARES) field campaign took place in the Sacramento valley air basin of California in June 2010. A wide range of instruments were deployed simultaneous at two ground sites located in Sacramento (T0, urban site) and Cool at the foothills of the Sierra Nevada Mountains (T1, rural site) to measure aerosol chemical composition, size distribution, and optical and hygroscopic properties, as well as trace gases and meteorological data [*Zaveri et al.*, 2012b]. In this project, we performed thorough analyses of the data acquired with a high-resolution time-of-flight aerosol mass spectrometer and a scanning mobility particle sizer deployed at the T1 site. The sources and processes of submicrometer particles over the Sierra foothills region were interpreted based on these results, together with measurement data of meteorological conditions, trace gases, and other particle species (e.g., black carbon) at T1. Aerosol data acquired at the T0 site were also included in this analysis to better understand aerosol processing on a regional scale. Our primary goals are to achieve a process-level understanding of organic aerosols in Northern California and to bridge between observations and models via synthesizing and translating the results and insights generated from this research into data products and formulations that may be directly used to inform and evaluate air quality models.

Particles were dominated by organics over the Sacramento and western Sierra Foothills area. The average mass loading of PM_1 at T1 in June 2010 was 3.0 μg m^{-3} and the average composition of PM_1 was 80% organics, 9.9% sulfate, 4.5% ammonium, 3.6% nitrate, 1.6% black carbon, and 0.1% nonrefractory chloride. Ammonium appeared to be in charge balance with observed anions (sum of SO_4^{2-} + NO_3^- + Cl^-) in particles, indicating that sulfate was mainly present in the form of $(NH_4)_2SO_4$. The average mass-based size distribution of particles indicated that sulfate was mainly present in the accumulation mode (D_{va} 200-600 nm) whereas organics showed broader distributions peaking at smaller sizes.

The T1 site was located at the foothills of the Sierra Nevada Mountains, where biogenic emissions from forests are periodically mixed with urban outflow from the Sacramento metropolitan area and the Bay Area transported by consistent southwest winds from Sacramento. This regular wind pattern has allowed us to study SOA formation in mixed anthropogenic and biogenic emissions. We performed positive matrix factorization to the high resolution mass spectra and identified three distinct OA factors, including two OOA types that appeared to be different oxidation (together representing 91% of total organic mass) and an HOA (9% of the organic mass). The more oxidized MO-OOA (O/C = 0.54) was found to represent biogenically influenced SOA, while the less oxidized LO-OOA (O/C = 0.42) corresponded to anthropogenically influenced SOA mainly formed in the air mass transported from the Sacramento area. The HOA factor corresponded to primary emissions from local sources.

The diurnal variation patterns of LO-OOA, ozone, and sulfate were very similar and all showed substantial daytime increases consistent with impacts from urban transport. However, the time series of LO-OOA and sulfate were poorly correlated, indicating different source regions of their precursor species and different formation mechanisms. For instance, the prominent droplet mode of sulfate and the tight correlation between sulfate and methanesulfonic acid indicate a significant influence of aqueous-phase reactions on sulfate production. A large fraction of this droplet mode may come from the San Francisco Bay Area, where oil refineries are the largest SO_2 sources identified in northern California and where aqueous reactions would have been promoted by fogs and low clouds during morning hours around the Bay Area. The

good correlations observed between MO-OOA and first generation isoprene photooxidation products (MVK and MACR) and between LO-OOA and ozone suggest that both SOA types were relatively fresh, which were consistent with their relatively low O/C ratios.

23 periods of urban plumes from T0 (Sacramento) to T1 (Cool) were identified using the WRF-Chem model. The average chemical composition of aerosols was overall similar in different air masses. PM_1 mass loading, however, was more than twice higher during the T0 to T1 transport periods than during northwesterly wind periods (3.9 vs. 1.8 μg/m^3). In addition, a second mode of sulfate in small sizes (D_{va} 100-150 nm) became conspicuous during the T0 to T1 transport periods, due to the frequent occurrence of new particle growth events in urban plumes. This mode was less obvious in air masses dominated by biogenic SOAs and almost disappeared during northwesterly wind periods. ΔOA/ΔCO, an indicator for SOA production, varied in the range of 5-196 μg/m^3/ppm during this study. Enhanced SOA formation was observed when urban emissions from Sacramento arrived at T1 and interacted with biogenic precursors. Moreover, the largest SOA formation was observed in urban plumes mixed with a high concentration of biogenic VOCs. For example, in air masses influenced by urban emissions, ΔOA/ΔCO values were on average above 90 μg/m^3/ppm in the presence of high biogenic VOCs (> 2 ppb), compared to 36 μg/m^3/ppm at low biogenic VOCs (< 0.7 ppb). The average ΔOA/ΔCO was 30 - 35 μg/m^3/ppm in air masses dominated by biogenic SOA with little anthropogenic influence (i.e., during the northwesterly wind periods).

During this study, new particle events were frequently observed at both T0 and T1, indicating that these events took place on a regional scale, predominantly during periods of dominant southwestern flow that transports urban plumes and anthropogenic emissions from the Sacramento metropolitan area and the San Francisco Bay Area near Carquinez Strait. Growth rates were on average higher at T0 (7.1±2.7 nm/hr) than at T1 (6.2±2.5 nm/hr), due to higher anthropogenic influences at T0. The evolution of the chemical composition and size distribution of these newly formed particles has been investigated in detail with an HR-ToF-AMS deployed at T1.

Our results indicate that the new particle growth was mainly driven by organics, with a small contribution of ammonium sulfate. For example, the average increase of the organic mass in ultrafine particles (40-120 nm in D_{va}, which corresponds to 30-85 nm in physical diameter, assuming no internal voids, sphericity = 1, and density = 1.4 g/cm^3) was 0.7 μg/m^3 during this period, approximately 7 times higher than that of sulfate (0.1 μg/m^3). Our results also indicate that aminium concentration was enhanced during the new particle growth. The size-resolved mass spectra of organics in the size range 40-120 nm (in D_{va}) during the growth events were very similar to the mass spectrum of anthropogenically-influenced SOA from urban plume. In addition, during the new particle growth event days, the concentrations of photo-oxidation products (formaldehyde, acetaldehyde, sum of methacrolein and methyl vinyl ketone) and species representative of urban emissions (e.g., BC, CO and toluene) were on average 1.5 - 2 times higher than during non-event days. These results suggest that new particle growth events were promoted by the interaction between biogenic emissions and transported urban plumes.

5. REFERENCES

IPCC: Summary for Policymakers, in Climate Change 2007: The Physical Science Basis. Contribution of Working Group I to the Fourth Assessment Report of the Intergovernmental Panel on Climate Change, edited by S. Solomon, D. Qin, M. Manning, Z. Chen, M. Marquis, K.

B. Averyt, M.Tignor and H. L. Miller, Cambridge University Press, Cambridge, United Kingdom and New York, NY, USA.

Ahlm, L., S. Liu, D. A. Day, L. M. Russell, R. Weber, D. R. Gentner, A. H. Goldstein, J. P. DiGangi, S. B. Henry, F. N. Keutsch, T. C. VandenBoer, M. Z. Markovic, J. G. Murphy, X. Ren, and S. Scheller (2012), Formation and growth of ultrafine particles from secondary sources in Bakersfield, California, J. Geophys. Res., 117, D00V08, 10.1029/2011jd017144

Aiken, A. C., P. F. DeCarlo, and J. L. Jimenez (2007), Elemental analysis of organic species with electron ionization high-resolution mass spectrometry, Analytical Chemistry, 10.1021/ac071150w,

Aiken, A. C., B. de Foy, C. Wiedinmyer, P. F. DeCarlo, I. M. Ulbrich, M. N. Wehrli, S. Szidat, A. S. H. Prevot, J. Noda, L. Wacker, R. Volkamer, E. Fortner, J. Wang, A. Laskin, V. Shutthanandan, J. Zheng, R. Zhang, G. Paredes-Miranda, W. P. Arnott, L. T. Molina, G. Sosa, X. Querol, and J. L. Jimenez (2010), Mexico city aerosol analysis during MILAGRO using high resolution aerosol mass spectrometry at the urban supersite (T0) - Part 2: Analysis of the biomass burning contribution and the non-fossil carbon fraction, Atmos. Chem. Phys., 10(12), 5315-5341, 10.5194/acp-10-5315-2010

Aiken, A. C., P. F. Decarlo, J. H. Kroll, D. R. Worsnop, J. A. Huffman, K. S. Docherty, I. M. Ulbrich, C. Mohr, J. R. Kimmel, D. Sueper, Y. Sun, Q. Zhang, A. Trimborn, M. Northway, P. J. Ziemann, M. R. Canagaratna, T. B. Onasch, M. R. Alfarra, A. S. H. Prevot, J. Dommen, J. Duplissy, A. Metzger, U. Baltensperger, and J. L. Jimenez (2008), O/C and OM/OC ratios of primary, secondary, and ambient organic aerosols with high-resolution time-of-flight aerosol mass spectrometry, Environ. Sci. Technol., 42(12), 4478-4485, 10.1021/es703009q

Aiken, A. C., D. Salcedo, M. J. Cubison, J. A. Huffman, P. F. DeCarlo, I. M. Ulbrich, K. S. Docherty, D. Sueper, J. R. Kimmel, D. R. Worsnop, A. Trimborn, M. Northway, E. A. Stone, J. J. Schauer, R. M. Volkamer, E. Fortner, B. de Foy, J. Wang, A. Laskin, V. Shutthanandan, J. Zheng, R. Zhang, J. Gaffney, N. A. Marley, G. Paredes-Miranda, W. P. Arnott, L. T. Molina, G. Sosa, and J. L. Jimenez (2009a), Mexico City aerosol analysis during MILAGRO using high resolution aerosol mass spectrometry at the urban supersite (T0) - Part 1: Fine particle composition and organic source apportionment, Atmos. Chem. Phys., 9(17), 6633-6653,

Aiken, A. C., D. Salcedo, M. J. Cubison, J. A. Huffman, P. F. DeCarlo, I. M. Ulbrich, K. S. Docherty, D. Sueper, J. R. Kimmel, D. R. Worsnop, A. Trimborn, M. Northway, E. A. Stone, J. J. Schauer, R. Volkamer, E. Fortner, B. d. Foy, J. Wang, A. Laskin, V. Shutthanandan, J. Zheng, R. Zhang, J. Gaffney, N. A. Marley, G. Paredes-Miranda, W. P. Arnott, L. T. Molina, G. Sosa, and J. L. Jimenez (2009b), Mexico City aerosol analysis during MILAGRO using high resolution aerosol mass spectrometry at the urban supersite (T0) – Part 1: Fine particle composition and organic source apportionment, Atmos. Chem. Phys. Discuss., 9, 8377-8427,

Alfarra, M. R. (2004), Insights Into Atmospheric Organic Aerosols Using An Aerosol Mass Spectrometer, Thesis thesis, University of Manchester, Manchester (U.K.).

Alfarra, M. R., D. Paulsen, M. Gysel, A. A. Garforth, J. Dommen, A. S. H. Prevot, D. R. Worsnop, U. Baltensperger, and H. Coe (2006), A mass spectrometric study of secondary organic aerosols formed from the photooxidation of anthropogenic and biogenic precursors in a reaction chamber, Atmos. Chem. Phys., 6, 5279-5293,

Alfarra, M. R., A. S. H. Prevot, S. Szidat, J. Sandradewi, S. Weimer, V. A. Lanz, D. Schreiber, M. Mohr, and U. Baltensperger (2007), Identification of the Mass Spectral Signature

of Organic Aerosols from Wood Burning Emissions, Environ. Sci. Technol., 41(16), 5770-5777, 10.1021/es062289b

Alfarra, M. R., H. Coe, J. D. Allan, K. N. Bower, H. Boudries, M. R. Canagaratna, J. L. Jimenez, J. T. Jayne, A. A. Garforth, S. M. Li, and D. R. Worsnop (2004), Characterization of urban and rural organic particulate in the lower Fraser valley using two aerodyne aerosol mass spectrometers, Atmos. Environ., 38(34), 5745-5758, 10.1016/j.atmosenv.2004.01.054

Allan, J. D., J. L. Jimenez, P. I. Williams, M. R. Alfarra, K. N. Bower, J. T. Jayne, H. Coe, and D. R. Worsnop (2003), Quantitative sampling using an Aerodyne Aerosol Mass Spectrometer. Part 1: Techniques of data interpretation and error analysis, Journal of Geophysical Research-Atmospheres, 108(D3), 4090, doi:4010.1029/2002JD002358,

Allan, J. D., P. I. Williams, W. T. Morgan, C. L. Martin, M. J. Flynn, J. Lee, E. Nemitz, G. J. Phillips, M. W. Gallagher, and H. Coe (2010a), Contributions from transport, solid fuel burning and cooking to primary organic aerosols in two UK cities, Atmos. Chem. Phys., 10, 647-668,

Allan, J. D., M. R. Alfarra, K. N. Bower, H. Coe, J. T. Jayne, D. R. Worsnop, P. P. Aalto, M. Kulmala, T. Hyotylainen, F. Cavalli, and A. Laaksonen (2006), Size and composition measurements of background aerosol and new particle growth in a Finnish forest during QUEST 2 using an Aerodyne Aerosol Mass Spectrometer, Atmospheric Chemistry and Physics, 6, 315-327, 10.5194/acp-6-315-2006

Allan, J. D., A. E. Delia, H. Coe, K. N. Bower, M. R. Alfarra, J. L. Jimenez, A. M. Middlebrook, F. Drewnick, T. B. Onasch, M. R. Canagaratna, J. T. Jayne, and D. R. Worsnop (2004), A generalised method for the extraction of chemically resolved mass spectra from aerodyne aerosol mass spectrometer data, J. Aerosol. Sci., 35(7), 909-922, 10.1016/j.jaerosci.2004.02.007

Apel, E. C., D. D. Riemer, A. Hills, W. Baugh, J. Orlando, I. Faloona, D. Tan, W. Brune, B. Lamb, H. Westberg, M. A. Carroll, T. Thornberry, and C. D. Geron (2002), Measurement and interpretation of isoprene fluxes and isoprene, methacrolein, and methyl vinyl ketone mixing ratios at the PROPHET site during the 1998 Intensive, J. Geophys. Res., 107(D3), 4034, 10.1029/2000jd000225

Asmi, E., A. Frey, A. Virkkula, M. Ehn, H. E. Manninen, H. Timonen, O. Tolonen-Kivimaki, M. Aurela, R. Hillamo, and M. Kulmala (2010), Hygroscopicity and chemical composition of Antarctic sub-micrometre aerosol particles and observations of new particle formation, Atmospheric Chemistry and Physics, 10(9), 4253-4271, 10.5194/acp-10-4253-2010

Barnes, I., J. Hjorth, and N. Mihalopoulos (2006), Dimethyl Sulfide and Dimethyl Sulfoxide and Their Oxidation in the Atmosphere, Chemical Reviews, 106(3), 940-975, 10.1021/cr020529+

Birmili, W., F. Stratmann, A. Wiedensohler, D. Covert, L. M. Russell, and O. Berg (1997), Determination of differential mobility analyzer transfer functions using identical instruments in series, Aerosol Sci. Technol., 27(2), 215-223, 10.1080/02786829708965468

Blando, J. D., and B. J. Turpin (2000), Secondary organic aerosol formation in cloud and fog droplets: a literature evaluation of plausibility, Atmospheric Environment, 34(10), 1623-1632,

Bond, T. C., and R. W. Bergstrom (2006), Light Absorption by Carbonaceous Particles: An Investigative Review, Aerosol Sci. Technol., 40(1), 27-67, 10.1080/02786820500421521

Bouvier-Brown, N. C., A. H. Goldstein, J. B. Gilman, W. C. Kuster, and J. A. de Gouw (2009), In-situ ambient quantification of monoterpenes, sesquiterpenes, and related oxygenated compounds during BEARPEX 2007: implications for gas- and particle-phase chemistry, Atmos. Chem. Phys., 9(15), 5505-5518,

Boy, M., and M. Kulmala (2002), Nucleation events in the continental boundary layer: Influence of physical and meteorological parameters, Atmospheric Chemistry and Physics, 2(1), 1-16, 10.5194/acp-2-1-2002

Brock, C. A., M. Trainer, T. B. Ryerson, J. A. Neuman, D. D. Parrish, J. S. Holloway, D. K. Nicks, Jr., G. J. Frost, G. Hübler, F. C. Fehsenfeld, J. C. Wilson, J. M. Reeves, B. G. Lafleur, H. Hilbert, E. L. Atlas, S. G. Donnelly, S. M. Schauffler, V. R. Stroud, and C. Wiedinmyer (2003), Particle growth in urban and industrial plumes in Texas, J. Geophys. Res., 108(D3), 4111, 10.1029/2002jd002746

Bzdek, B. R., and M. V. Johnston (2010), New Particle Formation and Growth in the Troposphere, Analytical Chemistry, 82(19), 7871-7878, 10.1021/ac100856j

Bzdek, B. R., C. A. Zordan, G. W. Luther, and M. V. Johnston (2011), Nanoparticle Chemical Composition During New Particle Formation, Aerosol Sci. Technol., 45(8), 1041-1048, 10.1080/02786826.2011.580392

Bzdek, B. R., C. A. Zordan, M. R. Pennington, G. W. Luther, and M. V. Johnston (2012), Quantitative Assessment of the Sulfuric Acid Contribution to New Particle Growth, Environmental Science & Technology, 46(8), 4365-4373, 10.1021/es204556c

Cahill, T. M., V. Y. Seaman, M. J. Charles, R. Holzinger, and A. H. Goldstein (2006), Secondary organic aerosols formed from oxidation of biogenic volatile organic compounds in the Sierra Nevada Mountains of California, J. Geophys. Res.-Atmos., 111(D16), D16312, 10.1029/2006jd007178

Canagaratna, M. R., J. T. Jayne, J. L. Jimenez, J. D. Allan, M. R. Alfarra, Q. Zhang, T. B. Onasch, F. Drewnick, H. Coe, A. Middlebrook, A. Delia, L. R. Williams, A. M. Trimborn, M. J. Northway, P. F. DeCarlo, C. E. Kolb, P. Davidovits, and D. R. Worsnop (2007), Chemical and microphysical characterization of ambient aerosols with the aerodyne aerosol mass spectrometer, Mass Spectrometry Reviews, 26(2), 185-222, 10.1002/mas.20115

Charron, A., W. Birmili, and R. M. Harrison (2007), Factors influencing new particle formation at the rural site, Harwell, United Kingdom, J. Geophys. Res., 112(D14), D14210, 10.1029/2007jd008425

Chen, Q., D. K. Farmer, J. Schneider, S. R. Zorn, C. L. Heald, T. G. Karl, A. Guenther, J. D. Allan, N. Robinson, H. Coe, J. R. Kimmel, T. Pauliquevis, S. Borrmann, U. Po uml schl, M. O. Andreae, P. Artaxo, J. L. Jimenez, and S. T. Martin (2009), Mass spectral characterization of submicron biogenic organic particles in the Amazon Basin, Geophys. Res. Lett., 36(20), L20806, 10.1029/2009gl039880

Chhabra, P. S., R. C. Flagan, and J. H. Seinfeld (2010), Elemental analysis of chamber organic aerosol using an aerodyne high-resolution aerosol mass spectrometer, Atmos. Chem. Phys., 10(9), 4111-4131, 10.5194/acp-10-4111-2010

Chhabra, P. S., N. L. Ng, M. R. Canagaratna, A. L. Corrigan, L. M. Russell, D. R. Worsnop, R. C. Flagan, and J. H. Seinfeld (2011), Elemental composition and oxidation of chamber organic aerosol, Atmos. Chem. Phys., 11(17), 8827-8845, 10.5194/acp-11-8827-2011

Clausnitzer, H., and M. J. Singer (1996), Respirable-Dust Production from Agricultural Operations in the Sacramento Valley, California, J. Environ. Qual., 25(4), 877-884, 10.2134/jeq1996.00472425002500040032x

Cottrell, L. D., R. J. Griffin, J. L. Jimenez, Q. Zhang, I. Ulbrich, L. D. Ziemba, P. J. Beckman, B. C. Sive, and R. W. Talbot (2008), Submicron particles at Thompson Farm during ICARTT measured using aerosol mass spectrometry, J. Geophys. Res.-Atmos., 113(D8), D08212, 10.1029/2007jd009192

Creamean, J. M., A. P. Ault, J. E. Ten Hoeve, M. Z. Jacobson, G. C. Roberts, and K. A. Prather (2011), Measurements of Aerosol Chemistry during New Particle Formation Events at a Remote Rural Mountain Site, Environmental Science & Technology, 45(19), 8208-8216, 10.1021/es103692f

Cubison, M., M. Alfarra, J. Allan, K. Bower, H. Coe, G. McFiggans, J. Whitehead, P. Williams, Q. Zhang, J. L. Jimenez, J. Hopkins, and J. Lee (2006), The characterisation of pollution aerosol in a changing photochemical environment, Atmospheric Chemistry and Physics, 6, 5573-5588,

Cubison, M. J., B. Ervens, G. Feingold, K. Docherty, I. Ulbrich, L. Shields, K. Prather, S. Hering, and J. L. Jimenez (2008), The Influence of Chemical Composition and Mixing State of Los Angeles Urban Aerosol on CCN number and Cloud Properties, Atmospheric Chemistry and Physics, 8, 5649-5667,

de Gouw, J., and C. Warneke (2007), Measurements of volatile organic compounds in the earths atmosphere using proton-transfer-reaction mass spectrometry, Mass Spectrom. Rev., 26(2), 223-257, 10.1002/mas.20119

de Gouw, J., and J.-L. Jimenez (2009), Organic Aerosols in the Earth's Atmosphere -- Organic Particles Are Abundant in the Troposphere and Important for Air Quality and Climate. But What Are Their Sources?, Environ. Sci. and Technol., 43, 7614-7618,

de Gouw, J. A., A. M. Middlebrook, C. Warneke, P. D. Goldan, W. C. Kuster, J. M. Roberts, F. C. Fehsenfeld, D. R. Worsnop, M. R. Canagaratna, A. A. P. Pszenny, W. C. Keene, M. Marchewka, S. B. Bertman, and T. S. Bates (2005), Budget of organic carbon in a polluted atmosphere: Results from the New England Air Quality Study in 2002, J. Geophys. Res.-Atmos., 110(D16), D16305, 10.1029/2004jd005623

de Gouw, J. A., C. A. Brock, E. L. Atlas, T. S. Bates, F. C. Fehsenfeld, P. D. Goldan, J. S. Holloway, W. C. Kuster, B. M. Lerner, B. M. Matthew, A. M. Middlebrook, T. B. Onasch, R. E. Peltier, P. K. Quinn, C. J. Senff, A. Stohl, A. P. Sullivan, M. Trainer, C. Warneke, R. J. Weber, and E. J. Williams (2008), Sources of particulate matter in the northeastern United States in summer: 1. Direct emissions and secondary formation of organic matter in urban plumes, J. Geophys. Res.-Atmos., 113(D8), D08301, 10.1029/2007jd009243

DeCarlo, P., J. G. Slowik, D. R. Worsnop, P. Davidovits, and J. L. Jimenez (2004), Particle morphology and density characterization by combined mobility and aerodynamic diameter measurements. Part 1: Theory, Aerosol Science & Technology, 38, 1185-1205,

DeCarlo, P. F., J. G. Slowik, D. R. Worsnop, P. Davidovits, and J. L. Jimenez (2004), Particle morphology and density characterization by combined mobility and aerodynamic diameter measurements. Part 1: Theory, Aerosol Sci. Technol., 38(12), 1185-1205, 10.1080/027868290903907

DeCarlo, P. F., J. R. Kimmel, A. Trimborn, J. Jayne, A. C. Aiken, M. Gonin, K. Fuhrer, T. Horvath, D. R. Worsnop, and J. L. Jimenez (2006a), A Field-Deployable High-Resolution Time-of-Flight Aerosol Mass Spectrometer, Analytical chemistry, 10.1021/ac061249n,

DeCarlo, P. F., J. R. Kimmel, A. Trimborn, M. J. Northway, J. T. Jayne, A. C. Aiken, M. Gonin, K. Fuhrer, T. Horvath, K. S. Docherty, D. R. Worsnop, and J. L. Jimenez (2006b), Field-deployable, high-resolution, time-of-flight aerosol mass spectrometer, Anal. Chem., 78(24), 8281-8289, 10.1021/ac061249n

DeCarlo, P. F., E. J. Dunlea, J. R. Kimmel, A. C. Aiken, D. Sueper, J. Crounse, P. O. Wennberg, L. Emmons, Y. Shinozuka, A. Clarke, J. Zhou, J. Tomlinson, D. R. Collins, D. Knapp, A. J. Weinheimer, D. D. Montzka, T. Campos, and J. L. Jimenez (2008), Fast airborne aerosol size and chemistry measurements above Mexico City and Central Mexico during the MILAGRO campaign, Atmos. Chem. Phys., 8(14), 4027-4048,

Dillon, M. B., M. S. Lamanna, G. W. Schade, A. H. Goldstein, and R. C. Cohen (2002), Chemical evolution of the Sacramento urban plume: Transport and oxidation, J. Geophys. Res.-Atmos., 107(D5-6), 4045, 10.1029/2001jd000969

Docherty, K. S., E. A. Stone, I. M. Ulbrich, P. F. Decarlo, D. C. Snyder, J. J. Schauer, R. E. Peltier, R. J. Weber, S. M. Murphy, J. H. Seinfeld, B. D. Grover, D. J. Eatough, and J. L. Jimenez (2008), Apportionment of Primary and Secondary Organic Aerosols in Southern California during the 2005 Study of Organic Aerosols in Riverside (SOAR-1), Environ. Sci. Technol., 42, 7655-7662,

Donahue, N. M., A. L. Robinson, C. O. Stanier, and S. N. Pandis (2006), Coupled Partitioning, Dilution, and Chemical Aging of Semivolatile Organics, Environmental Science & Technology, 40(8), 2635-2643, 10.1021/es052297c

Dunn, M. J., J.-L. Jiménez, D. Baumgardner, T. Castro, P. H. McMurry, and J. N. Smith (2004), Measurements of Mexico City nanoparticle size distributions: Observations of new particle formation and growth, Geophysical Research Letters, 31(10), L10102, 10.1029/2004gl019483

Dzepina, K., R. Volkamer, S. Madronich, P. Tulet, I. Ulbrich, Q. Zhang, C. D. Cappa, P. J. Ziemann, and J. L. Jimenez (2009), Evaluation of New Secondary Organic Aerosol (SOA) Models for a Case Study in Mexico City, Atmos. Chem. Phys., 9, 5681-5709,

Ervens, B., B. J. Turpin, and R. J. Weber (2011), Secondary organic aerosol formation in cloud droplets and aqueous particles (aqSOA): a review of laboratory, field and model studies, Atmos. Chem. Phys., 11(21), 11069-11102, 10.5194/acp-11-11069-2011

Farmer, D. K., A. Matsunaga, K. S. Docherty, J. D. Surratt, J. H. Seinfeld, P. J. Ziemann, and J. L. Jimenez (2010), Response of an aerosol mass spectrometer to organonitrates and organosulfates and implications for atmospheric chemistry, Proc. Natl. Acad. Sci. U. S. A., 107(15), 6670-6675, 10.1073/pnas.0912340107

Farmer, D. K., J. R. Kimmel, G. Phillips, K. S. Docherty, D. R. Worsnop, D. Sueper, E. Nemitz, and J. L. Jimenez (2011), Eddy covariance measurements with high-resolution time-of-flight aerosol mass spectrometry: a new approach to chemically resolved aerosol fluxes, Atmos. Meas. Tech., 4(6), 1275-1289, 10.5194/amt-4-1275-2011

Fast, J. D., W. I. Gustafson Jr, L. K. Berg, W. J. Shaw, M. Pekour, M. Shrivastava, J. C. Barnard, R. A. Ferrare, C. A. Hostetler, J. A. Hair, M. Erickson, B. T. Jobson, B. Flowers, M. K. Dubey, S. Springston, R. B. Pierce, L. Dolislager, J. Pederson, and R. A. Zaveri (2012),

Transport and mixing patterns over Central California during the carbonaceous aerosol and radiative effects study (CARES), Atmos. Chem. Phys., 12(4), 1759-1783, 10.5194/acp-12-1759-2012

Fuzzi, S., M. O. Andreae, B. J. Huebert, M. Kulmala, T. C. Bond, M. Boy, S. J. Doherty, A. Guenther, M. Kanakidou, K. Kawamura, V.-M. Kerminen, U. Lohmann, L. M. Russell, and U. Pöschl (2006), Critical assessment of the current state of scientific knowledge, terminology, and research needs concerning the role of organic aerosols in the atmosphere, climate, and global change, Atmos. Chem. Phys., 6, 2017-2038,

Ge, X., Q. Zhang, Y. Sun, C. R. Ruehl, and A. Setyan (2012), Effect of aqueous-phase processing on aerosol chemistry and size distributions in Fresno, California, during wintertime, Environmental Chemistry, 9(3), 221-235, 10.1071/EN11168

Ghan, S., and S. E. Schwartz (2007), Aerosol properties and processes: A path from field and laboratory measurements to global climate models, Bulletin of the American Meteorological Society, 88(7), 1059-1083, DOI:1010.1175/BAMS-1088-1057-1059,

Goldstein, A., and I. Galbally (2007), Known and Unexplored Organic Constituents in the Earth's Atmosphere, Environ. Sci. Technol., 41(5), 1514 - 1521,

Goldstein, A. H., C. D. Koven, C. L. Heald, and I. Y. Fung (2009), Biogenic carbon and anthropogenic pollutants combine to form a cooling haze over the southeastern United States, Proceedings of the National Academy of Sciences, 106(22), 8835-8840, 10.1073/pnas.0904128106

Goldstein, A. H., N. E. Hultman, J. M. Fracheboud, M. R. Bauer, J. A. Panek, M. Xu, Y. Qi, A. B. Guenther, and W. Baugh (2000), Effects of climate variability on the carbon dioxide, water, and sensible heat fluxes above a ponderosa pine plantation in the Sierra Nevada (CA), Agric. For. Meteorol., 101(2-3), 113-129,

Guo, H., D. W. Wang, K. Cheung, Z. H. Ling, C. K. Chan, and X. H. Yao (2012), Observation of aerosol size distribution and new particle formation at a mountain site in subtropical Hong Kong, Atmospheric Chemistry and Physics, 12(20), 9923-9939, 10.5194/acp-12-9923-2012

Hallquist, M., J. C. Wenger, U. Baltensperger, Y. Rudich, D. Simpson, M. Claeys, J. Dommen, N. M. Donahue, C. George, A. H. Goldstein, J. F. Hamilton, H. Herrmann, T. Hoffmann, Y. Iinuma, M. Jang, M. E. Jenkin, J. L. Jimenez, A. Kiendler-Scharr, W. Maenhaut, G. McFiggans, T. F. Mentel, A. Monod, A. S. H. Prévôt, J. H. Seinfeld, J. D. Surratt, R. Szmigielski, and J. Wildt (2009b), The formation, properties and impact of secondary organic aerosol: current and emerging issues, Atmos. Chem. Phys., 9(14), 5155-5236, 10.5194/acp-9-5155-2009

Hamed, A., H. Korhonen, S. L. Sihto, J. Joutsensaari, H. Jarvinen, T. Petaja, F. Arnold, T. Nieminen, M. Kulmala, J. N. Smith, K. E. J. Lehtinen, and A. Laaksonen (2011), The role of relative humidity in continental new particle formation, J. Geophys. Res.-Atmos., 116, 10.1029/2010jd014186

Hamed, A., J. Joutsensaari, S. Mikkonen, L. Sogacheva, M. Dal Maso, M. Kulmala, F. Cavalli, S. Fuzzi, M. C. Facchini, S. Decesari, M. Mircea, K. E. J. Lehtinen, and A. Laaksonen (2007), Nucleation and growth of new particles in Po Valley, Italy, Atmospheric Chemistry and Physics, 7(2), 355-376, 10.5194/acp-7-355-2007

Han, Y., Y. Iwamoto, T. Nakayama, K. Kawamura, T. Hussein, and M. Mochida (2013), Observation of new particle formation over a mid-latitude forest facing the North Pacific, Atmospheric Environment, 64(0), 77-84, 10.1016/j.atmosenv.2012.09.036

Herndon, S. C., T. B. Onasch, E. C. Wood, J. H. Kroll, M. R. Canagaratna, J. T. Jayne, M. A. Zavala, W. B. Knighton, C. Mazzoleni, M. K. Dubey, I. M. Ulbrich, J. L. Jimenez, R. Seila, J. A. de Gouw, B. de Foy, J. Fast, L. T. Molina, C. E. Kolb, and D. R. Worsnop (2008), Correlation of secondary organic aerosol with odd oxygen in Mexico City, Geophys. Res. Lett., 35(15), 10.1029/2008gl034058

Hildebrandt, L., G. J. Engelhart, C. Mohr, E. Kostenidou, V. A. Lanz, A. Bougiatioti, P. F. DeCarlo, A. S. H. Prevot, U. Baltensperger, N. Mihalopoulos, N. M. Donahue, and S. N. Pandis (2010), Aged organic aerosol in the Eastern Mediterranean: the Finokalia Aerosol Measurement Experiment-2008, Atmos. Chem. Phys., 10(9), 4167-4186, 10.5194/acp-10-4167-2010

Holmes, N. S. (2007), A review of particle formation events and growth in the atmosphere in the various environments and discussion of mechanistic implications, Atmospheric Environment, 41(10), 2183-2201, 10.1016/j.atmosenv.2006.10.058

Holzinger, R., A. Lee, K. T. Paw, and A. H. Goldstein (2005), Observations of oxidation products above a forest imply biogenic emissions of very reactive compounds, Atmos. Chem. Phys., 5, 67-75,

Holzinger, R., D. B. Millet, B. Williams, A. Lee, N. Kreisberg, S. V. Hering, J. Jimenez, J. D. Allan, D. R. Worsnop, and A. H. Goldstein (2007b), Emission, oxidation, and secondary organic aerosol formation of volatile organic compounds as observed at Chebogue Point, Nova Scotia, J. Geophys. Res.-Atmos., 112(D10), 10.1029/2006jd007599

Hoyle, C. R., M. Boy, N. M. Donahue, J. L. Fry, M. Glasius, A. Guenther, A. G. Hallar, K. H. Hartz, M. D. Petters, T. Petaja, T. Rosenoern, and A. P. Sullivan (2011), A review of the anthropogenic influence on biogenic secondary organic aerosol, Atmos. Chem. Phys., 11(1), 321-343, 10.5194/acp-11-321-2011

Huffman, J. A., K. S. Docherty, A. C. Aiken, M. J. Cubison, I. M. Ulbrich, P. F. DeCarlo, D. Sueper, J. T. Jayne, D. R. Worsnop, P. J. Ziemann, and J. L. Jimenez (2009), Chemically-Resolved Aerosol Volatility Measurements from Two Megacity Field Studies , 2009, Atmospheric Chemistry and Physics, 9(18), 7161-7182,

IPCC (2007), Climate Change 2007: The Scientific Basis, Contribution of Working Group I to the Third Assessment Report of the Intergovernmental Panel on Climate Change, edited by J. T. Houghton, Ding, Y., Griggs, D. J., Noguer, M., van der Linden, P. J., Dai X., Maskell, K., and Johnson, C. A., Cambridge Univ. Press, New York.

Jacob, D. J., B. D. Field, E. M. Jin, I. Bey, Q. Li, J. A. Logan, R. M. Yantosca, and H. B. Singh (2002), Atmospheric budget of acetone, J. Geophys. Res., 107(D10), 4100, 10.1029/2001jd000694

Jacob, D. J., B. D. Field, Q. Li, D. R. Blake, J. de Gouw, C. Warneke, A. Hansel, A. Wisthaler, H. B. Singh, and A. Guenther (2005), Global budget of methanol: Constraints from atmospheric observations, J. Geophys. Res., 110(D8), D08303, 10.1029/2004jd005172

Jacobson, M. C., H. C. Hansson, K. J. Noone, and R. J. Charlson (2000), Organic atmospheric aerosols: Review and state of the science, Reviews of Geophysics, 38(2), 267-294,

Jayne, J. T., D. C. Leard, X. F. Zhang, P. Davidovits, K. A. Smith, C. E. Kolb, and D. R. Worsnop (2000), Development of an aerosol mass spectrometer for size and composition analysis of submicron particles, Aerosol Sci. Technol., 33(1-2), 49-70, 10.1080/027868200410840

Jeong, C. H., G. J. Evans, M. L. McGuire, R. Y. W. Chang, J. P. D. Abbatt, K. Zeromskiene, M. Mozurkewich, S. M. Li, and A. R. Leaitch (2010), Particle formation and growth at five rural and urban sites, Atmospheric Chemistry and Physics, 10(16), 7979-7995, 10.5194/acp-10-7979-2010

Jimenez, J. L., J. T. Jayne, Q. Shi, C. E. Kolb, D. R. Worsnop, I. Yourshaw, J. H. Seinfeld, R. C. Flagan, X. Zhang, K. A. Smith, J. W. Morris, and P. Davidovits (2003), Ambient aerosol sampling with an Aerosol Mass Spectrometer, J. Geophys. Res., 108(D7), 8425, doi:8410:1029/2001JD001213,

Jimenez, J. L., M. R. Canagaratna, N. M. Donahue, A. S. H. Prevot, Q. Zhang, J. H. Kroll, P. F. DeCarlo, J. D. Allan, H. Coe, N. L. Ng, A. C. Aiken, K. S. Docherty, I. M. Ulbrich, A. P. Grieshop, A. L. Robinson, J. Duplissy, J. D. Smith, K. R. Wilson, V. A. Lanz, C. Hueglin, Y. L. Sun, J. Tian, A. Laaksonen, T. Raatikainen, J. Rautiainen, P. Vaattovaara, M. Ehn, M. Kulmala, J. M. Tomlinson, D. R. Collins, M. J. Cubison, E. J. Dunlea, J. A. Huffman, T. B. Onasch, M. R. Alfarra, P. I. Williams, K. Bower, Y. Kondo, J. Schneider, F. Drewnick, S. Borrmann, S. Weimer, K. Demerjian, D. Salcedo, L. Cottrell, R. Griffin, A. Takami, T. Miyoshi, S. Hatakeyama, A. Shimono, J. Y. Sun, Y. M. Zhang, K. Dzepina, J. R. Kimmel, D. Sueper, J. T. Jayne, S. C. Herndon, A. M. Trimborn, L. R. Williams, E. C. Wood, A. M. Middlebrook, C. E. Kolb, U. Baltensperger, and D. R. Worsnop (2009), Evolution of Organic Aerosols in the Atmosphere, Science, 326(5959), 1525-1529, 10.1126/science.1180353

John, W., S. M. Wall, J. L. Ondo, and W. Winklmayr (1990), Modes in the size distributions of atmospheric inorganic aerosol, Atmospheric Environment. Part A. General Topics, 24(9), 2349-2359, 10.1016/0960-1686(90)90327-j

Johnson, D., S. R. Utembe, M. E. Jenkin, R. G. Derwent, G. D. Hayman, M. R. Alfarra, H. Coe, and G. McFiggans (2006), Simulating regional scale secondary organic aerosol formation during the TORCH 2003 campaign in the southern UK, Atmos. Chem. Phys., 6, 403-418,

Jokinen, T., M. Sipilä, H. Junninen, M. Ehn, G. Lönn, J. Hakala, T. Petäjä, R. L. Mauldin Iii, M. Kulmala, and D. R. Worsnop (2012), Atmospheric sulphuric acid and neutral cluster measurements using CI-APi-TOF, Atmospheric Chemistry and Physics, 12(9), 4117-4125, 10.5194/acp-12-4117-2012

Kanakidou, M., K. Tsigaridis, F. J. Dentener, and P. J. Crutzen (2000), Human-activity-enhanced formation of organic aerosols by biogenic hydrocarbon oxidation, J. Geophys. Res., 105(D7), 9243-9354, 10.1029/1999jd901148

Kanakidou, M., J. H. Seinfeld, S. N. Pandis, I. Barnes, F. J. Dentener, M. C. Facchini, R. V. Dingenen, B. Ervens, A. Nenes, C. J. Nielsen, E. Swietlicki, J. P. Putaud, Y. Balkanski, S. Fuzzi, J. Horth, G. K. Moortgat, R. Winterhalter, C. E. L. Myhre, K. Tsigaridis, E. Vignati, E. G. Stephanou, and J. Wilson (2005a), Organic aerosol and global climate modelling: a review, Atmos. Chem. Phys., 5, 1053-1123,

Kerminen, V. M., M. Paramonov, T. Anttila, I. Riipinen, C. Fountoukis, H. Korhonen, E. Asmi, L. Laakso, H. Lihavainen, E. Swietlicki, B. Svenningsson, A. Asmi, S. N. Pandis, M. Kulmala, and T. Petäjä (2012), Cloud condensation nuclei production associated with

atmospheric nucleation: a synthesis based on existing literature and new results, Atmospheric Chemistry and Physics, 12(24), 12037-12059, 10.5194/acp-12-12037-2012

Kiendler-Scharr, A., Q. Zhang, T. Hohaus, E. Kleist, A. Mensah, T. F. Mentel, C. Spindler, R. Uerlings, R. Tillmann, and J. Wildt (2009b), Aerosol Mass Spectrometric Features of Biogenic SOA: Observations from a Plant Chamber and in Rural Atmospheric Environments, Environ. Sci. Technol., 43(21), 8166-8172, 10.1021/es901420b

Kleinman, L. I., P. H. Daum, Y.-N. Lee, G. I. Senum, S. R. Springston, J. Wang, C. Berkowitz, J. Hubbe, R. A. Zaveri, F. J. Brechtel, J. Jayne, T. B. Onasch, and D. Worsnop (2007), Aircraft observations of aerosol composition and ageing in New England and Mid-Atlantic States during the summer 2002 New England Air Quality Study field campaign, J. Geophys. Res., 112(D9), D09310, 10.1029/2006jd007786

Kleinman, L. I., S. R. Springston, P. H. Daum, Y. N. Lee, L. J. Nunnermacker, G. I. Senum, J. Wang, J. Weinstein-Lloyd, M. L. Alexander, J. Hubbe, J. Ortega, M. R. Canagaratna, and J. Jayne (2008a), The time evolution of aerosol composition over the Mexico City plateau, Atmos. Chem. Phys., 8(6), 1559-1575, 10.5194/acp-8-1559-2008

Komppula, M., H. Lihavainen, J. Hatakka, J. Paatero, P. Aalto, M. Kulmala, and Y. Viisanen (2003), Observations of new particle formation and size distributions at two different heights and surroundings in subarctic area in northern Finland, J. Geophys. Res., 108(D9), 4295, 10.1029/2002jd002939

Koponen, I. K., A. Virkkula, R. Hillamo, V.-M. Kerminen, and M. Kulmala (2003), Number size distributions and concentrations of the continental summer aerosols in Queen Maud Land, Antarctica, J. Geophys. Res., 108(D18), 4587, 10.1029/2003jd003614

Kroll, J. H., and J. H. Seinfeld (2008), Chemistry of secondary organic aerosol: Formation and evolution of low-volatility organics in the atmosphere, Atmosphere Environment, 42, 3593-3624,

Kulmala, M., J. Kontkanen, H. Junninen, K. Lehtipalo, H. E. Manninen, T. Nieminen, T. Petäjä, M. Sipilä, S. Schobesberger, P. Rantala, A. Franchin, T. Jokinen, E. Järvinen, M. Äijälä, J. Kangasluoma, J. Hakala, P. P. Aalto, P. Paasonen, J. Mikkilä, J. Vanhanen, J. Aalto, H. Hakola, U. Makkonen, T. Ruuskanen, R. L. Mauldin, J. Duplissy, H. Vehkamäki, J. Bäck, A. Kortelainen, I. Riipinen, T. Kurtén, M. V. Johnston, J. N. Smith, M. Ehn, T. F. Mentel, K. E. J. Lehtinen, A. Laaksonen, V.-M. Kerminen, and D. R. Worsnop (2013), Direct Observations of Atmospheric Aerosol Nucleation, Science, 339(6122), 943-946, 10.1126/science.1227385

Kuwata, M., S. R. Zorn, and S. T. Martin (2012), Using Elemental Ratios to Predict the Density of Organic Material Composed of Carbon, Hydrogen, and Oxygen, Environ. Sci. Technol., 46(2), 787-794, 10.1021/es202525q

Laaksonen, A., M. Kulmala, C. D. O'Dowd, J. Joutsensaari, P. Vaattovaara, S. Mikkonen, K. E. J. Lehtinen, L. Sogacheva, M. Dal Maso, P. Aalto, T. Petaja, A. Sogachev, Y. J. Yoon, H. Lihavainen, D. Nilsson, M. C. Facchini, F. Cavalli, S. Fuzzi, T. Hoffmann, F. Arnold, M. Hanke, K. Sellegri, B. Umann, W. Junkermann, H. Coe, J. D. Allan, M. R. Alfarra, D. R. Worsnop, M. L. Riekkola, T. Hyotylainen, and Y. Viisanen (2008), The role of VOC oxidation products in continental new particle formation, Atmospheric Chemistry and Physics, 8(10), 2657-2665,

Laitinen, T., M. Ehn, H. Junninen, J. Ruiz-Jimenez, J. Parshintsev, K. Hartonen, M. L. Riekkola, D. R. Worsnop, and M. Kulmala (2011), Characterization of organic compounds in 10-to 50-nm aerosol particles in boreal forest with laser desorption-ionization aerosol mass

spectrometer and comparison with other techniques, Atmospheric Environment, 45(22), 3711-3719, 10.1016/j.atmosenv.2011.04.023

Lambe, A. T., T. B. Onasch, P. Massoli, D. R. Croasdale, J. P. Wright, A. T. Ahern, L. R. Williams, D. R. Worsnop, W. H. Brune, and P. Davidovits (2011), Laboratory studies of the chemical composition and cloud condensation nuclei (CCN) activity of secondary organic aerosol (SOA) and oxidized primary organic aerosol (OPOA), Atmos. Chem. Phys., 11(17), 8913-8928, 10.5194/acp-11-8913-2011

Lanz, V. A., M. R. Alfarra, U. Baltensperger, B. Buchmann, C. Hüglin, and A. S. H. Prévôt (2007a), Source apportionment of submicron organic aerosols at an urban site by factor analytical modelling of aerosol mass spectra, Atmos. Chem. Phys., 7, 1503-1522,

Lanz, V. A., A. S. H. Prevot, M. R. Alfarra, S. Weimer, C. Mohr, P. F. DeCarlo, M. F. D. Gianini, C. Hueglin, J. Schneider, O. Favez, B. D'Anna, C. George, and U. Baltensperger (2010), Characterization of aerosol chemical composition with aerosol mass spectrometry in Central Europe: an overview, Atmos. Chem. Phys., 10(21), 10453-10471, 10.5194/acp-10-10453-2010

Lee, A., A. H. Goldstein, M. D. Keywood, S. Gao, V. Varutbangkul, R. Bahreini, N. L. Ng, R. C. Flagan, and J. H. Seinfeld (2006), Gas-phase products and secondary aerosol yields from the ozonolysis of ten different terpenes, J. Geophys. Res.-Atmos., 111(D7), D0730210.1029/2005jd006437

Lehtipalo, K., M. Sipilä, H. Junninen, M. Ehn, T. Berndt, M. K. Kajos, D. R. Worsnop, T. Petäjä, and M. Kulmala (2011), Observations of Nano-CN in the Nocturnal Boreal Forest, Aerosol Sci. Technol., 45(4), 499-509, 10.1080/02786826.2010.547537

Liu, S., M. Hu, Z. Wu, B. Wehner, A. Wiedensohler, and Y. Cheng (2008), Aerosol number size distribution and new particle formation at a rural/coastal site in Pearl River Delta (PRD) of China, Atmospheric Environment, 42(25), 6275-6283, 10.1016/j.atmosenv.2008.01.063

Lunden, M. M., D. R. Black, M. McKay, K. L. Revzan, A. H. Goldstein, and N. J. Brown (2006), Characteristics of fine particle growth events observed above a forested ecosystem in the Sierra Nevada Mountains of California, Aerosol Sci. Technol., 40(5), 373-388, 10.1080/02786820600631896

Mahowald, N. (2011), Aerosol Indirect Effect on Biogeochemical Cycles and Climate, Science, 334(6057), 794-796, 10.1126/science.1207374

Makela, J. M., S. Yli-Koivisto, V. Hiltunen, W. Seidl, E. Swietlicki, K. Teinila, M. Sillanpaa, I. K. Koponen, J. Paatero, K. Rosman, and K. Hameri (2001), Chemical composition of aerosol during particle formation events in boreal forest, Tellus Ser. B-Chem. Phys. Meteorol., 53(4), 380-393, 10.1034/j.1600-0889.2001.530405.x

Matthew, B. M., A. M. Middlebrook, and T. B. Onasch (2008), Collection efficiencies in an Aerodyne Aerosol Mass Spectrometer as a function of particle phase for laboratory generated aerosols, Aerosol Sci. Technol., 42(11), 884-898, 10.1080/02786820802356797

McKendry, I. G., A. M. Macdonald, W. R. Leaitch, A. van Donkelaar, Q. Zhang, T. Duck, and R. V. Martin (2008), Trans-Pacific dust events observed at Whistler, British Columbia during INTEX-B, Atmos. Chem. Phys., 8(20), 6297-6307,

McLafferty, F. W., and F. Turecek (1993), Interpretation of mass spectra, Fourth ed., University Science Books, Mill Valley, California.

Meng, Z., and J. H. Seinfeld (1994), On the Source of the Submicrometer Droplet Mode of Urban and Regional Aerosols, Aerosol Sci. Technol., 20(3), 253-265, 10.1080/02786829408959681

Middlebrook, A. M., R. Bahreini, J. L. Jimenez, and M. R. Canagaratna (2012), Evaluation of Composition-Dependent Collection Efficiencies for the Aerodyne Aerosol Mass Spectrometer using Field Data, Aerosol Sci. Technol., 46(3), 258-271, 10.1080/02786826.2011.620041

Modini, R. L., Z. D. Ristovski, G. R. Johnson, C. He, N. Surawski, L. Morawska, T. Suni, and M. Kulmala (2009), New particle formation and growth at a remote, sub-tropical coastal location, Atmospheric Chemistry and Physics, 9(19), 7607-7621, 10.5194/acp-9-7607-2009

Mohr, C., J. A. Huffman, M. J. Cubison, A. C. Aiken, K. S. Docherty, J. R. Kimmel, I. M. Ulbrich, M. Hannigan, and J. L. Jimenez (2009), Characterization of Primary Organic Aerosol Emissions from Meat Cooking, Trash Burning, and Motor Vehicles with High-Resolution Aerosol Mass Spectrometry and Comparison with Ambient and Chamber Observations, Environ. Sci. Technol., 43(7), 2443-2449, 10.1021/es8011518

Murphy, D. M. (2005), Atmospheric Science: Enhanced: Something in the Air, Science, 307(5717), 1888-1890,

Murphy, J. G., D. A. Day, P. A. Cleary, P. J. Wooldridge, D. B. Millet, A. H. Goldstein, and R. C. Cohen (2007), The weekend effect within and downwind of Sacramento - Part 1: Observations of ozone, nitrogen oxides, and VOC reactivity, Atmos. Chem. Phys., 7(20), 5327-5339,

Ng, N. L., M. R. Canagaratna, J. L. Jimenez, P. S. Chhabra, J. H. Seinfeld, and D. R. Worsnop (2011a), Changes in organic aerosol composition with aging inferred from aerosol mass spectra, Atmos. Chem. Phys., 11(13), 6465-6474, 10.5194/acp-11-6465-2011

Ng, N. L., M. R. Canagaratna, J. L. Jimenez, Q. Zhang, I. M. Ulbrich, and D. R. Worsnop (2011b), Real-Time Methods for Estimating Organic Component Mass Concentrations from Aerosol Mass Spectrometer Data, Environ. Sci. Technol., 45(3), 910-916, 10.1021/es102951k

Ng, N. L., M. R. Canagaratna, Q. Zhang, J. L. Jimenez, J. Tian, I. M. Ulbrich, J. H. Kroll, K. S. Docherty, P. S. Chhabra, R. Bahreini, S. M. Murphy, J. H. Seinfeld, L. Hildebrandt, N. M. Donahue, P. F. DeCarlo, V. A. Lanz, A. S. H. Prevot, E. Dinar, Y. Rudich, and D. R. Worsnop (2010b), Organic aerosol components observed in Northern Hemispheric datasets from Aerosol Mass Spectrometry, Atmos. Chem. Phys., 10(10), 4625-4641, 10.5194/acp-10-4625-2010

O'Dowd, C. D., J. L. Jimenez, R. Bahreini, R. C. Flagan, J. H. Seinfeld, K. Hameri, L. Pirjola, M. Kulmala, S. G. Jennings, and T. Hoffmann (2002), Marine aerosol formation from biogenic iodine emissions, Nature, 417(6889), 632-636,

Paatero, P., and U. Tapper (1994a), Positive Matrix Factorization - A Nonnegative Factor Model with Optimal Utilization of Error-Estimates of Data Values, Environmetrics, 5(2), 111-126,

Paatero, P., and U. Tapper (1994b), Positive matrix factorization: A non-negative factor model with optimal utilization of error estimates of data values, Environmetrics, 5, 111-126, 10.1002/env.3170050203

Pierce, J. R., W. R. Leaitch, J. Liggio, D. M. Westervelt, C. D. Wainwright, J. P. D. Abbatt, L. Ahlm, W. Al-Basheer, D. J. Cziczo, K. L. Hayden, A. K. Y. Lee, S. M. Li, L. M.

Russell, S. J. Sjostedt, K. B. Strawbridge, M. Travis, A. Vlasenko, J. J. B. Wentzell, H. A. Wiebe, J. P. S. Wong, and A. M. Macdonald (2012), Nucleation and condensational growth to CCN sizes during a sustained pristine biogenic SOA event in a forested mountain valley, Atmospheric Chemistry and Physics, 12(7), 3147-3163, 10.5194/acp-12-3147-2012

Pikridas, M., I. Riipinen, L. Hildebrandt, E. Kostenidou, H. Manninen, N. Mihalopoulos, N. Kalivitis, J. F. Burkhart, A. Stohl, M. Kulmala, and S. N. Pandis (2012), New particle formation at a remote site in the eastern Mediterranean, J. Geophys. Res., 117(D12), D12205, 10.1029/2012jd017570

Pope, C. A., M. Ezzati, and D. W. Dockery (2009), Fine-Particulate Air Pollution and Life Expectancy in the United States, New England Journal of Medicine, 360(4), 376-386, doi:10.1056/NEJMsa0805646

Raatikainen, T., P. Vaattovaara, P. Tiitta, P. Miettinen, J. Rautiainen, M. Ehn, M. Kulmala, A. Laaksonen, and D. R. Worsnop (2010), Physicochemical properties and origin of organic groups detected in boreal forest using an aerosol mass spectrometer, Atmos. Chem. Phys., 10(4), 2063-2077,

Rollins, A. W., J. L. Fry, J. F. Hunter, J. H. Kroll, D. R. Worsnop, S. W. Singaram, and R. C. Cohen (2010), Elemental analysis of aerosol organic nitrates with electron ionization high-resolution mass spectrometry, Atmos. Meas. Tech., 3(1), 301-310,

Salcedo, D., T. B. Onasch, M. R. Canagaratna, K. Dzepina, J. A. Huffman, J. T. Jayne, D. R. Worsnop, C. E. Kolb, S. Weimer, F. Drewnick, J. D. Allan, A. E. Delia, and J. L. Jimenez (2007), Technical note: use of a beam width probe in an Aerosol Mass Spectrometer to monitor particle collection efficiency in the field, Atmospheric Chemistry and Physics, 7, 549-556,

Saxena, P., and L. M. Hildemann (1996), Water-soluble organics in atmospheric particles: A critical review of the literature and application of thermodynamics to identify candidate compounds, Journal of Atmospheric Chemistry, 24(1), 57-109,

Schade, G. W., and A. H. Goldstein (2001), Fluxes of oxygenated volatile organic compounds from a ponderosa pine plantation, J. Geophys. Res.-Atmos., 106(D3), 3111-3123,

Schade, G. W., and A. H. Goldstein (2006), Seasonal measurements of acetone and methanol: Abundances and implications for atmospheric budgets, Glob. Biogeochem. Cycle, 20(1), GB1011, 10.1029/2005gb002566

Schwartz, S. E. (2008), Uncertainty in climate sensitivity: Causes, consequences, challenges, Energy & Environmental Science, 1(4), 430-453, 10.1039/b810350j

Seinfeld, J. H., and J. F. Pankow (2003), Organic atmospheric particulate material, Annual Review of Physical Chemistry, 54, 121-140,

Setyan, A., Q. Zhang, M. Merkel, W. B. Knighton, Y. Sun, C. Song, J. E. Shilling, T. B. Onasch, S. C. Herndon, D. R. Worsnop, J. D. Fast, R. A. Zaveri, L. K. Berg, A. Wiedensohler, B. A. Flowers, M. K. Dubey, and R. Subramanian (2012), Characterization of submicron particles influenced by mixed biogenic and anthropogenic emissions using high-resolution aerosol mass spectrometry: results from CARES, Atmos. Chem. Phys., 12(17), 8131-8156, 10.5194/acp-12-8131-2012

Sharkey, T. D., E. L. Singsaas, P. J. Vanderveer, and C. Geron (1996), Field measurements of isoprene emission from trees in response to temperature and light, Tree Physiol., 16(7), 649-654

Shilling, J. E., Q. Chen, S. M. King, T. Rosenoern, J. H. Kroll, D. R. Worsnop, P. F. DeCarlo, A. C. Aiken, D. Sueper, J. L. Jimenez, and S. T. Martin (2009), Loading-dependent elemental composition of alpha-pinene SOA particles, Atmos. Chem. Phys., 9(3), 771-782,

Shilling, J. E., R. A. Zaveri, J. D. Fast, L. Kleinman, M. L. Alexander, M. R. Canagaratna, E. Fortner, J. M. Hubbe, J. T. Jayne, A. Sedlacek, A. Setyan, S. Springston, D. R. Worsnop, and Q. Zhang (2013), Enhanced SOA formation from mixed anthropogenic and biogenic emissions during the CARES campaign, Atmos. Chem. Phys., 13(4), 2091-2113, 10.5194/acp-13-2091-2013

Slowik, J. G., C. Stroud, J. W. Bottenheim, P. C. Brickell, R. Y. W. Chang, J. Liggio, P. A. Makar, R. V. Martin, M. D. Moran, N. C. Shantz, S. J. Sjostedt, A. van Donkelaar, A. Vlasenko, H. A. Wiebe, A. G. Xia, J. Zhang, W. R. Leaitch, and J. P. D. Abbatt (2010), Characterization of a large biogenic secondary organic aerosol event from eastern Canadian forests, Atmos. Chem. Phys., 10(6), 2825-2845,

Smith, J. N., K. F. Moore, F. L. Eisele, D. Voisin, A. K. Ghimire, H. Sakurai, and P. H. McMurry (2005), Chemical composition of atmospheric nanoparticles during nucleation events in Atlanta, Journal of Geophysical Research: Atmospheres, 110(D22), D22S03, 10.1029/2005jd005912

Smith, J. N., M. J. Dunn, T. M. VanReken, K. Iida, M. R. Stolzenburg, P. H. McMurry, and L. G. Huey (2008), Chemical composition of atmospheric nanoparticles formed from nucleation in Tecamac, Mexico: evidence for an important role for organic species in nanoparticle growth, Geophysical Research Letters, 35(4), L04808, 10.1029/2007GL032523

Smith, J. N., K. C. Barsanti, H. R. Friedli, M. Ehn, M. Kulmala, D. R. Collins, J. H. Scheckman, B. J. Williams, and P. H. McMurry (2010), Observations of aminium salts in atmospheric nanoparticles and possible climatic implications, Proceedings of the National Academy of Sciences, 107(15), 6634-6639, 10.1073/pnas.0912127107

Spaulding, R. S., G. W. Schade, A. H. Goldstein, and M. J. Charles (2003), Characterization of secondary atmospheric photooxidation products: Evidence for biogenic and anthropogenic sources, J. Geophys. Res.-Atmos., 108(D8), 4247, 10.1029/2002jd002478

Spracklen, D. V., K. S. Carslaw, M. Kulmala, V. M. Kerminen, G. W. Mann, and S. L. Sihto (2006), The contribution of boundary layer nucleation events to total particle concentrations on regional and global scales, Atmospheric Chemistry and Physics, 6(12), 5631-5648, 10.5194/acp-6-5631-2006

Spracklen, D. V., J. L. Jimenez, K. S. Carslaw, D. R. Worsnop, M. J. Evans, G. W. Mann, Q. Zhang, M. R. Canagaratna, J. Allan, H. Coe, G. McFiggans, A. Rap, and P. Forster (2011), Aerosol mass spectrometer constraint on the global secondary organic aerosol budget, Atmos. Chem. Phys., 11(23), 12109-12136, 10.5194/acp-11-12109-2011

Stanier, C. O., A. Y. Khlystov, and S. N. Pandis (2004), Nucleation events during the Pittsburgh air quality study: Description and relation to key meteorological, gas phase, and aerosol parameters, Aerosol Sci. Technol., 38, 253-264, 10.1080/02786820390229570

Subramanian, R., G. L. Kok, D. Baumgardner, A. Clarke, Y. Shinozuka, T. L. Campos, C. G. Heizer, B. B. Stephens, B. de Foy, P. B. Voss, and R. A. Zaveri (2010), Black carbon over Mexico: the effect of atmospheric transport on mixing state, mass absorption cross-section, and BC/CO ratios, Atmos. Chem. Phys., 10(1), 219-237,

Sun, J. Y., Q. Zhang, M. R. Canagaratna, Y. M. Zhang, N. L. Ng, Y. L. Sun, J. T. Jayne, X. C. Zhang, X. Y. Zhang, and D. R. Worsnop (2010), Highly time- and size-resolved characterization of submicron aerosol particles in Beijing using an Aerodyne Aerosol Mass Spectrometer, Atmos. Environ., 44(1), 131-140, 10.1016/j.atmosenv.2009.03.020

Sun, Y., Q. Zhang, J. J. Schwab, K. L. Demerjian, W.-N. Chen, M.-S. Bae, H.-M. Hung, O. Hogrefe, B. Frank, O. V. Rattigan, and Y.-C. Lin (2010), Characterization of the Sources and Processes of Organic and Inorganic Aerosols in New York City with a High-Resolution Time-of-Flight Aerosol Mass Spectrometer, Atmospheric Chemistry and Physics Discussion, 10, 22669–22723, doi:22610.25194/acpd-22610-22669-22010

Sun, Y., Q. Zhang, A. M. Macdonald, K. Hayden, S.-M. Li, J. Liggio, P. S. K. Liu, K. G. Anlauf, W. R. Leaitch, A. Steffen, M. Cubison, D. R. Worsnop, A. van Donkelaar, and R. V. Martin (2009), Size-Resolved Aerosol Chemistry on Whistler Mountain, Canada with a High-Resolution Aerosol Mass Spectrometer during INTEX-B, Atmos. Chem. Phys., 9(3095-3111)

Sun, Y. L., Q. Zhang, J. J. Schwab, K. L. Demerjian, W. N. Chen, M. S. Bae, H. M. Hung, O. Hogrefe, B. Frank, O. V. Rattigan, and Y. C. Lin (2011), Characterization of the sources and processes of organic and inorganic aerosols in New York city with a high-resolution time-of-flight aerosol mass apectrometer, Atmos. Chem. Phys., 11(4), 1581-1602, 10.5194/acp-11-1581-2011

Takegawa, N., T. Miyakawa, K. Kawamura, and Y. Kondo (2007), Contribution of Selected Dicarboxylic and ω-Oxocarboxylic Acids in Ambient Aerosol to the m/z 44 Signal of an Aerodyne Aerosol Mass Spectrometer, Aerosol Sci. Technol., 41(4), 418-437, 10.1080/02786820701203215

Takegawa, N., T. Miyakawa, Y. Kondo, D. R. Blake, Y. Kanaya, M. Koike, M. Fukuda, Y. Komazaki, Y. Miyazaki, A. Shimono, and T. Takeuchi (2006), Evolution of submicron organic aerosol in polluted air exported from Tokyo, Geophysical Research Letters, doi:10.1029/2006GL025815

Ulbrich, I. M., M. R. Canagaratna, Q. Zhang, D. R. Worsnop, and J. L. Jimenez (2009), Interpretation of organic components from Positive Matrix Factorization of aerosol mass spectrometric data, Atmos. Chem. Phys., 9(9), 2891-2918

Ulbrich, I. M., M. R. Canagaratna, M. J. Cubison, Q. Zhang, N. L. Ng, A. C. Aiken, and J. L. Jimenez (2012), Three-dimensional factorization of size-resolved organic aerosol mass spectra from Mexico City, Atmos. Meas. Tech., 5(1), 195-224, 10.5194/amt-5-195-2012

Vaden, T. D., D. Imre, J. Beranek, M. Shrivastava, and A. Zelenyuk (2011), Evaporation kinetics and phase of laboratory and ambient secondary organic aerosol, Proc. Natl. Acad. Sci. U. S. A., 108(6), 2190-2195, 10.1073/pnas.1013391108

Vakkari, V., H. Laakso, M. Kulmala, A. Laaksonen, D. Mabaso, M. Molefe, N. Kgabi, and L. Laakso (2011), New particle formation events in semi-clean South African savannah, Atmospheric Chemistry and Physics, 11(7), 3333-3346, 10.5194/acp-11-3333-2011

Volkamer, R., J. L. Jimenez, F. San Martini, K. Dzepina, Q. Zhang, D. Salcedo, L. T. Molina, D. R. Worsnop, and M. J. Molina (2006), Secondary organic aerosol formation from anthropogenic air pollution: Rapid and higher than expected, Geophys. Res. Lett., 33(17), L17811, 10.1029/2006gl026899

Watson, J. G. (2002), Visibility: Science and regulation, J. Air Waste Manage. Assoc., 52(6), 628-713,

Weber, R. J., P. H. McMurry, R. L. Mauldin, D. J. Tanner, F. L. Eisele, A. D. Clarke, and V. N. Kapustin (1999), New Particle Formation in the Remote Troposphere: A Comparison of Observations at Various Sites, Geophysical Research Letters, 26(3), 307-310, 10.1029/1998gl900308

Weber, R. J., A. P. Sullivan, R. E. Peltier, A. Russell, B. Yan, M. Zheng, J. de Gouw, C. Warneke, C. Brock, J. S. Holloway, E. L. Atlas, and E. Edgerton (2007), A study of secondary organic aerosol formation in the anthropogenic-influenced southeastern United States, J. Geophys. Res.-Atmos., 112(D13), D13302, 10.1029/2007jd008408

Wen, J., Y. Zhao, and A. S. Wexler (2006), Marine particle nucleation: Observation at Bodega Bay, California, J. Geophys. Res., 111(D8), D08207, 10.1029/2005jd006210

Wiedensohler, A. (1988), An approximation of the bipolar charge distribution for particles in the submicron size range, J. Aerosol. Sci., 19(3), 387-389, 10.1016/0021-8502(88)90278-9

Wiedensohler, A., W. Birmili, A. Nowak, A. Sonntag, K. Weinhold, M. Merkel, B. Wehner, T. Tuch, S. Pfeifer, M. Fiebig, A. M. Fjäraa, E. Asmi, K. Sellegri, R. Depuy, H. Venzac, P. Villani, P. Laj, P. Aalto, J. A. Ogren, E. Swietlicki, P. Williams, P. Roldin, P. Quincey, C. Hüglin, R. Fierz-Schmidhauser, M. Gysel, E. Weingartner, F. Riccobono, S. Santos, C. Grüning, K. Faloon, D. Beddows, R. Harrison, C. Monahan, S. G. Jennings, C. D. O'Dowd, A. Marinoni, H. G. Horn, L. Keck, J. Jiang, J. Scheckman, P. H. McMurry, Z. Deng, C. S. Zhao, M. Moerman, B. Henzing, G. de Leeuw, G. Löschau, and S. Bastian (2012), Mobility particle size spectrometers: harmonization of technical standards and data structure to facilitate high quality long-term observations of atmospheric particle number size distributions, Atmos. Meas. Tech., 5(3), 657-685, 10.5194/amt-5-657-2012

Williams, B. J., A. H. Goldstein, D. B. Millet, R. Holzinger, N. M. Kreisberg, S. V. Hering, A. B. White, D. R. Worsnop, J. D. Allan, and J. L. Jimenez (2007), Chemical speciation of organic aerosol during the International Consortium for Atmospheric Research on Transport and Transformation 2004: Results from in situ measurements, J. Geophys. Res.-Atmos., 112(D10), D10S26, 10.1029/2006jd007601

Winklmayr, W., G. P. Reischl, A. O. Lindner, and A. Berner (1991), A New Electromobility Spectrometer for the Measurement of Aerosol Size Distributions in the Size Range from 1 to 1000 nm, J. Aerosol. Sci., 22(3), 289-296,

Wood, E. C., M. R. Canagaratna, S. C. Herndon, T. B. Onasch, C. E. Kolb, D. R. Worsnop, J. H. Kroll, W. B. Knighton, R. Seila, M. Zavala, L. T. Molina, P. F. DeCarlo, J. L. Jimenez, A. J. Weinheimer, D. J. Knapp, B. T. Jobson, J. Stutz, W. C. Kuster, and E. J. Williams (2010), Investigation of the correlation between odd oxygen and secondary organic aerosol in Mexico City and Houston, Atmos. Chem. Phys., 10(18), 8947-8968, 10.5194/acp-10-8947-2010

Worton, D. R., A. H. Goldstein, D. K. Farmer, K. S. Docherty, J. L. Jimenez, J. B. Gilman, W. C. Kuster, J. de Gouw, B. J. Williams, N. M. Kreisberg, S. V. Hering, G. Bench, M. McKay, K. Kristensen, M. Glasius, J. D. Surratt, and J. H. Seinfeld (2011), Origins and composition of fine atmospheric carbonaceous aerosol in the Sierra Nevada Mountains, California, Atmos. Chem. Phys., 11(19), 10219-10241, 10.5194/acp-11-10219-2011

Wu, Z., M. Hu, S. Liu, B. Wehner, S. Bauer, A. Maßling, A. Wiedensohler, T. Petäjä, M. Dal Maso, and M. Kulmala (2007), New particle formation in Beijing, China: Statistical analysis of a 1-year data set, J. Geophys. Res., 112(D9), D09209, 10.1029/2006jd007406

Yue, D. L., M. Hu, R. Y. Zhang, Z. B. Wang, J. Zheng, Z. J. Wu, A. Wiedensohler, L. Y. He, X. F. Huang, and T. Zhu (2010), The roles of sulfuric acid in new particle formation and growth in the mega-city of Beijing, Atmospheric Chemistry and Physics, 10(10), 4953-4960, 10.5194/acp-10-4953-2010

Zaveri, R. A., R. C. Easter, J. D. Fast, and L. K. Peters (2008), Model for Simulating Aerosol Interactions and Chemistry (MOSAIC), J. Geophys. Res.-Atmos., 113(D13), 10.1029/2007jd008782

Zaveri, R. A., W. J. Shaw, D. J. Cziczo, B. Schmid, R. A. Ferrare, M. L. Alexander, M. Alexandrov, R. J. Alvarez, W. P. Arnott, D. B. Atkinson, S. Baidar, R. M. Banta, J. C. Barnard, J. Beranek, L. K. Berg, F. Brechtel, W. A. Brewer, J. F. Cahill, B. Cairns, C. D. Cappa, D. Chand, S. China, J. M. Comstock, M. K. Dubey, R. C. Easter, M. H. Erickson, J. D. Fast, C. Floerchinger, B. A. Flowers, E. Fortner, J. S. Gaffney, M. K. Gilles, K. Gorkowski, W. I. Gustafson, M. Gyawali, J. Hair, R. M. Hardesty, J. W. Harworth, S. Herndon, N. Hiranuma, C. Hostetler, J. M. Hubbe, J. T. Jayne, H. Jeong, B. T. Jobson, E. I. Kassianov, L. I. Kleinman, C. Kluzek, B. Knighton, K. R. Kolesar, C. Kuang, A. Kubátová, A. O. Langford, A. Laskin, N. Laulainen, R. D. Marchbanks, C. Mazzoleni, F. Mei, R. C. Moffet, D. Nelson, M. D. Obland, H. Oetjen, T. B. Onasch, I. Ortega, M. Ottaviani, M. Pekour, K. A. Prather, J. G. Radney, R. R. Rogers, S. P. Sandberg, A. Sedlacek, C. J. Senff, G. Senum, A. Setyan, J. E. Shilling, M. Shrivastava, C. Song, S. R. Springston, R. Subramanian, K. Suski, J. Tomlinson, R. Volkamer, H. W. Wallace, J. Wang, A. M. Weickmann, D. R. Worsnop, X. Y. Yu, A. Zelenyuk, and Q. Zhang (2012b), Overview of the 2010 Carbonaceous Aerosols and Radiative Effects Study (CARES), Atmos. Chem. Phys., 12(16), 7647-7687, 10.5194/acp-12-7647-2012

Zhang, Q., D. R. Worsnop, M. R. Canagaratna, and J. L. Jimenez (2005a), Hydrocarbon-like and oxygenated organic aerosols in Pittsburgh: Insights into sources and processes of organic aerosols, Atmos. Chem. Phys., 5, 3289-3311, doi:10.5194/acp-5-3289-2005

Zhang, Q., J. L. Jimenez, D. R. Worsnop, and M. Canagaratna (2007a), A case study of urban particle acidity and its influence on secondary organic aerosol, Environ. Sci. Technol., 41(9), 3213-3219, 10.1021/es061812j

Zhang, Q., M. R. Canagaratna, J. T. Jayne, D. R. Worsnop, and J. L. Jimenez (2005b), Time- and size-resolved chemical composition of submicron particles in Pittsburgh: Implications for aerosol sources and processes, J. Geophys. Res.-Atmos., 110(D7), D07S09, 10.1029/2004jd004649

Zhang, Q., C. O. Stanier, M. R. Canagaratna, J. T. Jayne, D. R. Worsnop, S. N. Pandis, and J. L. Jimenez (2004), Insights into the chemistry of new particle formation and growth events in Pittsburgh based on aerosol mass spectrometry, Environmental Science & Technology, 38(18), 4797-4809, 10.1021/es035417u

Zhang, Q., M. R. Alfarra, D. R. Worsnop, J. D. Allan, H. Coe, M. R. Canagaratna, and J. L. Jimenez (2005c), Deconvolution and quantification of hydrocarbon-like and oxygenated organic aerosols based on aerosol mass spectrometry, Environ. Sci. Technol., 39(13), 4938-4952, 10.1021/es048568l

Zhang, Q., J. Jimenez, M. Canagaratna, I. Ulbrich, N. Ng, D. Worsnop, and Y. Sun (2011), Understanding atmospheric organic aerosols via factor analysis of aerosol mass spectrometry: a review, Analytical and Bioanalytical Chemistry, 401(10), 3045-3067, 10.1007/s00216-011-5355-y

Zhang, Q., J. D. Allan, J. Tian, J. L. Jimenez, M. R. Canagaratna, I. Ulbrich, A. Kiendler-Scharr, H. Coe, D. R. Worsnop, A. H. Goldstein, and B. J. Williams (2009), Identification and characterization of biogenic and anthropogenic SOA components at Chebogue Point during ICARTT 2004 Based on Aerosol Mass Spectrometry Journal of Geophysical Research (in prepare),

Zhang, Q., J. L. Jimenez, M. R. Canagaratna, J. D. Allan, H. Coe, I. Ulbrich, M. R. Alfarra, A. Takami, A. M. Middlebrook, Y. L. Sun, K. Dzepina, E. Dunlea, K. Docherty, P. F. DeCarlo, D. Salcedo, T. Onasch, J. T. Jayne, T. Miyoshi, A. Shimono, S. Hatakeyama, N. Takegawa, Y. Kondo, J. Schneider, F. Drewnick, S. Weimer, K. Demerjian, P. Williams, K. Bower, R. Bahreini, L. Cotrell, R. J. Griffin, J. Rautiainen, J. Y. Sun, Y. M. Zhang, and D. R. Worsnop (2007b), Ubiquity and Dominance of Oxygenated Species in Organic Aerosols in Anthropogenically-Influenced Northern Hemisphere Mid-latitudes, Geophys. Res. Lett., 34, L13801, doi:10.1029/2007GL029979,

Zhang, Y. M., X. Y. Zhang, J. Y. Sun, W. L. Lin, S. L. Gong, X. J. Shen, and S. Yang (2011), Characterization of new particle and secondary aerosol formation during summertime in Beijing, China, Tellus Ser. B-Chem. Phys. Meteorol., 63(3), 382-394, 10.1111/j.1600-0889.2011.00533.x

Ziemba, L. D., R. J. Griffin, L. D. Cottrell, P. J. Beckman, Q. Zhang, R. K. Varner, B. C. Sive, H. Mao, and R. W. Talbot (2010), Characterization of aerosol associated with enhanced small particle of number concentrations in a suburban forested environment, J. Geophys. Res.-Atmos., 115, D12206, 10.1029/2009jd012614